UNIVERSITÀ DEGLI STUDI DI MILANO

Doctoral School in Pharmaceutical Sciences – XXXIV cycle

DIPARTIMENTO DI SCIENZE FARMACEUTICHE

Quantitative Lipidomics and Proteomics in Medicinal Chemistry

CHIM/08

SILVIA RADREZZA

R12190

Tutor: Prof. Marina CARINI; Prof. Alfonsina D'AMATO

Coordinator: Prof. Giancarlo ALDINI

Academic year 2020/2021

INDEX

GENERAL ABSTRACT

The ‘omics sciences are currently in development offering a new and combined perspective of cellular and organismal environment. Among these, genomics and proteomics are among the most developed while lipidomics is still an emergent field. The importance to provide a strong methodological approach paired to a rigorous data interpretation is explained by the recent discovery of the lipids’ key role not only as structural components and energetic source but also in many biological processes (*i.e.,* second messengers, regulators of inter-cellular interactions and of surface charge, involvement in metabolic diseases, cancer etc.).

Thanks to the recent significant advances, mass spectrometry is the most suitable analytical method in many of ‘omics sciences despite their integration is still at the beginning and a careful optimization of protocols is needed. Nevertheless, considering the molecular complexity, only a multi-omics vision can give a complete picture of intra- and extra-cellular processes in physiological and pathological conditions as well as in response to an environmental or chemical exposure to finally contribute to the field of precision medicine.

So, the work herein aims to provide proteomics and lipidomics perspectives, both as single and integrated approaches, to different research questions by high-resolution mass spectrometry.

At first, the investigation on skin hairless mice proteome allowed me to show how an endogenous peptide, β-alanil-L-histidine (a.k.a. carnosine), is acting in defense of UV-A damages. Indeed, several major protein systems shown an alteration by UV-A treatment including calcium signaling, mitochondrial function or sirtuin expression, which were all restored by a preventive treatment of the skins by a topical application of carnosine. These proteomics alterations could result (at least in part) from ROS generated by UV-A, or/and the generation of lipid oxidation products (HNE, acrolein) resulting from the peroxidation of polyunsaturated fatty acids in the irradiated skins. The implication of such agents is emphasized by the potent efficacy of carnosine in restoring a normal proteomic profile of UV-A-treated skins, in accordance with its ability to neutralize the formation of adducts on proteins and their subsequent modification, thereby restoring their function.

Moving to lipidomics, the biological importance recently demonstrated by fatty acid esters of hydroxy fatty acids (FAHFAs) asked for a tailored method optimization for their identification and quantification in human matrix. In fact, increasing evidence on the physiological roles of FAHFAs, including anti-inflammatory, anti-diabetic and immunomodulatory ones, motivates a more extensive characterization of these lipids as possible biomarkers and therapeutic targets for pathological conditions such as diabetes or obesity. Nevertheless, the low concentration in human tissues, the large structure heterogeneity and that the major amount of FAHFAs in cells is incorporated into

triacylglycerols challenge current analytical methods for their accurate identification and quantification. The achieved samples' preparation and instrumental method optimization successfully enabled to isolate, detect, and quantify endogenous FAHFAs for the first time on human adipose tissue revealing significant alterations based on metabolic status (obese insulin sensitive or resistant vs lean subjects) and adipose tissue portions (visceral vs subcutaneous). These results will be useful to better understand the biological potentiality of this bioactive lipids in metabolic pathologies.

Then, the two multi-omics studies herein conducted were aimed to evaluate molecular effects of low-molecular-weight hyaluronic acid (LMW-HA) in proteome and lipidome of normal human dermal fibroblasts and to analyze lipidome and proteome profile changes induced by γ-Oryzanol (Orz) prevention treatment in obese-induced rats, respectively.

LMW-HA showed an impact both on proteome and lipidome profile, mainly at 0.50 % of concentration. The proteomics results were not only confirmed but also corroborated by lipidomics and integratomics ones. Indeed, mitochondria functionality, cells maturation and lipids metabolism were concordantly demonstrated. About lipidome changes, we saw a particular increasing of ceramides, triacylglycerols and cholesterol esters involved in the skin moisturizing and epidermis renewal and so supporting the beneficial role of low-molecular weight as cosmetic ingredient. Nevertheless, the correct balance between their synthesis and degradation is essential for the skin wellness and further studies are necessary for the deepening of these dynamics.

The Orz's effects assessment, instead, provided only marginal significant alterations both in plasma's proteome and lipidome probably due to the weakness of the animal model. Further thoughts and experiments are needed to confirm the biological relevance of Orz mainly showed in biological tests so far.

To conclude, although a lot of questions related to these research topics are still unanswered and other omics should be included in an integrative vision (metabolomics for example), during this multidisciplinary PhD journey I appreciated the complexity and the value of omics sciences in deepening our knowledge about several research fields approaching more and more the precision medicine goal.

I

Introduction

1.1 Precision medicine and networking analysis

– A general perspective –

The past half century has seen a tremendous progress in technology of many fields, including science, allowing the start of the omics' era characterized by an unheard-of large data availability at relatively low costs and efforts. The term *'omics* refers to the comprehensive study of the roles, relationships, and actions of various types of molecules in cells of an organism (1,2). Nevertheless, since the complete mapping of human genome by Guyer et al. (1993) (3) at the beginning of ninety's, the way to approach science is highly changed and expanded through the development of a whole range of additional omics technologies with different research goals. Among all, omics data help to clarify the molecular mechanisms and to provide both potential biomarkers and pharmacological targets for a more detailed patient stratification boosting the "precision medicine" approach as end goal (2).

Despite the concept of precision medicine is not new (before it was called "personalized medicine"), the interest on it is constantly increasing also thanks to the "Precision Medicine Initiative" carried on by National Research Council (NRC) and the public support of President Barrack Obama in 2015 (4). Mainly driven by *big data* collecting all the medical records for each individual and sub-population, precision medicine is referred as "*the tailoring of medical treatment to the individual characteristics of each patient. It does not literally mean the creation of drugs or medical devices that are unique to a patient, but rather the ability to classify individuals into subpopulations that differ in their susceptibility to a particular disease or in their response to a specific treatment*" (4). The promise of precision medicine, therefore, is that a greater understanding of individual data will lead to personalized treatment and improved outcomes.

Studies aimed to optimize tailored treatments maximizing effects and resources are constantly increasing by number and covered areas. One of the first and successful example of precision medicine comes from Piccart-Gebhart MJ., (2005) (5) by targeting of the single gene mutation in the human epidermal growth factor receptor 2 (HER2) gene in breast cancer cells by the monoclonal antibody Trastuzumab. Morello et al., (2019) (6) showed instead a pathway-based characterization of sporadic amyotrophic lateral sclerosis (SALS) subtypes and identified 24 potential candidates for genomic-based patient stratification. Coupled to genomics, also lipidomics is attracting an increasing

interest in precision medicine (7). Being lipids essential in many biological aspects, they are becoming great candidates as unique biomarkers or prognostic indicators. At this regard, Eisfeld et al., (2017) (8) identified in plasma samples from patients with Ebola virus disease (EVD) reporting outstanding predictive ability of survival at the early stage of diagnosis of 11 biomarkers including lipids, metabolites, cytokines, proteins and one clinical index, thereby helping to improve the prognostic treatment of those high-risk patients.

1.1.1 Integratomics and network analyses

From the study of the entire genes population in a cell or organism (genomics) focused on "what can happen", the interested has moved forward to see "what seems to be happening" through the measurement of gene transcripts (transcriptomics), "what makes it happen" by the proteins expression (proteomics), and finally on "what is actually happening or happened" driven by metabolites (metabolomics). Further than these principal ones, a corollary of other omics are becoming popular such as lipidomics, metagenomics, glycomics, connectomics, cellomics, foodomics etc. (9–14). All these steps, also known as "omics cascade", have taken place greatly expanding our knowledge about biological and phenotypical processes in cellular and organismal environment in health and disease conditions but also in pharmaceutical, food and nutrition, veterinary, environmental etc. fields (15).

Although each approach could offer a broad understanding of the biological processes, single omics studies don't consider the complex molecular interplay despite of the phenotypes resulting from different signalling pathways involve at the same time various types of biological actors. Therefore, combining multiple omics data (*i.e.*, genomics, transcriptomics, proteomics, metabolomics) in a "multi-omics" vision is needed to detail molecular mechanisms and for a better comprehension of health and diseases as well as the cause-effect relations.

So, the principal aim of multi-omics approach (also referred as "integratomics") is to identify unrevealed key factors acting on cell signalling, interactions, and for prediction of phenotype in a more realistic way of a singular omics science. Moreover, that allows to supply missing data or

information in any single data type also reducing, after a suitable data curation, the possibilities of misinterpretation providing instead more reliable results (16).

Indeed, many studies related not only on health conditions but also on different research areas such as food and nutrition, system microbiology, microbiomes, system biology, plants etc. (17–20) demonstrated so far the added value of integration of omics data although mainly of them are focused on genomics and proteomics. Currently increasing is the integration with metabolomics data, including lipidomics ones, despite the novelty and complexity of their (bio)interpretation (21).

In line with this goal, "LipidGenie", a large-scale genome-lipid association for lipid identification was recently assembled by Linke et al. (2020) (22). Despite of it is not possible to directly predict lipid identities from genome, shared genetic regulation could facilitate lipid identification. Indeed, metabolites including lipids were defined as linkers between genome and phenotype in pathologies like Alzheimer, type 2 diabetes, and various types of cancer since the metabolic profile alterations could result from genetic variations (further than environmental and lifestyle factors) or, in turn, they can modulate the activity of specific genes and related proteins (23, 24). Among the few integrating studies involving lipidomics, Xu et al. (2020) (20) demonstrated as five protein modules are involved in positive regulation of cytokine production, neutrophil mediated immunity, and humoral immune response were also correlated with Alzheimer's disease risk loci acting in immune and complement systems and in lipid metabolism. Instead, Di Carlo et al. (2021) (25), combing proteomics and lipidomics data, demonstrated a crucial role of fatty acid elongation and alteration in cardiolipin acyl chain composition in pancreatic cancer stem cells representing an attractive therapeutic target in pancreatic ductal adenocarcinomas.

1.1.2 Integrations challenges and strategies

The heterogeneity of datasets intra- and, above all, inter-omics is one of the biggest challenges for their integrations mainly due to differences on experimental design, sample processing, analytical methods, data quality and management (17,26). Indeed, so far there aren't defined protocols neither

for pre-integrations steps nor for post-integration analyses especially for emerging omics (*i.e.*, lipidomics) leaving to the researchers to find the best and reliable approach. However, it's well known as an appropriate raw data curation is fundamental for any kind of analyses.

The data curation, also called "dimensional reduction", includes deletion of batch effect, normalization (by internal standards and proteins concentration in case of lipidomics for example) and replacement of missing values for each dataset before the integration (1,17).

Then, for their integration specific methods were developed. Nevertheless, the appropriate integration strategy depends on the study aim and data availability. In fact, multi-omics data could be resulted from same sample/individual (the optimal scenario but not often feasible), just a partial overlapping set from the same sample/individual or coming from completely different sets. So, not "one fits all".

Two general integration paradigms have been described and referred as:

I) simultaneous or statistical-based integration approach when all omics data are available at the same time and the analysis is driven by inference from the data themselves (intrinsic integration) applying for example principal component analysis (PCA) or Bayesian correlation (*i.e.*, univariate correlation, matrix-based correlation, or matrix factorization) to identify links or overall patterns across multiple omics dataset based (17,27).

II) stepwise or network-based integration when the datasets are analysed by themselves, and the results subsequently integrated by networking approach. After having identified the molecules or pathways of interest deriving from one's own experimental data, the information is then integrated with external literature resources or public databases in an approach called "knowledge-based". In that way, it's possible to expand own scale analysis maybe lacking of information (1,27).

Having applied the knowledge-based approach also in one of my projects, I'll focus on it my attention.

1.1.3 Knowledge-based approach for network analyses

In the knowledge-based integration strategies external information are merged to those provided by experimental analyses. Indeed, prior knowledge derived from scientific publication and/or databases could include more complete functional relationships, pharmacogenomics links or genomics annotations.

Due to the increasing spread of multi-omics vision, over the last decades many efforts were put for the creation of extensive databases collecting molecules annotations, biological pathways, and interactions networks. Below some examples of the most popular, comprehensive, and open-source database:

- "The Human Genome Project" (1990 - 2004) (28) represents the first public and large database on genomics and so the starting point for many others in different research field
- "The Kyoto Encyclopaedia of Gene and Genomes" (KEGG) (29) covers around 11.000 reactions and about 19.000 compounds (https://www.kegg.jp/kegg/docs/statistics.html - last check at 08/09/2021) offering one of the first resource (released in 1995) to link genome with higher-order information (proteins and metabolites)
- "Recon3D" (30) contains genome-scale metabolic reconstruction useful for computational modelling
- "Reactome" (31) is mainly focused on human biological reactions at multiple levels
- "Wikipathways" (32–34) is an open, collaborative platform to describe models of biological pathways
- "STRING" (35) is a tool for protein-protein interactions
- "LIPID MAPS Structure Database (LMSD)" (36) represents a comprehensive source for lipids nomenclature and structure providing also internal tools for data analysis and interpretation (*i.e.*, LipidFinder, BioPan etc.)
- "ChEBI" (37) maps lipids to the chemical ontology

- "SwissLipids" (38) is an expert curated knowledge resource dedicated to lipids and their biology, designed to better integrate lipidomics data with biological knowledge;

Then, some large consortia interested on specific clinical conditions or biological status are developing their own dataset such as "The Cancer Genome Atlas" (TCGA), the "integrative Human Microbiome Project" (iHMP) or NCI60 cell lines dataset (39–41). Nevertheless, to further improve databases completeness and reproducibility of experiments the sharing of all results is fundamental in accessible repositories or dedicated web-services (42).

To use these heterogeneous resources for knowledge-based interactions, all experimental data must be converted into platform-specific identifiers (ID). "Omics Discovery Index" (OmicsDI) platform helps on the coordination among different omics datasets (43). However, many resources such as MetaboAnalystR (https://www.metaboanalyst.ca/faces/upload/ConvertView.xhtml) for metabolites, have developed their internal ID codes increasing the numbers of IDs referring to the same entry or analogous. This overlap is critical especially for metabolites and lipids considering the intrinsic challenge to discriminate isobaric species at side-chain level causing a loss of information or an underestimation of their presence (1).

1.1.3.1 Different types of knowledge-based integration

The knowledge-based integration is based on the following strategies mainly described as (1,17,27):

i) Sub-network identification and analysis if based on context-specific networks selection in which the less important and/or known molecules can be pointed out. As cons there is the potential lack of interactions with sparse information and the necessity of large dataset

ii) Overrepresentation analysis (ORA) aimed to identify entries overrepresented in the predefined input lists compared to what it's expected by chance

iii) Functional set enrichment analysis (FSEA) that, in contrast to ORA, compares all entries (not a subset) to known pathways or functional genes expression with quantitative purpose (p value)

iv) *In silico* approach is aimed to discover and characterize pathways by prediction of possible connections overcoming the limitations of what is already known or used in ORA and FSEA analyses

v) Cluster integration mainly used for grouping separately known and unknown molecules with similar phenomenological behaviour

vi) Composite network approach that combines information of experimental data and knowledge-based resources (other studies and databases) drawing also indirect associations

The composite network approach is currently becoming the most popular due to its versatility and completeness expanding the user's information in one single analysis without any other additional experiments. Indeed, to create a qualitative network the required information is only the gene name (if proteins or genes) or the converted IDs if lipids for examples. In case the goal is to verify the trend, so quantification, the fold-change expression is also needed.

Although the development of integrations algorithms is still on-going and many aspects are uncovered or "weak", the real challenge in these days is the post-integrations interpretation of multi-omics networks to reach meaningful results.

If the analyses of genome and proteome is almost routine nowadays, metabolic and lipidomics ones are still at the beginning, less standardized and easy to be biased. For example, if the metabolic reaction of interested is at membrane level, a large network could contain many other unrelated information that could compromise the output reading. Further than that, the data source (plasma, cells etc.) must be considered as well as the reactions kinetic rates (16,27). Metabolites, lipids, post-

translations modifications of proteins can change very quickly being directly related to enzymes, intracellular metabolic reactions for example can happen from secs to hours but the activation of the response can take longer, hours to days. So, only molecules with the similar turn-over and referred to the same biological system should be merged.

1.1.4 Networking analysis and visualization

To our knowledge, Ingenuity Pathways Analysis (IPA; https://digitalinsights.qiagen.com/) is the only functional analysis and knowledge discovery web-based tool giving quantitative output (z score, p-value, fold change) for intra- and inter-omics pathways and networks. That's done by the merge of user's experimental data (current and/or previous ones) with its own database, constantly curated that collects (so far) almost 50.000 public human, mouse, and rat's datasets (*i.e.*, UniProt, Entrez Gene, GEO, TCGA, OMIM, scientific publications etc.) including both microarray and RNA-Seq gene expression, miRNA, SNP, metabolomics, and proteomics data. In general, lists of genes or chemicals can be analysed using IPA. It also has a search capability for information on genes, proteins, chemicals, and drugs allowing interactive building of networks to represent biological systems. The significance indicates the probability of association of molecules from the experimental dataset with the pathway by random chance alone. The overall activation/inhibition states of canonical pathways are predicted based on a z-score algorithm.

Indeed, through IPA software, I was able to identify the most relevant signaling and metabolic pathways, molecular networks, and biological functions for list of genes-related proteins and/or lipids further than prediction of the direction of downstream effects on biological and disease processes as well as of upstream transcription factors and to compare affected pathways and phenotypes across multiple testing conditions.

A key component of networking analyses is visualization. Indeed, statics alone is not enough to highlight the results especially with a large-size dataset. In multi-omics network, nodes represent a

biological entry (metabolite, gene, protein etc.) and edges the known direct or indirect interactions. Moreover, to help the comprehension, nodes size reflects the topological degree, node colour the expression (up- or down-regulation) or abundance, and node shape the molecule type (enzyme, lipid etc.). In the Figure 1 an example of visualization network obtained with IPA database.

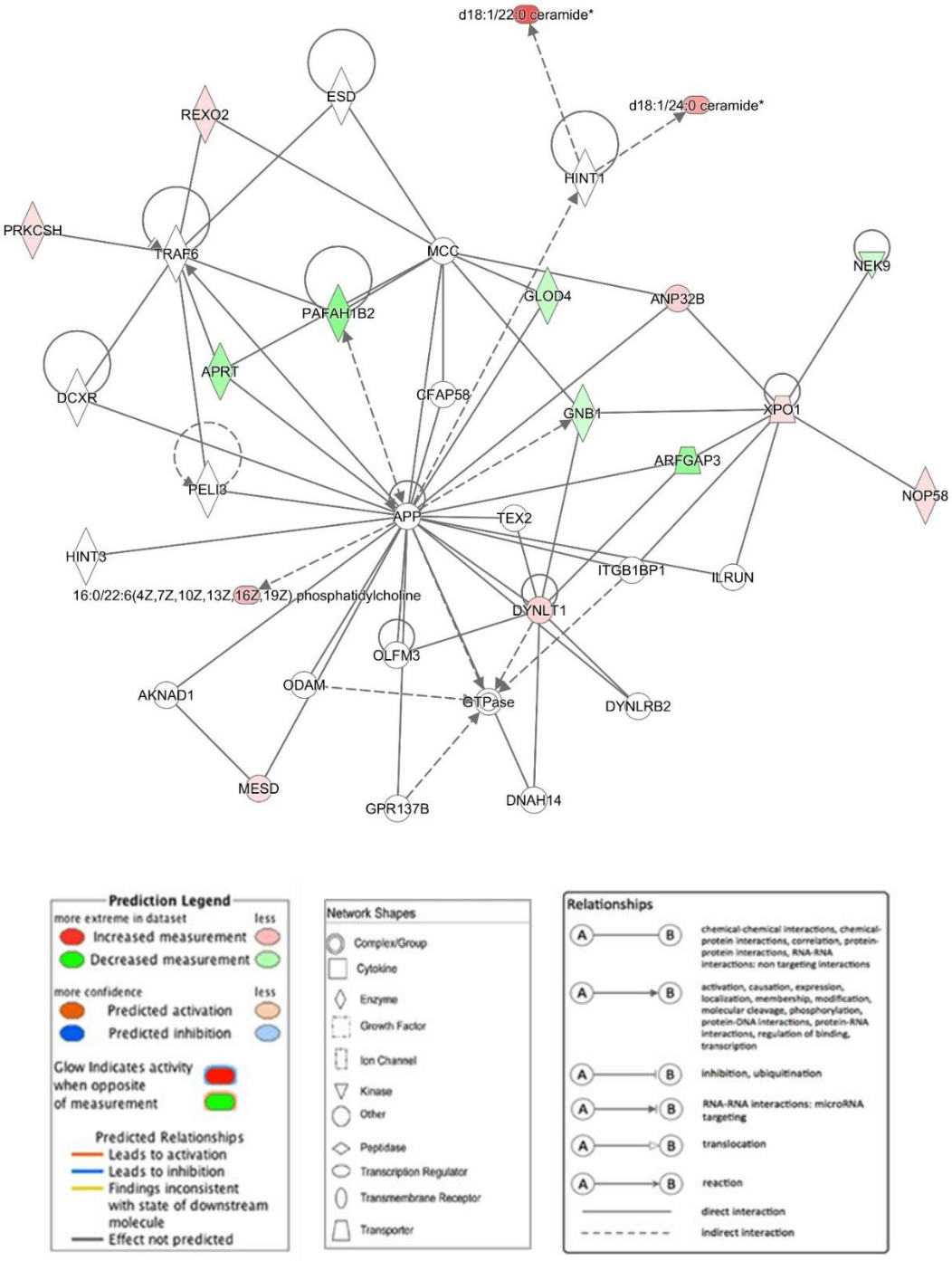

Figure 1. Example of IPA network merging genes (proteins) and lipids. In the charts below the colours and shapes legends (Qiagen).

Further than IPA, there are many visualization options and mostly web-based such as Cytoscape (https://cytoscape.org/), MetaboAnalyst (https://www.metaboanalyst.ca/), String (https://string-db.org/) or BioPan (https://www.lipidmaps.org/biopan/) despite they can provide only qualitative and intra-omics outputs.

1.2 Omics

– Focus on Proteomics and Lipidomics –

During my PhD, I have had experience in the field of proteomics and lipidomics both as single omics and in combination as the new multi-omics approach aims to.

1.2.1 PROTEOMICS

The past decades have marked the period of greatest development of proteomics, alongside genomics, by the boosting of biological mass spectrometry (MS), genome sequencing and bioinformatics tools (44).

Proteomics is the qualitative and quantitative study of complete sets of all expressed proteins (proteome) in a cell or in a subcellular compartment, tissue, biofluid, or organism in the given context. In addition, proteomics also encompasses the study of proteins isoforms, modifications, their interactions, and complexes (45). Since the proteome is the linker between genotype and phenotype, proteomics emerges as an area that promises translational research including biomarkers discovery, early diagnosis of diseases, predicting disease prognosis, and identifying druggable targets for new therapies (45,46).

Considering the broader experience in proteomics field than, for example, lipidomics, the experimental protocols and data analysis steps are better consolidated and standardized especially for unmodified proteins and comprehensive proteome analyses. In this case proteins are nowadays typically digested with specific proteases (trypsin, lys-C or chemo-trypsin). Then, the resulting peptide mixtures are separated and detected by high performance liquid chromatography (HPLC) coupled to a mass spectrometer mainly operating in high-resolution such as Orbitrap or Q-TOF generating (tandem) mass spectra subsequently matched to theoretical spectra for their identification and quantification (44).

1.2.1.1 Labelled and label-free quantitative proteomics

Quantitative MS-based proteomics could be performed by labelling-based or label-free approaches. Although labelling with isobaric tag, isotope-coded affinity tag, stable isotope etc. can provide a more accurate inter-sample quantification, it's costly, time consuming and requires additional steps for the sample preparation. It's case of experiments such as TMT (Tandem mass tags), SILAC (Stable isotope labelling by amino acids in cell culture) or iTRAQ (Isobaric Tags for Relative and Absolute Quantitation) (47–49).

Label-free proteomics instead is more versatile, easy to apply and less expensive becoming the most common approach with as well great levels of accuracy and sensitivity quantification (50).

For all these reasons, during my PhD I have had mostly experience with label-free approach generally based on:

- Data-dependent acquisition (DDA) that is the more used MS method for the proteins detection and identification followed by data-independent one (DIA) both operating in high-resolution mode (51)
- Proteins quantification is almost always performed by spectra count or, above all, peak intensity (50). In the first case, the quantification is based on the number of MS/MS spectra of peptides derived from a given protein. In the peak intensity-based approach instead, proteins are quantified according to the ion intensities of the acquired peptides offering more accurate information

To facilitate MS raw data analysis, several software were developed such as Proteome Discoverer (Thermo Scientific ™), MaxQuant, MetaMorpheus, Mascot, PEAKS etc (52–55).

Among them, for proteins identification and quantification, I used MaxQuant-LFQ (label-free quantitation) against Andromeda search engine that summarizes observed peptide intensities based on peptide ratios at the protein-level before performing a statistical analysis on protein abundance for their relative quantitation. Then, MaxQuant-LFQ normalizes the signal from each run combining the information from peptide level (52). The missing values, one of the most important problem in label-

free proteomics (56), is here solved by "match between runs" strategy that, despite of it could causes false transfer, it is the more used strategy so far (57). After that, I visualized the obtained results with Perseus (https://maxquant.net/perseus/).

Label-free proteomics applications: some examples

The impact of label-free proteomics on many research fields, from system biology to pharmaceutics, food, veterinary science etc. is doubtless. Below some examples of its current applications.

Optimization of the dosage of medicines to maximize their efficacy with limited toxicity is an urgent need pointed out by the Food and Drug Administration (FDA) last guidance (58). Precise and reliable quantification of proteins involved in drug metabolism and impact is essential to achieve this goal. At this regard, Couto et al. (2019) (59) studied microsomes from human liver applying label-free proteomics to better explore the clearance of drugs. This comprehensive analysis offers a useful perspective of the abundance of drug metabolising enzymes, particularly belonging to cytochrome (CYPs) and glucuronosyltransferase (UGTs) families, and drug transporters in human liver microsomal fractions. Moreover, a decreased expression of specific enzymes and transporters was associated to an increasing body max index (BMI).

Tierney et al. (2021) (60) instead, working on multiple myeloma (the second most prevalent haematological malignancy), explored the patients' sensitivity to currently used drugs by liquid-chromatography coupled to high-resolution MS (LC-HRMS)-based proteomics. Comparative analyses allowed to separate the most and least sensitive patients as well as to identify several proteins significantly involved in the drug's lack of efficacy. Indeed, five classes of focal adhesion-related proteins predicted low sensitivity suggesting that targeting this pathway could modulate drug resistance.

Moreover, thanks to the huge data availability provides by omics sciences, an increasing number of projects are born to create tissue- or organ-specific atlas facilitating translational research.

Paired to global initiatives driven for example by "Human Proteome Organization" (HUPO; https://www.proteinatlas.org/) or "Clinical Proteomic Tumor Analysis Consortium" (CPTAC; https://proteomics.cancer.gov/programs/cptac), more tailored ones are becoming of interest. Among them, Dyring-Andersen et al. (2020) (61) investigated healthy human skin proteome resulting on a spatial and cell-type resolved quantitative proteomic atlas comprehensive of 10.701 proteins with the relative function, location, and cellular origin.

1.2.2 LIPIDOMICS

Among omics, lipidomics is still an emerging field. The importance to provide a strong methodological approach paired to a rigorous data interpretation is explained by the recent discovery of the lipids' key role in many biological processes. Indeed, more than passive structural cellular membrane's components or energetic source they are crucial small biomolecules acting as second messengers in signal transduction, regulators of intra- intercellular interactions and of surface charge (62). Again, most of lipids are involved in many diseases such as diabetes, obesity, hypertension, cancer, neurodegenerative and dermatological ones (63).

Lipids represent the last step of "omics cascade" (64). Genome is the first step determining the genotype and the predisposition of what could happen to the subject. On the contrary, metabolome including lipidome influences the phenotype and so it's able to report the actual health status. For this reason, metabolomics (and so lipidomics) is more convenient for biomarker discovery and prognostic factors. Nevertheless, although lipidomics is a sub-field of metabolomics, due to its complexity it requires totally different analytical and data interpretation approaches.

1.2.2.1 Lipidome's complexity

Despite there isn't a universal definition of lipids yet, the most used nowadays says the lipids are *"hydrophobic or amphipathic small molecules that originate entirely or in part by carbanion-based condensations of thioesters and/or by carbocation-based condensations of isoprene units"* (65). In fact, most natural lipids are different combinations of hydrophobic fatty acyl chain and polar head group attached to several backbone structures. Since 2005, LIPID MAPS consortium (36) offers one of the most complete collection of lipid structures (LMSD) with around 45.000 entries subdivided into eight categories *i.e.*, fatty acyls (FA), glycerolipids (GL), glycerophospholipids (GP), sphingolipids (SP), sterol lipids (ST), prenol lipids (PR), saccharolipids (SL), and polyketides (PK), each of them containing several classes and/or subclasses (Figure 2).

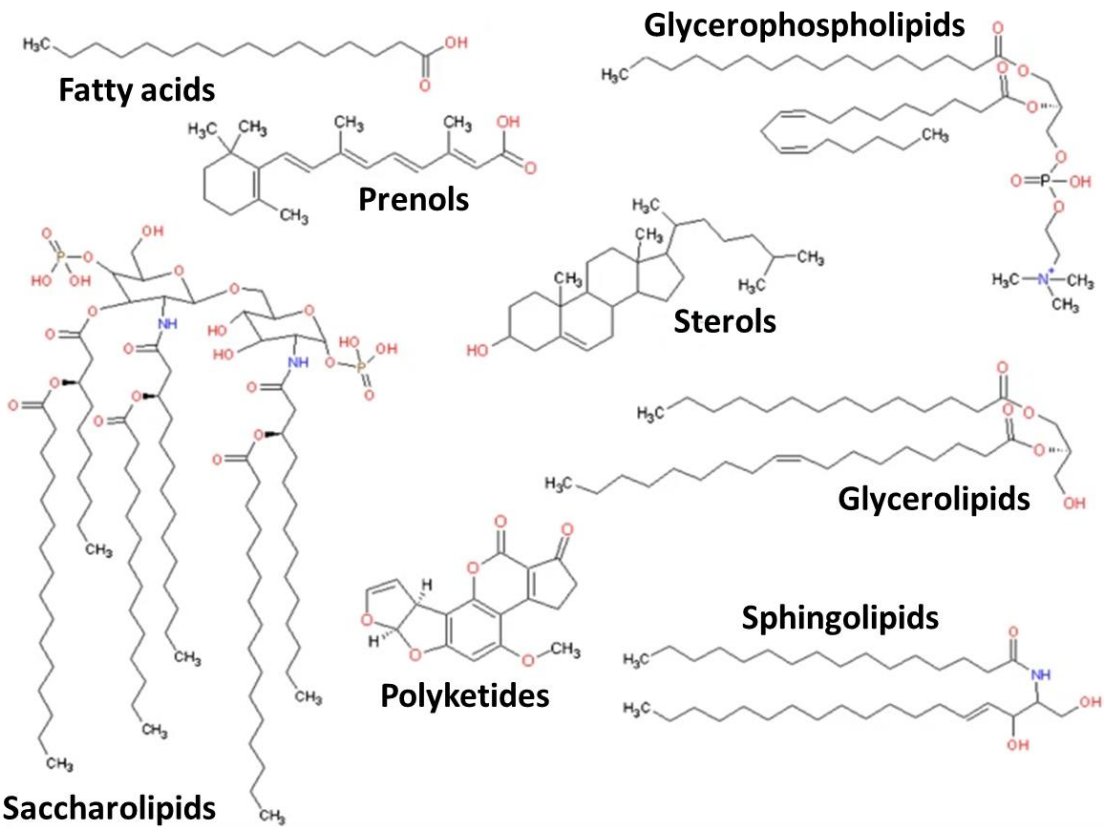

Figure 2. Eight categories of lipid structures based on LIPID MAPS consortium classification, *i.e.*, fatty acyls (FA), glycerolipids (GL), glycerophospholipids (GP), sphingolipids (SP), sterol lipids (ST), prenol lipids (PR), saccharolipids (SL), and polyketides (PK).

The structural diversity is one of the biggest challenges in lipidomics with ten to hundreds of thousands distinct chemical structures in a biological system characterized by different properties (66). Type of head group, fatty acid chain length, level of unsaturation, double bond position, type of double bonds (acyl-, alkyl- or alkenyl-), *cis-trans* geometric isomerism and branched functional groups are all aspects that influence the lipids' structure and their physio-chemical properties (polarity or ionization efficiency in MS for example) (67).

Due to this diversification, the lipidome analyses are still complicated despite the huge progresses in the analytical and bioinformatic fields. Indeed, it's impossible to cover all lipids in a biological matrix in a single method both in the sample preparation stage and instrumental one (Figure 3).

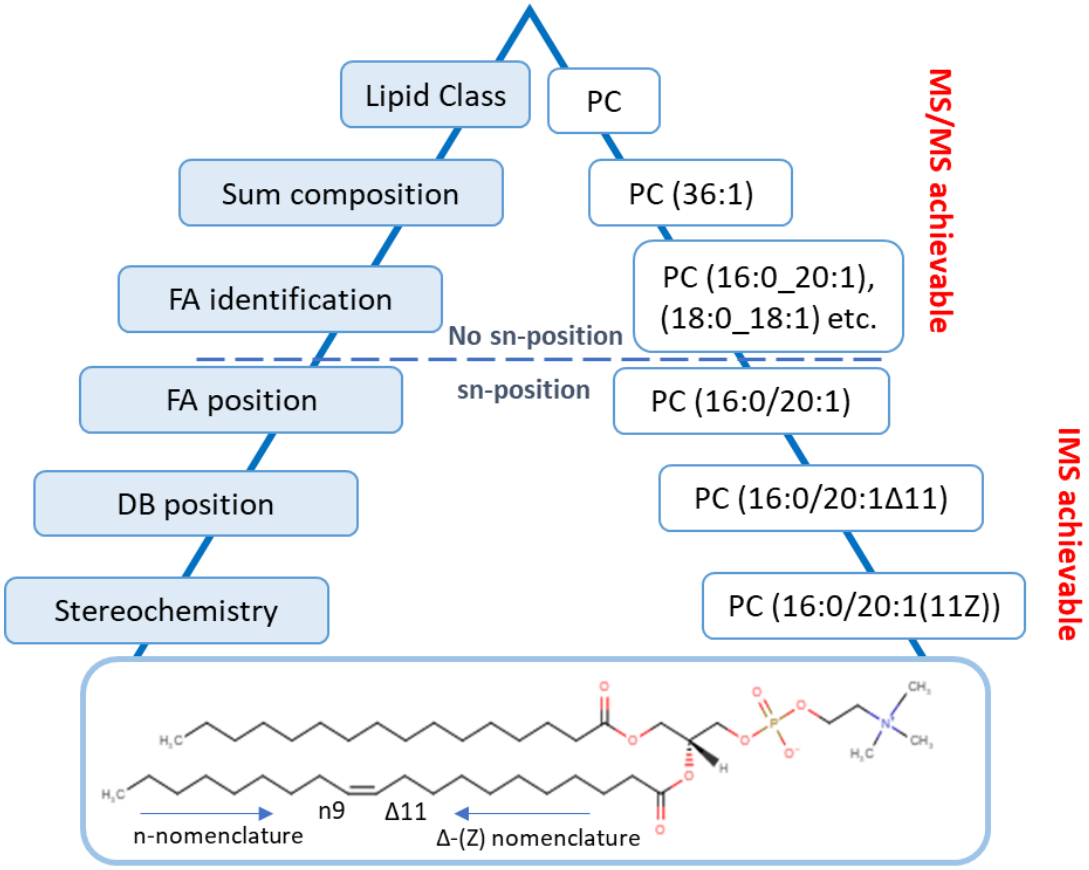

Figure 3. Levels of structural description of lipids. PC = phosphatidylcholine; MS = mass spectrometry; IMS= ion mobility mass spectrometry; FA = fatty acid chain; DB = double bond.

Further than the lipidome complexity, sample preparation procedure, lipid standard type and amount, extraction protocol, solvents, reagents, lab equipment (vials, caps, tips etc.) must be optimized and selected carefully to avoid contaminations (plasticizers for instance), artefacts or scarce data quality (64). Indeed, for example, there isn't a universal extraction procedure. On the contrary, it's highly dependent on the class of interest even if lately, MTBE extraction (68) has partially substituted the classic Folch (69) and Bligh and Dyer (70) methods chloroform-based due to its less toxicity and similar performance.

The storage is equally important. It's preferable stored samples at -80°C, in organic solvents (isopropanol for example), avoid as much as possible freeze-thaw cycles to reduce lipids hydrolysis

and to limit the storage time according to the sample type. Useful to contrast oxidation both during storage and extraction procedure is the addition of antioxidants like butylated hydroxytoluene (BHT).

1.2.2.2 Analytical strategies and current challenges for mass-spectrometry based lipidomics

During the last decade the improvement of detection techniques including mass-spectrometry boosted lipidomics analyses regarding availability and quality of data. Thanks to the enormous advantages offered by high-resolution MS (HRMS) compared to the older low-resolution, huge improvements are reached in terms of mass accuracy, sensitivity, and peak resolution despite there are still challenges and a reliable identification is the first one.

The huge lipids diversity briefly explained above leads many potential mass spectra overlaps of molecular and adduct ions. Indeed, isomeric species (same elemental composition but different structure) cannot be separated without fragmentation, and, above all, isobaric ones (same nominal mass) require high resolution approaches (71).

Among all the analytical techniques, liquid-chromatography (LC) coupled to HRMS is the most common approach in lipidomics. Chromatographic methods further improved detection and quantification reliability mainly reducing ion suppression (67,72). Superior performances are showed by ultrahigh-performance liquid chromatography (UHPLC) compared to the standard HPLC (high-performance liquid chromatography) and, more recently, supercritical fluid chromatography (UHPSCF). Moreover, it's becoming popular the multi-dimensional LC (MDLC) with orthogonal separations that allows a better peak capacity in complex matrixes even if the single lipid separation (one by one) is still not possible (64,67).

Normal-phase LC (NPLC), hydrophilic interaction liquid chromatography (HILIC) and reversed-phase LC (RPLC) are the most used chromatographic techniques in lipidomics. Among them, I applied RPLC due to its higher versatility, higher polarity coverage, and ability to efficiently separate lipids from the same class according to their fatty acid chain composition and number of double bonds.

However, despite the high-resolution, mass spectrometry-based lipidomics has strengths and limitations. On the identification step, thousands of lipids are now easily detected in short time (8-30 mins) thanks to a faster flow rate, higher column temperature tolerance and step gradient (73,74). Nevertheless, especially in complex matrixes, some bioactive lipids are often missed due to their low abundance, scarce ionization efficiency or instability. Sterols for example are hard to be ionized (and so detected) causing an underestimation. To overcome these issues, suitable modifier (*i.e.*, ammonium formate), ion source type (Electrospray ionization or ESI; Heated electrospray ionization or HESI; Atmospheric pressure chemical ionization or APCI etc.) and ionization modes (collision-induced dissociation or CID; Higher-energy C-trap dissociation or HCD etc.) are important factors to consider. Data-dependent acquisition (DDA) is the classic acquisition technique in untargeted lipidomics for a comprehensive lipidome analysis followed by data-independent approaches (DIA). While DDA offers a high-quality MS2 spectra, fragmenting only precursor ions above a pre-determined threshold but loosing info about those less abundant, DIA is able to provide a complete MS2 fingerprints that, nevertheless, is difficult to destruct.

When the features of interest are known, we can speak about targeted lipidomics. In this case, MS-based multiple reaction monitoring (MRM) and parallel-reaction monitoring (PRM) acquisition modes are the most used. The main advantage of targeted analysis consists in a more successful detection of low abundant species with, as opposite, longer time of acquisition for large dataset.

Nevertheless, the recent AcquireX data acquisition workflow (Thermo Scientific™) for HRMS enhances intelligence-driven mass spectrometry to better determine in real-time which precursors to select for enhanced MS/MS or MS^n (MS2, MS3, and/or MS4) interrogation (depending on the mass spectrometer), how to fragment the precursor to generate structurally diagnostic product ions, and how to connect one experiment to another for effective study evaluation. As main advantages, AquireX combined with DDA enables a significant increasing of compounds characterization by in-depth fragmentation spectra and so of the number of compounds with confident identification.

Worthy to be mentioned it is also the shotgun lipidomics where the crude lipid extract is directly injected (without LC separation) into the ion source at a constant concentration by LC autosampler or a chip-based automated syringe (*i.e.,* Advion TriVersa NanoMate). This approach is very useful in untargeted lipidomics allowing rapid identification of hundreds of lipids. On the other hands, the low abundant or with low ionization efficiency species are often scarcely detected. Dilution of samples are so recommended to reduce the ion suppression and eventual lipids aggregation (75–77).
Based on instrumentation possibilities, sample types and projects aim, during this PhD work I gained experience in HESI-HRMS by Q-Exactive Plus (Thermo Scientific) operating in DDA and PRM mode.

In MS-lipidomics, further than identification challenge mainly related to the instrumental performances and the analytical approach, the quantitation is the second one due to lack of a precise relationship between peak intensity and concentration. Moreover, the lipids standards commercial availability is extremely less than the actual lipids content and diversification supporting the possibility only for a relative quantification. The basic prerequisite of any lipidomics quantitation is the use of at least one no endogenous internal standard (IS) per each lipid subclass to be quantified in a suitable proportion compared to the endogenous lipids content. Starting from short fatty acid chains (*i.e.,* 12:0, 14:0) and odd ones (*i.e.*, 17:0, 17:1), less common in mammals but still sometimes present, recently the deuterated form (in single or mixture) became popular.
Among these, in my experiment I used SPLASH Lipidomix (Avanti Polar) containing a deuterated form for the most representative classes (n=12). Determination of endogenous analytes concentration is usually achieved by IS and protein concentration or cell number.

Another difficulty in lipidomics is the lack of standardized protocols with only few reporting guidelines available for lipidomics data. In fact, multiple analytical methods are applied, making it difficult to compare and reproduce the results. At this regard, “The Lipidomics Standard Initiative”

was recently established to create guidelines for major lipidomics workflows (78). In addition, O'Donnell et al. (2020) (79) provided a set of guidelines for lipidomics submissions aiming to contribute to improving reproducibility and standards in published works.

1.2.2.3 Bioinformatics software in lipidomics

Both untargeted and targeted lipidomics analyses provide very large and complex dataset. In parallel to the recent advances in MS technologies, the bioinformatics developments enable researchers to routinely identify hundreds of unique molecular lipid species (80). Nowadays, there are various bioinformatics software tools and packages that can handle datasets of this size. Nevertheless, in this section I'd describe only those I had have experience with *i.e.*, LipidLynxX, LipidHunter, LipoStar and MSDIAL (81–85).

- LipidLynxX is a free web-based tool that allows conversion of diverse lipid annotations (unmodified and modified lipids) to unified identifiers and perform cross-ID matching to support lipidomics data integration and usability of publicly available lipid identification dataset
- LipidHunter is an open source software easy to use for bottom-up identification of both LC-MS and shotgun data. It works by assembling detected fragments to the matching precursor using pre-defined fragmentation rules and a reference list of lipids building blocks. Applying a bottom-up approach it does not require structural or spectra databases and can be easily adjusted to fit user-specific analytical conditions
- LipoStar is a license-based high-throughput software for LC-MS data obtained from different vendors (Thermo, Sciex etc.) with advanced lipid identification and quantification protocols, statistical tools working with or without preformed databases. The new realising version will be also inter-connected with other software like LipidHunter for unmodified lipids and LPPTiger (86) for those oxidized

- MS-DIAL, a free web-based software, provides a stream pipeline for untargeted metabolomics including lipidomics for both DDA and DIA data and, in the last version, also ion mobility. With a large *in silico* fragmentation spectra database (117 lipids subclasses) it allows a broad identification, coupled to multivariate analyses for relative quantification and network visualization

1.2.2.4 Applications of MS-based lipidomics: some examples

Despite of all the emerging bioinformatics tools, understanding the biological relevance and effect on the function of other biomolecules (*i.e.*, proteins) and so the integration with other omics sciences is still a big challenge in the field of lipidomics (80). More explored, instead, is the impact and relations of lipidome itself in many fields like disease, nutrition, food and pharmaceutical mainly through MS-based accurate measurement of all lipids within a single biological fluid, cells, or tissue (67). Diet can, for example, influence the circulating lipid levels as well as tissue lipidome. About this relation, using LC-MS/MS-based lipidomics, Miller et al. (2019) (87) observed differential lipid accumulation in the brain, white and brown adipose tissue. It was also described the brain-adipose tissue crosstalk by studying the innervation state of adipose tissue in the mice fed by six custom diets. Gong et al., (2020) (88), by untargeted and targeted mass spectrometry-based lipidomics characterized three plasma metabolites (PC (18:1/p-16:0), PC (o-22:3/22:3), and PC (p-18:1/16:1)), as biomarkers in the risk prediction for metabolic syndrome, providing a basis for exploring their relationship with diet for future diagnosis or treatment.

Moreover, specific ceramides and phosphatidylcholines demonstrated good cardiovascular mortality prediction effect in multiple large-scale cohorts, and the synergistic performance with high-sensitivity troponin-T could be more effective in risk classification (89).

Then, Boyd et al. (2021) (90) showed as dietary enrichment with ω-6 PUFAs, highly present in Western-style diet, has a role in the aetiology of peripheral neuropathy acting as risk factor for chronic pain.

1.2.3 MULTI-OMICS: A summary and nowadays examples

In summary, as highlighted before, different omics approaches cover multiple parts of the patho- / physiology of clinical conditions while the analysis of just one single omics provides a partial and biased picture of the underlying biology. The precision medicine, the end goal of omics sciences, is more than just one genetic information. On the contrary it requires a multi-omics vision to be taken in the clinical practise. Despite its added and well-known value in many diseases and pharmaceutical research (91–93), the precision medicine is still in infancy as well as multi-omics studies. In fact, the generation of comprehensive and unbiased data truly based on integrative approach is just began, generally expensive, time-consuming, and highly dependent on the sample's availability and quality but at the same time very promising.

One of the biggest examples is the "Trans-Omics for Precision Medicine" (TOPMED), initiative of the NHLBI (94), started in 2014 that collects omics data for a wide range of study cohorts and based on already existing studies and sample material with the aim of discovery new therapeutical targets and active drugs, biomarkers, pathogenic mechanisms etc.

Starting from the end of 2019, we are facing severe acute respiratory syndrome coronavirus 2 (SARS-CoV-2) pandemic also known as COVID-19. Also this pandemic took advantages from omics data offering at the same time a great support to the personalized treatments. Gordon et al. (2020) (95) for example, studying SARS-CoV-2 protein-protein interaction by proteomic/cheminformatics analysis, was able not only to identify drugs and clinical molecules that might perturb the viral-human interactions, but also to give a mechanistic context to these potentially therapeutic perturbations. This work demonstrated for example as azithromycin, chloramphenicol tigecycline, and linezolid have an off-target effect on mitochondrial ribosome that interact with the SARS-CoV-2 Nsp8 protein, helping to better understand the viral-host complexes by the identification of protein biomarkers at every step of the disease, such as at different time of virus infection which will inform more targeted drug design. Then, Bojkova et al. (2020) (96) provided the proteome profile of SARS-CoV-2-infected host cells

revealing therapy targets. More in detail, it was demonstrated that SARS-CoV-2 reshapes central cellular pathways such as translation, splicing, carbon metabolism, protein homeostasis and nucleic acid metabolism. On the other hand, specific inhibitors targeting these pathways prevented viral replication in cells. Still on COVID-19, Schwarz et al., (2020) (97) reported that a loss of specific immune regulatory eicosanoids and docosanoids lipid mediators and increased pro-inflammatory species (AA-derived products of ALOX5 and cytochrome P450 (CYP)) contribute the progression from moderate to severe disease combining lipidomics, cytokine and chemokine quantitative analysis and single cell RNA sequencing analysis. This study pointed out not only mechanistic insights into the immune regulation in COVID-19 but also a potentially new therapeutic option. Moreover, Janneh et al., (2021) (98) showed as sphingosine profile and acid ceramidase level in serum provides a sensitive and selective serologic biomarker for the early identification of asymptomatic versus symptomatic COVID-19 patients.

To conclude, only with the generation of different omics datasets from the same biological samples will we be able to develop the necessary analytical and annotation tools or pharmaceutical strategies that will help us to extract, understand, and improve biological and clinically relevant information. Indeed, to truly advance in precision medicine, the multi-omics approach is necessary.

REFERENCES

1. Wörheide MA, Krumsiek J, Kastenmüller G, Arnold M. Multi-omics integration in biomedical research – A metabolomics-centric review . 1141, Analytica Chimica Acta. Elsevier B.V.; 2021 . p. 144–62.
2. Olivier M, Asmis R, Hawkins GA, Howard TD, Cox LA. The need for multi-omics biomarker signatures in precision medicine . Int J Mol Sci; 2019, 20
3. Guyer MS, Collins FS. The Human Genome Project and the Future of Medicine. Am J Dis Child . 1993 Nov 1 ;147(11):1145–52.
4. Precision Medicine Initiative | The White House . . https://obamawhitehouse.archives.gov/precision-medicine
5. Piccart-Gebhart MJ, Procter M, Leyland-Jones B, Goldhirsch A, Untch M, Smith I, et al. Trastuzumab after Adjuvant Chemotherapy in HER2-Positive Breast Cancer. N Engl J Med .

2005 Oct 20 ;353(16):1659–72.

6. Morello G, Guarnaccia M, Spampinato AG, Salomone S, D'Agata V, Conforti FL, et al. Integrative multi-omic analysis identifies new drivers and pathways in molecularly distinct subtypes of ALS. Sci Rep . 2019 Jul 10 ;9(1):1–18.

7. O'Donnell VB, Ekroos K, Liebisch G, Wakelam M. Lipidomics: Current state of the art in a fast moving field. Wiley Interdiscip Rev Syst Biol Med . 2020 Jan 1 ;12(1):e1466.

8. Eisfeld AJ, Halfmann PJ, Wendler JP, Kyle JE, Burnum-Johnson KE, Peralta Z, et al. Multi-platform 'Omics Analysis of Human Ebola Virus Disease Pathogenesis. Cell Host Microbe . 2017 Dec 13 ;22(6):817-829.e8.

9. Braconi D, Bernardini G, Millucci L, Santucci A. Foodomics for human health: current status and perspectives . Expert Rev Proteomics; 2018 . 15 p. 153–64.

10. Primiceri E, Chiriacò MS, Rinaldi R, Maruccio G. Cell chips as new tools for cell biology-results, perspectives and opportunities . Lab on a Chip. The Royal Society of Chemistry; 2013 . 13 p. 3789–802.

11. Sporns O, Tononi G, Kötter R. The human connectome: A structural description of the human brain . PLoS Computational Biology. Public Library of Science; 2005 . 1. 0245–51.

12. Raman R, Raguram S, Venkataraman G, Paulson JC, Sasisekharan R. Glycomics: An integrated systems approach to structure-function relationships of glycans . Nat Methods; 2005 . 2 p. 817–24.

13. Riesenfeld CS, Schloss PD, Handelsman J. Metagenomics: Genomic analysis of microbial communities . Annu Rev Genet; 2004 . 38 p. 525–52. /

14. Wenk MR. The emerging field of lipidomics . Nat Rev Drug Discov; 2005 . 4 p. 594–610.

15. Kyle JE, Aimo L, Bridge AJ, Clair G, Fedorova M, Helms JB, et al. Interpreting the lipidome: bioinformatic approaches to embrace the complexity . Metabolomics. Springer; 2021 . 17, p. 1–10.

16. Kopczynski D, Coman C, Zahedi RP, Lorenz K, Sickmann A, Ahrends R. Multi-OMICS: a critical technical perspective on integrative lipidomics approaches . Biochim Biophys Acta Mol Cell Biol Lipids; 2017 . 1862, p, 808–811

17. Misra BB, Langefeld C, Olivier M, Cox LA. Integrated omics: Tools, advances and future approaches . Journal of Molecular Endocrinology. Bioscientifica Ltd; 2019 . 62, p. R21–45.

18. Chella Krishnan K, Kurt Z, Barrere-Cain R, Sabir S, Das A, Floyd R, et al. Integration of Multi-omics Data from Mouse Diversity Panel Highlights Mitochondrial Dysfunction in Non-alcoholic Fatty Liver Disease. Cell Syst . 2018 Jan 24 ;6(1):103-115.e7.

19. Chang P, Niu Y, Zhang X, Zhang J, Wang X, Shen X, et al. Integrative proteomic and metabolomic analysis reveals metabolic phenotype in mice with cardiac-specific deletion of natriuretic peptide receptor a. Mol Cell Proteomics . 2021 ;20.

20. Xu J, Bankov G, Kim M, Wretlind A, Lord J, Green R, et al. Integrated lipidomics and proteomics network analysis highlights lipid and immunity pathways associated with Alzheimer's disease. Transl Neurodegener . 2020 Sep 21 ;9(1):1–15.

21. Alves MA, Lamichhane S, Dickens A, McGlinchey A, Ribeiro HC, Sen P, et al. Systems biology approaches to study lipidomes in health and disease. Biochim Biophys Acta - Mol Cell

Biol Lipids. 2021 Feb 1;1866(2):158857.

22. Linke V, Overmyer KA, Miller IJ, Brademan DR, Hutchins PD, Trujillo EA, et al. A large-scale genome–lipid association map guides lipid identification. Nat Metab . 2020 Sep 21 ;2(10):1149–62.

23. Fiehn O. Metabolomics – the link between genotypes and phenotypes. Plant Mol Biol 2002 ;48(1):155–71.

24. Tayanloo-Beik A, Sarvari M, Payab M, Gilany K, Alavi-Moghadam S, Gholami M, et al. OMICS insights into cancer histology; Metabolomics and proteomics approach . Clinical Biochemistry. Clin Biochem; 2020 . 84, p. 13–20.

25. Di Carlo C, Sousa BC, Manfredi M, Brandi J, Dalla Pozza E, Marengo E, et al. Integrated lipidomics and proteomics reveal cardiolipin alterations, upregulation of HADHA and long chain fatty acids in pancreatic cancer stem cells. Sci Reports 2021 Jun 24 ;11(1):1–13.

26. Yan J, Risacher SL, Shen L, Saykin AJ. Network approaches to systems biology analysis of complex disease: Integrative methods for multi-omics data. Brief Bioinform . 2017 Nov 27 ;19(6):1370–81.

27. Li S. Computational Methods and Data Analysis for Metabolomics In Methods in Molecular Biology . Springer US. New York, NY,2020 . (Methods in Molecular Biology; 2104).

28. Hood L, Rowen L. The human genome project: Big science transforms biology and medicine. Genome Med . 2013 Sep 13 ;5(9):1–8.

29. Kanehisa M, Goto S. KEGG: Kyoto Encyclopedia of Genes and Genomes . Nucleic Acids Research. Oxford Academic; 2000 . 28, p. 27–30.

30. Brunk E, Sahoo S, Zielinski DC, Altunkaya A, Dräger A, Mih N, et al. Recon3D enables a three-dimensional view of gene variation in human metabolism. Nat Biotechnol 2018;36(3):272–81.

31. Fabregat A, Sidiropoulos K, Viteri G, Forner O, Marin-Garcia P, Arnau V, et al. Reactome pathway analysis: A high-performance in-memory approach. BMC Bioinformatics . 2017 Mar 2 ;18(1):1–9.

32. Martens M, Ammar A, Riutta A, Waagmeester A, Slenter DN, Hanspers K, et al. WikiPathways: connecting communities. Nucleic Acids Res . 2021 Jan 8 ;49(D1):D613–21.

33. Kutmon M, Riutta A, Nunes N, Hanspers K, Willighagen EL, Bohler A, et al. WikiPathways: Capturing the full diversity of pathway knowledge. Nucleic Acids Res . 2016 ;44(D1):D488–94.

34. Slenter DN, Kutmon M, Hanspers K, Riutta A, Windsor J, Nunes N, et al.WikiPathways: a multifaceted pathway database bridging metabolomics to other omics research. Nucleic Acids Res. 2018 Jan 4;46(D1):D661-D667

35. Szklarczyk D, Gable AL, Nastou KC, Lyon D, Kirsch R, Pyysalo S, et al. The STRING database in 2021: Customizable protein-protein networks, and functional characterization of user-uploaded gene/measurement sets. Nucleic Acids Res . 2021 Jan 8 ;49(D1):D605–12.

36. LIPID MAPS Lipidomics gateway . Lipid Maps. 2019 . https://www.lipidmaps.org/data/structure/

37. Hastings J, Owen G, Dekker A, Ennis M, Kale N, Muthukrishnan V, et al. ChEBI in 2016:

Improved services and an expanding collection of metabolites. Nucleic Acids Res . 2016 ;44(D1):D1214–9.

38. Aimo L, Liechti R, Hyka-Nouspikel N, Niknejad A, Gleizes A, Götz L, et al. The SwissLipids knowledgebase for lipid biology. Bioinformatics . 2015 Feb 6 ;31(17):2860–6.

39. The integrative human microbiome project: Dynamic analysis of microbiome-host omics profiles during periods of human health and disease corresponding author . Cell Host Microbe; 2014 . 16, p. 276–89.

40. Tomczak K, Czerwińska P, Wiznerowicz M. The Cancer Genome Atlas (TCGA): An immeasurable source of knowledge . Wspolczesna Onkologia. Contemp Oncol (Pozn); 1A, 2015 . p. A68–77.

41. Shoemaker RH. The NCI60 human tumour cell line anticancer drug screen. Nat Rev Cancer; 2006 . p. 813–23.

42. Data Repository Guidance | Scientific Data . . https://www.nature.com/sdata/policies/repositories

43. Perez-Riverol Y, Bai M, Da Veiga Leprevost F, Squizzato S, Park YM, Haug K, et al. Discovering and linking public omics data sets using the Omics Discovery Index ., Nat Biotechnol; 2017 . 35 p. 406–9.

44. Halder A, Verma A, Biswas D, Srivastava S. Recent advances in mass-spectrometry based proteomics software, tools and databases. Drug Discovery Today: Technologies. Elsevier; 2021.

45. Tyers M, Mann M. From genomics to proteomics . Nature 2003 - 422 p. 193–7.

46. Wilkins MR, Sanchez JC, Gooley AA, Appel RD, Humphery-Smith I, Hochstrasser DF, et al. Progress with proteome projects: Why all proteins expressed by a genome should be identified and how to do it. Biotechnol Genet Eng Rev . 1996 Dec 1 ;13(1):19–50.

47. Ross PL, Huang YN, Marchese JN, Williamson B, Parker K, Hattan S, et al. Multiplexed protein quantitation in Saccharomyces cerevisiae using amine-reactive isobaric tagging reagents. Mol Cell Proteomics . 2004 ;3(12):1154–69.

48. Ong SE, Mann M. A practical recipe for stable isotope labeling by amino acids in cell culture (SILAC). Nat Protoc . 2007 Jan ;1(6):2650–60.

49. Thompson A, Schäfer J, Kuhn K, Kienle S, Schwarz J, Schmidt G, et al. Tandem mass tags: A novel quantification strategy for comparative analysis of complex protein mixtures by MS/MS. Anal Chem . 2003 Apr 15 ;75(8):1895–904.

50. Zhao L, Cong X, Zhai L, Hu H, Xu JY, Zhao W, et al. Comparative evaluation of label-free quantification strategies. J Proteomics . 2020 Mar 20 ;215.

51. Sajic T, Liu Y, Aebersold R. Using data-independent, high-resolution mass spectrometry in protein biomarker research: Perspectives and clinical applications . Proteomics Clin Appl; 2015 . 9, p. 307–21.

52. Cox J, Neuhauser N, Michalski A, Scheltema RA, Olsen J V., Mann M. Andromeda: A peptide search engine integrated into the MaxQuant environment. J Proteome Res . 2011 Apr 1 ;10(4):1794–805.

53. Protein Identification & Quantification Software, PTM & Variant Search

https://www.bioinfor.com/peaks-studio/

54. Access Mascot for free | Protein identification software for mass spec data . . https://www.matrixscience.com/search_form_select.html

55. Solntsev SK, Shortreed MR, Frey BL, Smith LM. Enhanced Global Post-translational Modification Discovery with MetaMorpheus. J Proteome Res . 2018 May 4 ;17(5):1844–51.

56. Zhang B, Kä L, Zubarev RA. DeMix-Q: Quantification-centered dataprocessing workflow. Mol Cell Proteomics . 2016 Apr 1 ;15(4):1467–78.

57. Lim MY, Paulo JA, Gygi SP. Evaluating False Transfer Rates from the Match-between-Runs Algorithm with a Two-Proteome Model. J Proteome Res . 2019 Nov 1 ;18(11):4020–6.

58. August O, Pharmacokinetic B. Program of physiologically-based pharmacokinetic and pharmacodynamic modeling (PBPK Program) . 2018 . p. 2012–4. https://www.fda.gov/about-fda/center-drug-evaluation-and-research-cder/program-physiologically-based-pharmacokinetic-and-pharmacodynamic-modeling-pbpk-program

59. Couto N, Al-Majdoub ZM, Achour B, Wright PC, Rostami-Hodjegan A, Barber J. Quantification of Proteins Involved in Drug Metabolism and Disposition in the Human Liver Using Label-Free Global Proteomics. Mol Pharm . 2019 ;16(2):632–47.

60. Tierney C, Bazou D, Majumder MM, Anttila P, Silvennoinen R, Heckman CA, et al. Next generation proteomics with drug sensitivity screening identifies sub-clones informing therapeutic and drug development strategies for multiple myeloma patients. Sci Rep . 2021 ;11(1):1–15.

61. Dyring-Andersen B, Løvendorf MB, Coscia F, Santos A, Møller LBP, Colaço AR, et al. Spatially and cell-type resolved quantitative proteomic atlas of healthy human skin. Nat Commun 2020;11(1):1–14.

62. Shevchenko A, Simons K. Lipidomics: Coming to grips with lipid diversity . Nat Rev Mol Cell Biol; 2010 . 11, p. 593–8.

63. Han X. Lipidomics for studying metabolism . Nature Reviews Endocrinology. 2016 . 12, p. 668–79.

64. Holčapek M, Liebisch G, Ekroos K. Lipidomic Analysis. Anal Chem . 2018 Apr 3 ;90(7):4249–57.

65. Fahy E, Subramaniam S, Brown HA, Glass CK, Merrill AH, Murphy RC, et al. A comprehensive classification system for lipids. J Lipid Res . 2005 ;46(5):839–61.

66. Antonny B. Mechanisms of membrane curvature sensing. Annu Rev Biochem . 2011 Jul 7 ;80:101–23.

67. Xu T, Hu C, Xuan Q, Xu G. Recent advances in analytical strategies for mass spectrometry-based lipidomics. Anal Chim Acta. 2020;1137:156–69.

68. Matyash V, Liebisch G, Kurzchalia T V., Shevchenko A, Schwudke D. Lipid extraction by methyl-terf-butyl ether for high-throughput lipidomics. In: Journal of Lipid Research . J Lipid Res; 2008 . p. 1137–46.

69. Folch J, Lees M SSG. A simple method for the isolation and purification of total lipides from animal tissues. J Biol Chem. 1957;497–509.

70. Bligh EG, Dyer WJ. A rapid method of total lipid extraction and purification. Can J Biochem

Physiol . 1959 ;37(8):911–7.

71. Züllig T, Köfeler HC. High Resolution Mass Spectrometry in Lipidomics . Mass Spectrometry Reviews. Mass Spectrom Rev; 2021 . 40, p. 162–76.

72. Züllig T, Trötzmüller M, Köfeler HC. Lipidomics from sample preparation to data analysis: a primer. Anal Bioanal Chem 2019;412(10):2191–209.

73. Lagerborg KA, Watrous JD, Cheng S, Jain M. High-throughput measure of bioactive lipids using non-targeted mass spectrometry. Methods Mol Biol; 2019 . p. 17–35.

74. Xuan Q, Zheng F, Yu D, Ouyang Y, Zhao X, Hu C, et al. Rapid lipidomic profiling based on ultra-high performance liquid chromatography–mass spectrometry and its application in diabetic retinopathy. Anal Bioanal Chem . 2020 Jun 1 ;412(15):3585–94.

75. Han X, Gross RW. Global analyses of cellular lipidomes directly from crude extracts of biological samples by ESI mass spectrometry: A bridge to lipidomics . J Lipid Res; 2003 . 44, p. 1071–9.

76. Yang K, Han X. Accurate quantification of lipid species by electrospray ionization mass spectrometry - Meets a key challenge in lipidomics . MDPI; 2011 . 1, p. 21–40

77. Southam AD, Weber RJM, Engel J, Jones MR, Viant MR. A complete workflow for high-resolution spectral-stitching nanoelectrospray direct-infusion mass-spectrometry-based metabolomics and lipidomics. Nat Protoc . 2017 Feb 1 ;12(2):255–73.

78. Liebisch G, Ahrends R, Arita M, Arita M, Bowden JA, Ejsing CS, et al. Lipidomics needs more standardization . Nature Metabolism; 2019 1,. p. 745–7.

79. Odonnell VB, Fitzgerald GA, Murphy RC, Liebisch G, Dennis EA, Quehenberger O, et al. Steps Toward Minimal Reporting Standards for Lipidomics Mass Spectrometry in Biomedical Research Publications . Circulation: Genomic and Precision Medicine. Lippincott Williams & Wilkins Hagerstown, MD; 2020 . p. 737–41.

80. Kyle JE, Aimo L, Bridge AJ, Clair G, Fedorova M, Helms JB, et al. Interpreting the lipidome: bioinformatic approaches to embrace the complexity . Metabolomics; 2021 . 17

81. Ni Z, Angelidou G, Lange M, Hoffmann R, Fedorova M. LipidHunter Identifies Phospholipids by High-Throughput Processing of LC-MS and Shotgun Lipidomics Datasets. Anal Chem . 2017 Sep 5 ;89(17):8800–7.

82. Ni Z, Fedorova M. LipidLynxX: A data transfer hub to support integration of large scale lipidomics datasets. bioRxiv . 2020 Apr 10 ;2020.04.09.033894.

83. Tsugawa H, Cajka T, Kind T, Ma Y, Higgins B, Ikeda K, et al. MS-DIAL: Data-independent MS/MS deconvolution for comprehensive metabolome analysis. Nat Methods . 2015 May 28;12(6):523–6.

84. Tsugawa H, Ikeda K, Takahashi M, Satoh A, Mori Y, Uchino H, et al. A lipidome atlas in MS-DIAL 4. Nat Biotechnol . 2020 Jun 15;38(10):1159–63.

85. Goracci L, Tortorella S, Tiberi P, Pellegrino RM, Di Veroli A, Valeri A, et al. Lipostar, a Comprehensive Platform-Neutral Cheminformatics Tool for Lipidomics. Anal Chem . 2017 Jun 6;89(11):6257–64.

86. Ni Z, Angelidou G, Hoffmann R, Fedorova M. LPPtiger software for lipidome-specific prediction and identification of oxidized phospholipids from LC-MS datasets. Sci Rep . 2017

Nov 9 ;7(1):1–14.

87. Miller JL, Blaszkiewicz M, Beaton C, Johnson CP, Waible S, Dubois AL, et al. A peroxidized omega-3-enriched polyunsaturated diet leads to adipose and metabolic dysfunction. J Nutr Biochem. 2019;64:50–60.

88. Gong L li, Yang S, Zhang W, Han F fei, Lv Y li, Xuan L ling, et al. Discovery of metabolite profiles of metabolic syndrome using untargeted and targeted LC–MS based lipidomics approach. J Pharm Biomed Anal. 2020;177:112848.

89. Hilvo M, Meikle PJ, Pedersen ER, Tell GS, Dhar I, Brenner H, et al. Development and validation of a ceramide- And phospholipid-based cardiovascular risk estimation score for coronary artery disease patients. Eur Heart J . 2020 Jan 14 ;41(3):371–80.

90. Boyd JT, LoCoco PM, Furr AR, Bendele MR, Tram M, Li Q, et al. Elevated dietary ω-6 polyunsaturated fatty acids induce reversible peripheral nerve dysfunction that exacerbates comorbid pain conditions. Nat Metab . 2021;3(6):762–73.

91. Sun Y V., Hu YJ. Integrative Analysis of Multi-omics Data for Discovery and Functional Studies of Complex Human Diseases. Adv Genet . 2016;93:147–90.

92. Hasin Y, Seldin M, Lusis A. Multi-omics approaches to disease . Genome Biology. BioMed Central; 2017 . 18, p. 1–15.

93. Turanli B, Karagoz K, Gulfidan G, Sinha R, Mardinoglu A, Arga KY. A Network-Based Cancer Drug Discovery: From Integrated Multi-Omics Approaches to Precision Medicine. Curr Pharm Des . 2019 Jan 15 ;24(32):3778–90.

94. Trans-Omics for Precision Medicine (TOPMed) Program | NHLBI, NIH . . https://www.nhlbi.nih.gov/science/trans-omics-precision-medicine-topmed-program

95. Gordon DE, Jang GM, Bouhaddou M, Xu J, Obernier K, O'Meara MJ, et al. A SARS-CoV-2-human protein-protein interaction map reveals drug targets and potential drug-repurposing. bioRxiv . 2020 Mar 27;19:2020.03.22.002386.

96. Bojkova D, Klann K, Koch B, Widera M, Krause D, Ciesek S, et al. Proteomics of SARS-CoV-2-infected host cells reveals therapy targets. Nature . 2020 May 14 ;583(7816):469–72.

97. Schwarz B, Sharma L, Roberts L, Peng X, Bermejo S, Leighton I, et al. Severe SARS-CoV-2 infection in humans is defined by a shift in the serum lipidome resulting in dysregulation of eicosanoid immune mediators. medRxiv Prepr Serv Heal Sci . 2020.

98. Janneh AH, Kassir MF, Dwyer CJ, Chakraborty P, Pierce JS, Flume PA, et al. Alterations of lipid metabolism provide serologic biomarkers for the detection of asymptomatic versus symptomatic COVID-19 patients. Sci Rep . 2021 Jul 9 ;11(1):1–10.

II

Aim of the work

The aim of my research has been to integrate quantitative proteomics methodologies with lipidomics analysis for a more complete, multi-omics vision of intra- and extra-cellular processes in several biological conditions (both physiological and pathological ones, environmental and chemical exposure). This integrated approach could contribute to the field of precision medicine.

During the first part of my PhD, I was focused on learning and deepening the concepts and techniques mainly related to label-free proteomics as well as to the world of cell cultures, all important aspects that I then applied to my projects. Prof. Carini's lab indeed has a long experience in the proteomics field covering different topics from oxidative stress to drug metabolism in cells and tissues.

My attention was on:

- Evaluation of molecular effects of low-molecular-weight hyaluronic acid in human dermal fibroblasts through advanced quantitative proteomics
- Effects' study of carnosine on nude mice skin to prevent UV-A damage

Then, to create my wealth of knowledge in lipidomics I spent seven months at the lab of Prof. Dr. Ralf Hoffman under Dr. Maria Fedorova's supervision (AG Bioanalytik Institut für Bioanalytische Chemie Fakultät für Chemie und Mineralogie, Universität Leipzig) since their consolidate experience in this field of research. Thanks to her brilliant skills and support I have had the opportunity to learn the fundamentals of lipidomics from the sample preparation to instrumental and data analyses and biological interpretation working with different matrixes and large sample size.

My work was mainly related to:

- Optimization of a reliable, reproducible, and fast methodology based on high resolution MS for the characterization and relative quantification of fatty acid esters of hydroxy fatty acids (FAHFAs) in human white adipose tissue of obese patients

Once back, I applied by my own what I learnt also integrating the previous proteomics results to the new lipidomics ones. In particular, I worked on:

- Semi-quantitative lipidomics evaluation of molecular effects of low-molecular-weight hyaluronic acid in human dermal fibroblasts
- Integration of proteomics and lipidomics data related to the molecular effects of low-molecular-weight hyaluronic acid in human dermal fibroblasts
- Analysis of lipidome and proteome profile changing induced by γ-Oryzanol prevention treatment in obese-induced rats

III

Proteomics

Study 1

Evaluation of molecular effects of low-molecular-weight hyaluronic acid in human dermal fibroblasts through advanced quantitative proteomics

(doi:10.1016/j.jpba.2020.113199)

ABSTRACT

Hyaluronic acid (HA) is physiologically synthesized by several human cell types but it is also a widespread ingredient of commercial products, from pharmaceuticals to cosmetics. Despite its extended use, the precise intra- and extra-cellular effects of HA at low-molecular-weight (LWM-HA) are currently unclear. At this regard, the aim of this study was to deepen identification and quantification proteome's changes in normal human dermal fibroblasts after 24 hours treatment with 0.125, 0.25 and 0.50 % LMW-HA (20-50 kDa) respectively, vs controls. To do this, a label-free quantitative proteomic approach based on high-resolution mass spectrometry was used. Overall, 2328 proteins were identified of which 39 significantly altered by 0.125 %, 149 by 0.25 % and 496 by 0.50 % LMW-HA. Protein networking results indicated that the biological effects involve the enhancement of intracellular activity at all concentrations, as well as the extracellular matrix reorganization, proteoglycans, and collagen biosynthesis. Moreover, the cell's wellness was confirmed, although mild inflammatory and immune responses were induced at the highest concentration. The more complete comprehension of intra- and extra-cellular effects of LMW-HA here provided by an advanced analytical approach and protein networking will be useful to further exploit its features and improve current formulations.

1. INTRODUCTION

The extracellular environment, also referred as extracellular matrix (ECM), is principally formed by glycosaminoglycans involved in several biological functions mainly related to their molecular structure (1). Among these, hyaluronic acid (HA), an unbranched glycosaminoglycan formed by repetitive disaccharide units of N-acetyl-D-glucosamine and D-glucuronic acid linked through alternating ß-1,3- and ß-1,4-glycosidic bonds, is synthesized in humans by different hyaluronan synthase isoforms (HAS1, HAS2 and HAS3). Hyaluronidases (HYALs) and reactive oxygen species (ROS) are instead responsible for around 30% of its degradation. The remaining is systemically metabolized by endothelial cells of the lymphatic vessel and liver (2). Because of the diverse degrees of physiological enzymatically and non-enzymatically polymerization, HA is usually classified as low-molecular-weight (LMW-HA) when $\leq 10^6$ Da, or as high-molecular-weight (HMW-HA) when $> 10^6$ Da. Nevertheless, a precise cutoff is not defined.

About biological functions, endogenous HMW-HA demonstrated a positive role in the control of tissue hydration, inflammatory and immune processes, tissue repair, and endothelial cellular growth (3, 4, 5). On the other hand, endogenous LWM-HA may induce pro-inflammatory activity stimulating cytokines, chemokines and growth factors as well as the ECM remodeling, uncontrolled cellular growth, and angiogenesis during wound healing (3, 6). Since last century, HA has been attracting the attention of many industrial fields, from pharmaceutical to cosmetic ones due to its widespread distribution in humans and its diversified physiochemical proprieties including biocompatibility, biodegradability, mucoadhesivity, viscoelasticity and hygroscopicity (7). In cosmetics HA is widely used as anti-ageing especially for its ability to induce tissue boost, skin hydration and collagen stimulation (8). As an example, Pavicic et al. (9) demonstrated that HMW-HA improves only hydration in aged skin probably because of its low skin penetration, while LMW-HA (50-800 kDa) shows better results on skin elasticity. Moreover, exogenous LWM-HA has showed to cross the *corneum stratum* (10, 11) and the epidermis (12) more easily than the HMW-HA, supporting its

currently increasing use in the topical formulations, although the detailed intra- and extra-cellular changes induced by exogenous LMW-HA are poorly described.

The aim of this work is to quantitatively describe the proteome alterations induced by 20-50 kDa LMW-HA in normal human dermal fibroblasts by advanced mass spectrometric technique and network analysis. Indeed, the current development of 'omics sciences (genomics, proteomics, metabolomics etc.) supported by performing analytical tools is showing a new molecular panorama due to a huge amount of data available. To own our knowledge, this is the first proteomic study applied to exogenous 20-50 kDa LWM-HA to gain a deeper insight into its molecular effects at fibroblast level. Therefore, the results here obtained will allow reaching a more complete comprehension about biological processes influenced by 20-50 kDa LWM-HA, useful information for the improvement also of existing cosmetics formulations and for the optimization of personalized treatments.

2. MATERIAL AND METHODS

2.1 Chemicals

Primary cell line (NHDF-Ad 28887), glutamine and penicillin-streptomycin antibiotic were purchased by Lonza Bioscence (Basel, Switzerland); Dulbecco's Modified Eagle's Medium (DMEM), trypsin-EDTA (0.5% 10×), sodium pyruvate, were purchased by Gibco® (Thermo Fisher Scientific, Bremen, Germany); Renovyhal 20–50 kDa here referred as low-molecular hyaluronic acid (LMW-HA) was purchased by Soliance (Pomacle, France); Fetal bovine serum (FBS) and phosphate buffered saline (PBS) were purchased by Euroclone® (Milano, Italia); 2,5-diphenyl-2H-tetrazolium bromide (MTT) reduction assay, Bradford kit reagents, protease inhibitor cocktail, DL-dithiothreitol (DTT), iodocetamide (IAA), ammonium formate (NH_4HCO_2) MS grade, acetonitrile (MeCN), and formic acid (FA) (all UHPLC/MS-CC/SFC grade) were brought by Sigma-Aldrich (Taufkirchen, Germany); Real Time Glo-MT kit assay was purchased by Promega (Milano, Italy); lysis buffer

reagents (urea, TrisHCl, sodium chloride) were purchased by BioRad Laboratories Inc. (Segrate, Milan, Italy); Trypsin Sequencing Grade was purchased by Roche (Monza, Italy); C-18 resin ZipTip were purchased by Merck (Millipore, Milan, Italy). Water was purified in-house (resistance > 18 MΩ cm−1; total organic content < 10 ppb) with a Milli-Q H2O purification system (Millipore, Bedford, MA, USA).

2.2 Cell culture

Adult normal human dermal fibroblasts at 7th passage, were cultured as a monolayer in Dulbecco's Modified Eagle's Medium containing 10% FBS, 1% glutamine and 1% penicillin-streptomycin antibiotic, at 37 °C in a humidified atmosphere of 5% CO_2**.**

2.3 Cell viability assays

The viability of cells was evaluated using MTT reduction assay and Real Time Glo-MT kit assay. Briefly, 9x10^3 NHDF-Ad cells were seeded on a 96-well plate overnight. Different concentrations of LMW-HA (0.125 %, 0.25 %, 0.50 %, 1.00 % and 2.50 % w/v, respectively) dissolved in DMEM were added to the cells, in biological duplicate, for 24 hours. As control, untreated cells were incubated as well in biological duplicate. For the viability cells' assessment, the MTT and RealTime Glo-MT assays were performed following the standard protocols. All statistical analyses were done by the GraphPad software (v 6.0).

2.4 Cell treatment

Three experimental conditions were planned considering the results of cell viability assays and the usual concentrations in the cosmetic products. NHDF-Ad (7th passage) seeded in T75 flasks were treated in biological duplicate with 0.125 %, 0.25 % and 0.5 % LMW-HA (w/v) respectively for 24 hours considering the physiological turn-over. Two untreated flasks were used as control.

2.5 Sample preparation

Once treated, all cells were trypsinized, counted using the automatic counter TC20™ (Bio-Rad®), and pelleted by two cycles of centrifuge at 400 g, room temperature for 5 min. The whole protein was extracted by using a buffer composed by 8 M urea in 50 mM Tris-HCl, 30 mM NaCl at 8.5 pH and 1 % of protease inhibitor cocktail followed by centrifugation at 14000 x g, 4° C for 30 min. The amount of proteins was quantified by the Bradford Reagent following the standard procedure. 20 µg of proteins in 50 mM NH_4HCO_3 were reduced with 5 mM DL-dithiothreitol (DTT) for 30 min at 52 °C, then centrifuged at 500 rpm and alkylated with 15 mM iodoacetamide for 20 min in the dark at room temperature. The trypsin digestion was performed in 1:20 enzyme: protein ratio (w/w) overnight at 37 °C.

2.6 High-resolution mass spectrometry analysis (nLC-HRMS)

To increase the quality of instrumental analysis, the digested samples were further purified and concentrated by 0.2 µL C-18 resin ZipTip.Tryptic peptides were analyzed using a Dionex Ultimate 3000 nano-LC system (Sunnyvale CA, USA) connected to Orbitrap Fusion™ Tribrid™ Mass Spectrometer (Thermo Scientific, Bremen, Germany) equipped with a nano-electrospray ion source (nESI). Peptide mixtures were pre-concentrated onto an Acclaim PepMap 100 - 100 µm × 2 cm C18 and separated on EASY-Spray column, 25 cm × 75 µm ID packed with Thermo Scientific Acclaim PepMap RSLC C18, 3 µm, 100 Å. The temperature was set to 35 °C and the flow rate was 300 nL min^{-1}. Mobile phases were the following: 0.1% formic acid (FA) in water (solvent A); 0.1% FA in water/acetonitrile with 2/8 ratio (solvent B). The elution gradient was from 96% buffer A to 40% buffer B for 110 min. MS spectra were collected over an *m/z* range of 375-1500 Da at 120,000 resolutions, operating in data dependent (DDA) scan mode, cycle time 3 sec between master scans. Higher-energy collision dissociation (HCD) was performed with collision energy set at 35 eV in positive polarity. Each sample was analyzed in three technical replicates.

2.7 Data analysis

The instrumental raw files were analysed with MaxQuant software v1.6.6.0 (13) set on *Uniprot_Homosapiens* database against the Andromeda search engine. The quantification of peptides and related proteins for each control and treated sample in biological duplicate and technical triplicates was based on the label-free quantitative (LFQ) intensities. Trypsin as the digestive enzyme, variable modification of carbamidomethylation of cysteine (+57.021 Da), fixed modification of methionine oxidation (+15.995 Da), N-terminal acetylation (+42.011 Da) and LFQ minimum ratio count to 2 were set as further parameters. The interpretation and visualization of results from MaxQuant software were performed by a two-sample t-test using Perseus (v1.6.1.3, Max Planck Institute of Biochemistry, Germany). The proteins variation (log2 fold change) was evaluated 0.125 % LMW-HA vs control, 0.25 % LMW-HA vs control and 0.50 % LMW-HA vs control respectively. Statistical parameters ($p < 0.05$; $q < 0.05$, q= FDR adjusted p-value) were set to identify the differentially expressed proteins between samples. The proteins were selected with a minimum of two peptides. Variability of biological replicates were measured using the scatter plot with Pearson correlation coefficient values of the LFQ intensities. The network protein analyses related to significantly altered proteins were carried out through Reactome, STRING (v 11.0) and Ingenuity Pathways Analysis (last release; Qiagen) based on Gene Ontology database.

3. RESULTS

Considering the widespread use of HA in topical formulations and the lack of deep knowledge about intra- and extra-cellular biological effects of LMW-HA, the goal of this study was to quantify the proteome's changes induced by different concentrations of LMW-HA in normal human dermal fibroblasts. In Figure 1 the general workflow.

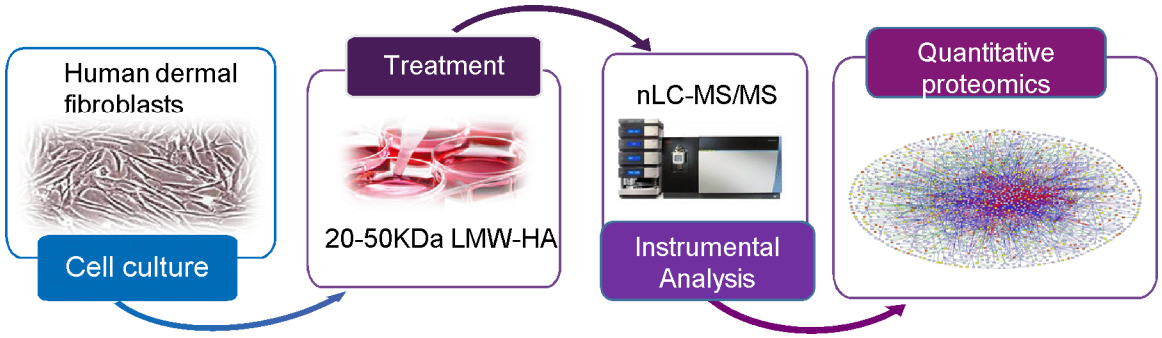

Figure 1. Experimental workflow

3.1 Treatments with LMW-HA: identification and differential proteomic analysis

Based on the MTT and RealTime-Glo results (Figure 2) and the plausible exposition in the real setting, 0.125, 0.25 and 0.50 % LMW-HA were selected for the treatments. Automatic count of cells supported the cell viability results.

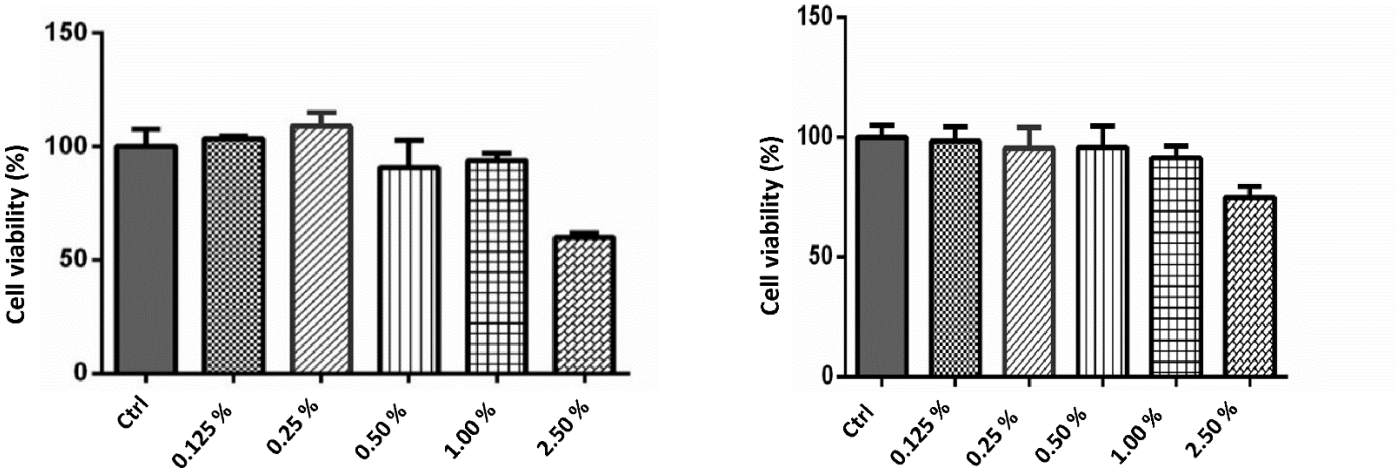

Figure 2. Cell viability assays. MTT (right) and RealTime Glo (left) with LWM-HA 0.125 %, 0.25 %, 0.50 %, 1.00 % and 2.50 % vs control.

After the treatment in biological duplicate with 0.125, 0.25 and 0.50 % LWM-HA respectively, applying MS-based label-free quantitative (LFQ) proteomic analysis, a total of 2328 proteins were identified and quantified. The quality and reproducibility of biological and technical replicates were confirmed by multi-scatter plot (Pearson coefficient values ≥ 0.98). As consequence of 0.125 %

LWM-HA, 39 proteins resulted significantly altered (25 up-regulated, 14 down-regulated) (Figure 3a), 149 by 0.25 % LWM-HA (72 up-regulated, 77 down-regulated) (Figure 3b) and 496 by 0.50 % LWM-HA (334 up-regulated, 172 down-regulated) (Figure 3c). Moreover, some of these were affected by all LWM-HA concentrations tested or by at least two out of three concentrations (examples in Table 1).

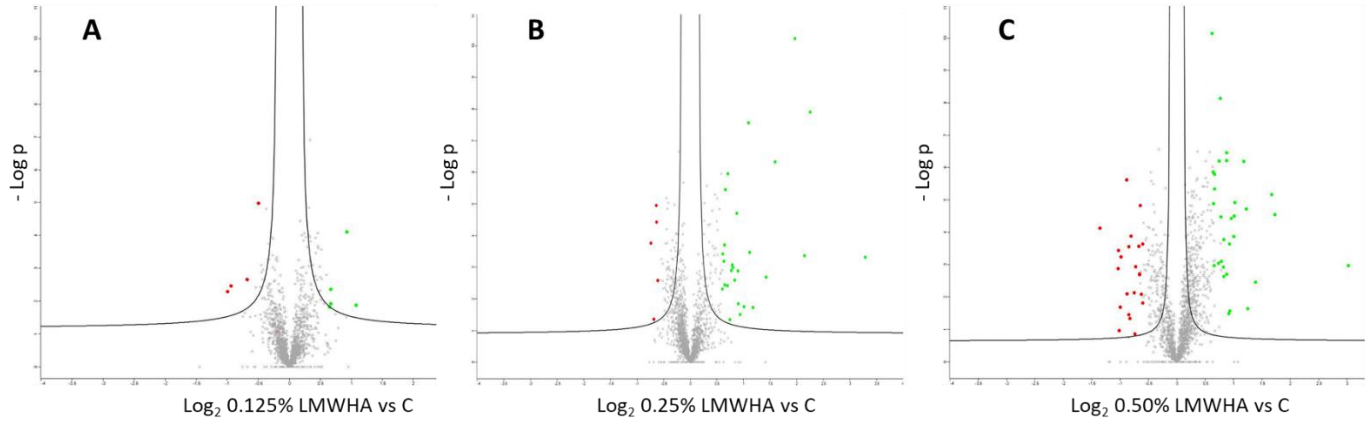

Figure 3. Distribution of differentially regulated proteins with a) LWM-HA 0.125 %, b) LWM-HA 0.25 % and c) LWM-HA 0.50 %. Green dots indicate up-regulation (log2 fold change ≥ 0.6), red dots represent down-regulation (log2 fold change ≤ -0.6); Log2 fold change on x-axis against -log p-value on y-axis.

3.2 Protein Network Analyses

After the identification and quantification of differentially regulated proteins, we applied protein network analyses using String, Reactome and Ingenuity Pathways Analysis (IPA) based on Gene Ontology (GO) terms to describe functional protein modules and pathways.

3.2.1 Proteome's changes induced by 0.125 % LWM-HA

This study demonstrated limited proteome's changes related to 0.125 % LWM-HA. Nevertheless, despite the low number of significantly altered proteins compared to controls (n=39), we mainly showed a noticeable increase of intracellular reorganization and mitochondrial activity (14). In

details, we found a pronounced overexpression of organelle (FDR= 0.023) and mitochondrial matrix (FDR = 3.2 e-04) reorganization. The low number of down-regulated proteins (n=14) did not allow us the identification of relevant nodes.

3.2.2 Proteome's changes induced by 0.25 % LWM-HA

By increasing the concentration of LWM-HA from 0.125 to 0.25 % a more robust biological effect was observed with the significant alteration of 149 proteins involved both in intra- and extra-cellular environment (examples in Table 1).

Regarding the intracellular activity, we observed an up-regulation of several pathways such as chromosome organization (FDR = 0.004) and oxidation-reduction process (FDR = 0.04) (Figure 4) but also cellular component organization or biogenesis involving 40 genes (FDR = 1.8 e-04), and protein processing (FDR = 0.04). More interesting were the LWM-HA effects outside the cell by raising the expression of proteins involved in collagen binding (FDR = 0.02) and extracellular matrix organization (FDR = 0.004) (Figure 4), elastic fibers formation (FDR = 0.03) or syndecans interactions (FDR = 0.01). ECM proteoglycans biosynthesis was also enriched (FDR = 0.01) especially for dermatan sulfate (HSPG2; fold change = 9.74) and chondroitin sulfate (CSPG4; fold change = 1.73). Conversely, a reduced expression of several immune pathways such as IL-12 signaling (FDR = 9.92 e-07) and neutrophil degranulation (FDR= 0.12) was observed, suggesting a great cells' wellness when exposed to the medium concentration (0.25 % LWM-HA).

3.2.3 Proteome's changes induced by 0.50 % LWM-HA

The main intra- and extracellular impact was shown in cells treated with 0.50 % LWM-HA. We found in fact the highest number of significantly altered proteins, 496 vs 149 and 36 with 0.125 and 0.25 % LWM-HA, respectively, and related pathways. The intracellular effects were mainly supported by an increasing of cells' proliferation by translation process (FDR = 6.02 e-11), lipid metabolism (FDR = 7.75 e-06) and immune process (FDR = 4.4 e-04) (Figure 4). More in details, cells growth was

demonstrated by an enhancement of VEGFA-VEGFR2 complex (p value= 3.35 e-03), RNA expression (p value = 6.72 e-05) and fibroblasts proliferation pathway (p value = 7.50 e-03) (Figure 5, up). Furthermore, mitochondrial activity by acid citric cycle II (p value = 1.89 e-04), EIF2 pathway (p value= 9.34 e-05) and Wnt signaling (FDR = 0.07) were also increased and, in line with the previous concentration (0.25%) we observed a pronounced extracellular activity by an over-expression of HSPG2 (fold change = 8.15), FN1 (fold change = 3.18) and CPSG4 (fold change = 1.77) suggesting a high ECM reorganization mainly based on proteoglycans biosynthesis (examples in Table 1). Nevertheless, 0.50 % LWM-HA seemed to provide an increasing immune response by an up-regulation of IL-12 family signaling (FDR= 1.04 e-05) (Figure 4) as well as IL-2 (p value = 3.21 e-03; z score = 1.34), IL-4 (p value = 6.91 e-03; z score = 1.63) and TNF signaling (p value = 2.73 e-01; z score = 1.78) (Figure 5 down). In addition, also IL-1 family signaling (FDR = 3.72 e-04), NF-kB pathway (FDR = 2.15 e-05), and neutrophil degranulation (FDR = 0.007) showed an increasing vs control.

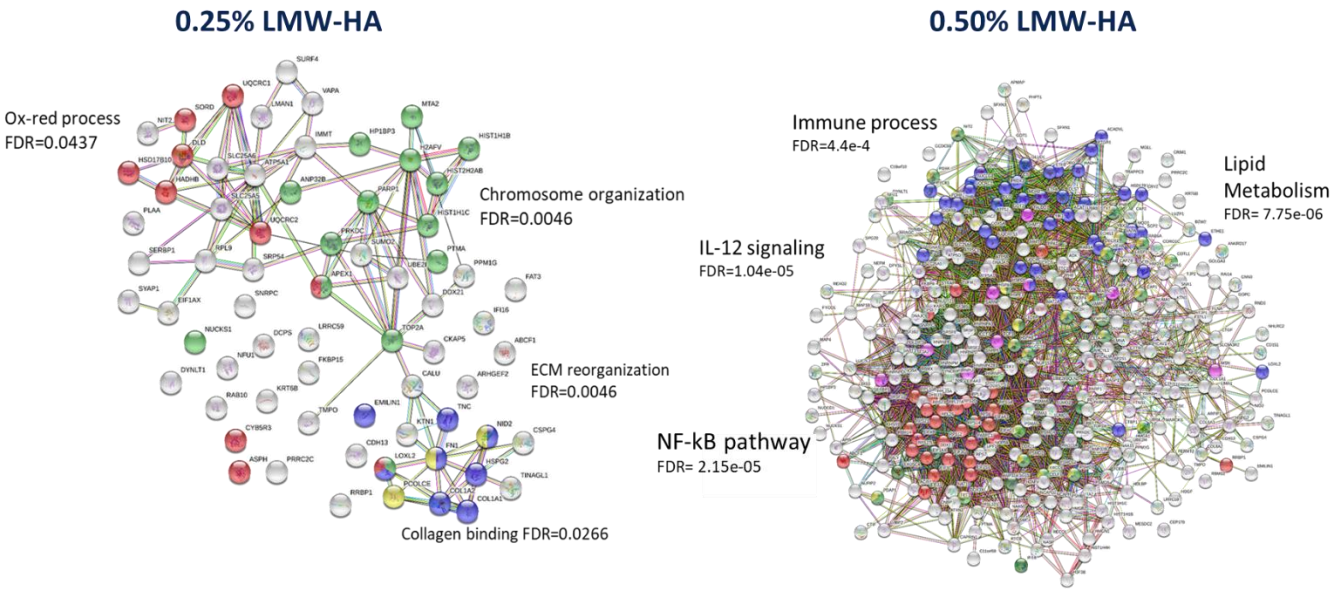

Figure 4. Networking of up-regulated proteins by (left) LMW-HA 0.25 % and (right) LMW-HA 0.50 % obtained by STRING software. In label some of the most interesting pathways significantly altered.

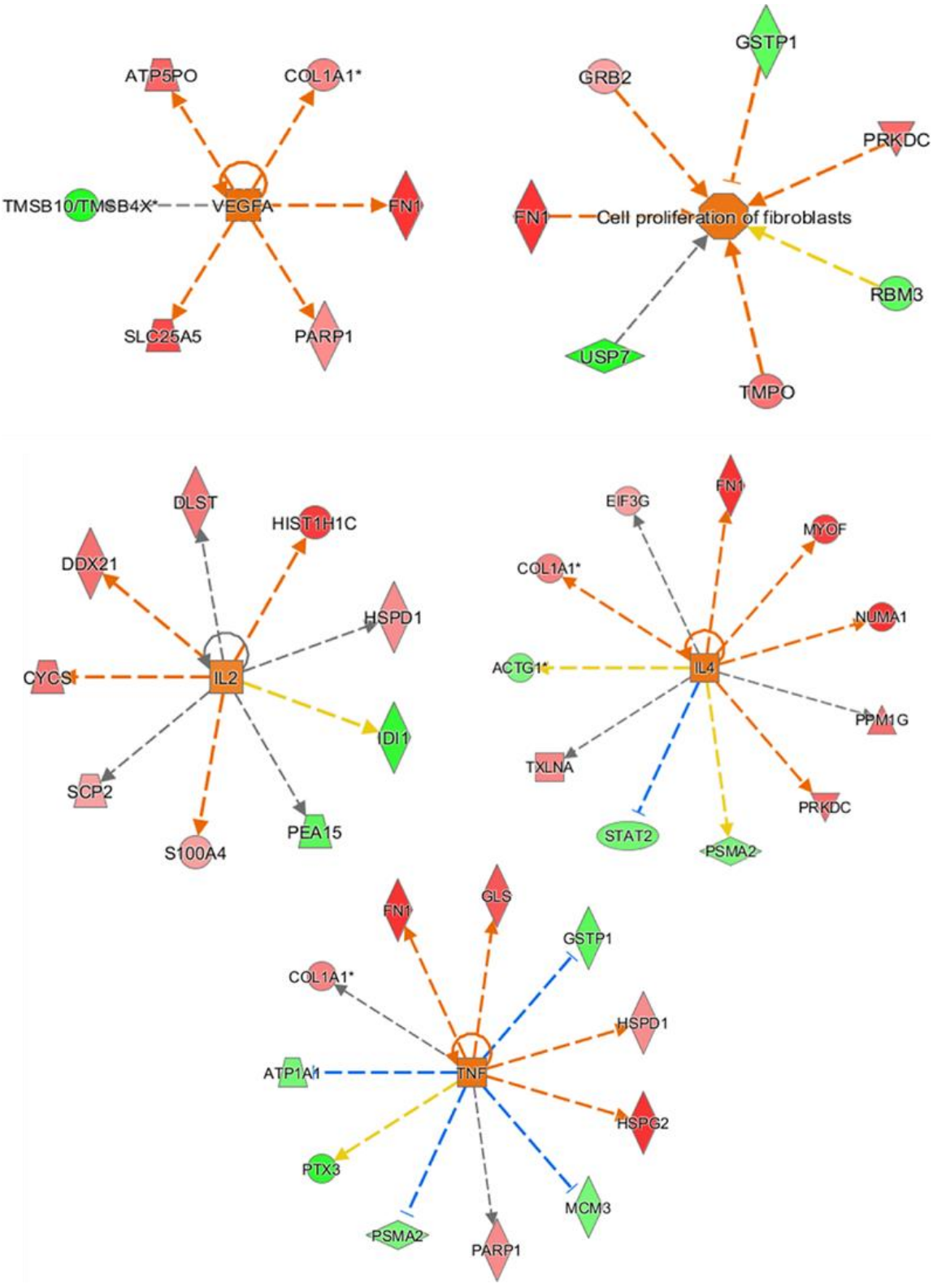

Figure 5. Graphical representation obtained by IPA software of (up) Proliferation's pathways enhanced by LMW-HA 0.50 % and (down) pathways involved in immune response significantly altered by LWM-HA 0.50%. In red the increased genes, in green those decreased. The color intensity is positive related to the up- or down-gene's regulation; orange line leads to activation, yellow lines for findings inconsistent with state of downstream molecule; grey line for effect not predicted.

Table 1. Examples of differentially regulated proteins by LWM-HA concentrations (0.125 %, 0.25 % and 0.50 %, respectively). In bold those more relevant for the networking explanation.

Accession numbers	Protein name	Gene Name	T0.125% vs C	T0.25% vs C	T0.50% vs C
Q2L6I2	ATP-binding cassette sub-family F member 1	ABCF1	1.36	1.56	1.55
Q9Y6K8	Adenylate kinase isoenzyme 5	AK5	0.73	0.76	0.71
Q53F35	Acidic leucine-rich nuclear phosphoprotein 32 family member B	ANP32B	1.37	1.41	1.56
A0A087WZT3	BolA-like protein 2	BOLA2	0.71	0.74	-
A8K651	Complement component 1 Q subcomponent-binding protein, mitochondrial	C1QBP	1.41	-	1.46
Q6IAW5	Calumenin	CALU	1.24	1.21	1.29
C9JEZ4	Cdc42 effector protein 3	CDC42EP3	-	0.73	0.80
Q6UVK1	**Chondroitin sulfate proteoglycan 4**	**CSPG4**	**-**	**1.73**	**1.77**
Q5VTU3	Dynein light chain Tctex-type 1	DYNLT1	-	1.38	1.50
P47813	Eukaryotic translation initiation factor 1A	EIF1AX	1.57	1.52	1.46
Q9Y6C2	**EMILIN-1**	**EMILIN1**	**-**	**4.75**	**3.31**
A0A0A0MT60	Peptidyl-prolyl cis-trans isomerase;FK506-binding protein 15	FKBP15	1.59	1.31	1.32
A0A024R462	**Fibronectin**	FN1	-	3.91	3.18
Q53TX0	Glutaminase kidney isoform, mitochondrial	GLS	1.39	-	1.51
B2R6K4	Guanine nucleotide-binding protein G(I)/G(S)/G(T) subunit beta-1	GNB1	-	0.72	0.83
F5GZQ3	Trifunctional enzyme subunit beta, mitochondrial	HADHB	1.41	1.78	2.04
P16401	Histone H1.5	HIST1H1B	1.90	3.01	2.33
P16403	Histone H1.2	HIST1H1C	1.30	2.14	1.83
Q8IUE6	Histone H2A type 2-B	HIST2H2AB	2.11	1.87	-
X6RGJ2	Heterochromatin protein 1-binding protein 3	HP1BP3	1.44	1.63	1.56
A0A0S2Z410	3-hydroxyacyl-CoA dehydrogenase type-2	HSD17B10	1.34	1.40	1.67
A0A024RAB6	**Basement membrane-specific heparan sulfate proteoglycan core protein**	**HSPG2**	**-**	**9.74**	**8.15**
B4DT20	MICOS complex subunit MIC60	IMMT	-	1.23	1.70
B4DWZ7	LanC-like protein 2	LANCL2	-	0.72	0.82
P30533	Alpha-2-macroglobulin receptor-associated protein	LRPAP1	-	0.77	0.84
Q8IV28	Nidogen-2	NID2	-	2.17	1.77
Q15113	Procollagen C-endopeptidase enhancer 1	PCOLCE	-	1.46	1.25
B4DDC8	Protein phosphatase 1G	PPM1G	1.26	1.29	1.48

4. CONCLUSIONS

A deepening knowledge of molecular effects induced by any active principle is fundamental to support its use, due to demonstration of safety and efficacy. Although the general attention was mainly focused on the intracellular environment, an increasing number of evidence has pointed out the biological importance also of the extracellular one. Indeed, the extracellular matrix (ECM) has showed to be involved in several physiological and pathological pathways (1). High-molecular-weight hyaluronic acid (HWM-HA) is one of the major ECM's constituents, but also a widespread commercial ingredient for its superficial hydration proprieties. More recently, LMW-HA became commercially available especially for anti-aging use (8). Despite its diffusion, the detailed intra- and extra- cellular impact of commercially available low-molecular-weight HA (LMW-HA) is not yet defined. At this regard, the objective of this study was to describe and quantify the proteins profile's change induced by different concentrations of 20-50 kDa LWM-HA (0.125 %, 0.25 % and 0.50 % respectively) on normal human dermal fibroblasts. To do this, a quantitative proteomics approach was applied considering the large number of molecular information available by omics science, including proteomics, and the currently improvement of instrumental technique. The high-resolution mass spectrometric technique coupled with nano-LC was here used and the results were explained by network and pathways analyses. In line with previous evidence (3, 6) but in a deeper way, here we demonstrated both an intra- and extra-cellular impact of 20-50 kDa LWM-HA. Indeed, the 24 hours treatment with LWM-HA induced, for example, an increasing of cell proliferation and growth as well as of extracellular matrix reorganization or proteoglycans biosynthesis. Moreover, at the highest concentration (0.50 %) the inflammatory and immune responses were activated, among all, by the stimulation of lymphocytes, interleukins (IL-12, IL-1, IL-2, IL-4 etc.) or necrosis tumor factor signaling. However, the global cells' wellness was still sustained as demonstrated, for example, by the significant up-regulation of Eukaryotic Initiation Factor 2 (EIF2) pathway implicated in the protein synthesis, of citrate acid cycle that is a pivotal factor of mitochondrial functionality and of

fibroblasts proliferation. In addition, 0.50 % LWM-HA enhanced the VEGFA-VEGFR2 signaling that is actively involved in angiogenesis by inducing the proliferation, survival and migration of endothelial cells, and by increasing endothelial permeability (15,16). As further confirmation of the cells' viability and ECM reorganization after the 0.25 and 0.50 % LMW-HA treatment, a significant upregulation was demonstrated by FN1 and HSPG2 genes. FN1 encodes for fibronectin, a glycoprotein of the extracellular matrix that plays a key role in cell adhesion and migration processes as well as in wound healing binding membrane-spanning receptor proteins as integrins but also collagen, fibrin, and heparan sulfate proteoglycans (*i.e.* syndecans, gypicans and perlecans) (17,18). Then, proteoglycan-2 (HSPG2) encodes exactly for heparan sulfate proteoglycans (HSPGs) that show angiogenic and growth-promoting attributes primarily by acting as a coreceptor for basic fibroblast growth factor (FGF2) (19) as well as a cross-linker among many extracellular matrix components and cell-surface molecules (laminin, prolargin, collagen type IV etc.). Additionally, as resulted also in this study, HSPGs demonstrated a pivotal role in regulating developmental signaling pathways including transforming growth factor-β or β-catenin independent Wnt signaling (17), where Wnt are lipid-modified proteins strictly associated with cell surface and ECM.

This study has strong points and limitations. The first includes: i) the analytical instruments and the applied methodology, that allowed us a detailed and quantified description of a huge number of proteins; ii) the investigation of less known form of HA (i.e. LMW-HA); iii) the network analysis conducted by several software, which allowed to depict a complete intra- and extra-cellular overview; iv) the primary and healthy selected cell line; v) the LMW-HA concentrations tested that reflected those commonly used. About the main limitations, it should be noted that a simple *in vitro* environment like that of cells, less complex that whole skin, could offer a limited view of the biological effects of a compound.

In conclusion, treating normal human dermal fibroblast with hyaluronic acid at low-molecular-weight resulted in positive intra- and extra-cellular effects enhancing the nucleus and mitochondria

functionality as well as the ECM reorganization. In addition, the inflammatory and immune activity induced by the highest concentration seemed to be well tolerated. As next step, considering the close connection between proteins and other metabolites, also the lipidome profile's changes will be analyzed to provide a more complete comprehension about the *in vitro* molecular effects of LWM-HA supporting and improving its commercial use and safety.

REFERENCES

1. Vallet SD, Clerc O, Ricard-Blum S. Glycosaminoglycan–Protein Interactions: The First Draft of the Glycosaminoglycan Interactome. Journal of Histochemistry & Cytochemistry. 2021;69(2):93-104.
2. P. Heldin, C.Y. Lin, C. Kolliopoulos, Y.H. Chen, S.S. Skandalis, Regulation of hyaluronan biosynthesis and clinical impact of excessive hyaluronan production. Matrix Biol (2019) 78-79:100-117
3. J.M. Cyphert, C.S. Trempus, S. Garantziotis, Size Matters: Molecular Weight Specificity of Hyaluronan Effects in Cell Biology. Int J Cell Biol (2015)
4. Abatangelo, G.; Vindigni, V.; Avruscio, G.; Pandis, L.; Brun, P. Hyaluronic Acid: Redefining Its Role. *Cells* 2020, *9*, 1743.
5. Y.R. Jung, C. Hwang, J.M. Ha, D.K. Choi, K.C. Sohn, Y. Lee, Hyaluronic Acid Decreases Lipid Synthesis in Sebaceous Glands. J Invest Dermatol 137 (2017) 1215-1222.
6. L. Vistejnova, B. Safrankova, K. Nesporova, R. Slavkovsky, M. Hermannova, P. Hosek, Low molecular weight hyaluronan mediated CD44 dependent induction of IL-6 and chemokines in human dermal fibroblasts potentiates innate immune response. Cytokine 70 (2014) 97-103
7. A. Fallacara, E. Baldini, S. Manfredini, S. Vertuani, Hyaluronic Acid in the Third Millennium. Polymers, 10 (2018)
8. S.N.A. Bukhari, N.L. Roswandi, M. Waqas, H. Habib, F. Hussain, S. Khan, et al. Hyaluronic acid, a promising skin rejuvenating biomedicine: A review of recent updates and pre-clinical and clinical investigations on cosmetic and nutricosmetic effects. Int J Biol Macromol, 120 (2018) 1682-1695
9. Snetkov, P.; Zakharova, K.; Morozkina, S.; Olekhnovich, R.; Uspenskaya, M. Hyaluronic Acid: The Influence of Molecular Weight on Structural, Physical, Physico-Chemical, and Degradable Properties of Biopolymer. Polymers 2020, 12

10. F. Cilurzo, G. Vistoli, C.G. Gennari, F. Selmin, F. Gardoni, S. Franzè, et al. The role of the conformational profile of polysaccharides on skin penetration: the case of hyaluronan and its sulfates. Chem Biodivers 11 (2014) 551-561

11. M. Essendoubi, C. Gobinet, R. Reynaud, J.F. Angiboust, M. Manfait, O. Piot, Human skin penetration of hyaluronic acid of different molecular weights as probed by Raman spectroscopy. Skin Res Technol 22 (2016) 55-62

12. M. Farwick, G. Gauglitz, T. Pavicic, T. Köhler, M. Wegmann, K. Schwach-Abdellaoui, et al., Fifty-kDa hyaluronic acid upregulates some epidermal genes without changing TNF-α expression in reconstituted epidermis. Skin Pharmacol Physiol 24 (2011) 210-7.

13. J. Cox, M.Y. Hein, C.A. Luber, I. Paron, N. Nagaraj, M. Mann, Accurate proteome-wide label-free quantification by delayed normalization and maximal peptide ratio extraction, termed MaxLFQ. Mol Cell Proteomics 13 (2014) 2513-26

14. Radrezza S, Baron G, Nukala SB, Depta G, Aldini G, Carini M, D'Amato A. Advanced quantitative proteomics to evaluate molecular effects of low-molecular-weight hyaluronic acid in human dermal fibroblasts. J Pharm Biomed Anal. 2020 Jun 5;185:113199.

15. S. Gariboldi, M. Palazzo, L. Zanobbio, S. Selleri, M. Sommariva, L. Sfondrini, et al. Low molecular weight hyaluronic acid increases the self-defense of skin epithelium by induction of beta-defensin 2 via TLR2 and TLR4. J Immunol 181 (2008) 2103-10

16. L. Claesson-Welsh, M. Welsh, VEGFA and tumour angiogenesis. J Intern Med 273 (2013) 114-27

17. X. Lin, Functions of heparan sulfate proteoglycans in cell signaling during development. Development 131 (2004) 6009-21

18. J.Patten , K.Wang, Fibronectin in development and wound healing, Advanced Drug Delivery Reviews (2021) 170, 353-368

19. De Araújo R., Lôbo M., Trindade K., Silva D.F., Pereira N., Fibroblast Growth Factors: A Controlling Mechanism of Skin Aging, Skin Pharmacol Physiol (2019);32:275–282

Study 2

Study of carnosine's effect on nude mice skin to prevent UV-A damage

(doi.org/10.1016/j.freeradbiomed.2021.07.010)

ABSTRACT

The skin is an important barrier against external attacks from bacteria, radicals, or radiations. Ultraviolet-A (UV-A) radiations cause significant impairment of this barrier, inducing inflammation, oxidative stress, and wrinkle formation, thereby promoting photoaging. Previous studies reported that carnosine, a potent antioxidant, and carbonyl scavenger agent, may prevent photoaging features in the skin of hairless mice exposed to UV-A radiations. In the present study, we used a quantitative proteomic approach to analyse the changes evoked by carnosine in the skin proteome of hairless mice exposed to UV-A. This approach allowed to quantify more than 2480 proteins, among them consistent differences were observed for 89 proteins in UV-A exposed *vs* control unexposed skins, and 252 proteins in UV-A-exposed skin preventively treated by carnosine (UVAC) *vs* UV-A. Several functional pathways were altered in the skins of UV-A exposed hairless mice, including the integrin-linked kinase, calcium signaling, fibrogenesis, cell migration and filament formation. An impairment of mitochondrial function and metabolism was observed, with an up-regulation of cytochrome C oxidase 6B1 and NADH: ubiquinone oxidoreductase S8. Skins pre-treated by carnosine were prevented from UV-A induced proteome alterations. In conclusion, our study emphasizes the potency of a proteomic approach to identify the consequences of UV radiations in the skins, and points out the capacity of carnosine to prevent the alterations of skin proteome evoked by UV-A.

1. INTRODUCTION

The skin is an efficient defensive barrier against external insults. Nevertheless, long-term ultraviolet (UV) radiation exposure can result in alterations of its structure and functionality via direct and indirect effects (1–3). The solar UV wavebands are mainly constituted by UV-A (315–400 nm) and a small portion of UV-B (280–315 nm) while short-wave UV-C (100–280 nm) are completely absorbed by the stratospheric ozone. UV-A can deeply penetrate the skin dermis up to the basal layer and are considered as a main cause for skin photoaging (4,5). Skin photoaging is characterized by the formation of wrinkles, a loss of skin tone and elasticity, dryness, and stiffening (1,2,6,7). At the molecular and biochemical level, chronic exposure to UV-A progressively leads to a disorganization of the extracellular matrix (ECM), alteration of DNA, dysregulated autophagy, chronic inflammation, alteration of fatty acids, carbohydrates or protein structure, all events involved in skin aging and the increasing of the risk of developing skin cancers (5,8). The mechanisms leading to skin damages are not fully understood and may derive (at least in part) from the generation of reactive oxygen species (ROS) and subsequent lipid peroxidation (9). Salvayre et al. (2015) (10) previously reported that lipid peroxidation products such as hydroxynonenal (HNE) and acrolein are generated in the skin dermis of hairless mice chronically exposed to UV-A radiations. These agents form adducts on extracellular matrix components such as elastin, with possible implication in solar elastosis (10,11). HNE and acrolein may contribute to dermis fibroblast senescence by promoting the expression of senescence markers such as γ-H2AX or the modification of cytoskeletal proteins such as vimentin, in the skin of UV-irradiated hairless mice or in cultured fibroblasts (12). Many other systems could be affected by ROS or lipid oxidation products generated by UV-A, with consequences on protein function, signaling, antioxidant systems or gene expression. Several compounds are used to protect the skin against UV radiations, among them antioxidants and carbonyl scavengers (13,14). In this context, we reported that a topical treatment of the hairless mice skin with carnosine, an endogenous β-alanyl-L-histidine dipeptide with antioxidant and carbonyl

scavenger properties, significantly prevented the visible signs of photoaging (15). At the molecular level, carnosine prevented the modification of elastin as well as the process of fibroblast senescence evoked by HNE or acrolein (10, 12). Carnosine readily reacts with aldehydes like acrolein or HNE to form nonreactive adducts, preventing the process of protein modification and subsequent alteration of cells and tissues (16,17). It is likely that carnosine treatment exerts a larger scale of protective responses in UV-irradiated skin, and a deeper characterization of its effects may allow a better understanding of skin alterations evoked by UV radiations. The current development of 'omics sciences (genomics, proteomics, metabolomics etc.) supported by performing analytical tools is showing a new molecular panorama with the availability of a huge amount of data. Proteomic studies represent a suitable technique for analysing and characterizing the nature and alterations of proteins in various pathophysiological areas (18–20), particularly in the skin (21) and a proteomic atlas of human skin (https://skin.science/) has been established (22). The quantitative distribution of skin structural proteins, obtained by label free quantitative proteomics, is an important resource for translational research in this area too (22, 23). Dermatological diseases, such as human malignant melanomas (24), eczema (25), psoriasis (26), were characterized by the alteration of proteome in the different states, control versus disease. Moreover, murine skin protein profiling was also described during ageing (27) and in psoriasis-like disease (28). However, and surprisingly, only few studies were focused on the murine or human skin proteome or its protection by antioxidants and related compounds, upon exposure to UV-radiations. The present study was designed to provide an in-depth description of the murine skin proteome of hairless mice exposed to UV-A radiations and the preventive effect of carnosine, using a label-free quantitative proteomics approach by high-resolution mass spectrometry. These analyses were carried out on murine skin samples from Negre-Salvayre's previous study showing that carnosine may prevent several photoaging features in the skin of UV-A irradiated hairless mice (10,12).

2. MATERIALS AND METHODS

2.1 Chemicals

Lysis buffer reagents (urea, TrisHCl, sodium chloride) were purchased by BioRad Laboratories, Inc. (Segrate, Milan, Italy); Bradford kit reagents, protease inhibitor cocktail, DL-dithiothreitol (DTT), iodocetamide (IAA), ammonium bicarbonate (NH_4HCO_3) ammonium formate (NH_4HCO_2) MS grade, acetonitrile (MeCN), and formic acid (FA) (all UHPLC/MS-CC/SFC grade) were brought by Sigma-Aldrich (Taufkirchen, Germany); lysC and Trypsin Sequencing Grade were purchased by Roche (Monza, Italy); C-18 resin ZipTip were purchased by Merck (Millipore, Milan, Italy). Water was purified in-house (resistance > 18 MΩ cm−1; total organic content < 10 ppb) with a Milli-Q H2O purification system (Millipore, Bedford, MA, USA).

2.2 Experimental treatment

Skin samples used in this work were provided by Negre-Salvayre's lab (10) (experimental protocol N°12/1048/10/13, approved by the French legislation and the local ethical committee for animal experiments). Briefly, this study was carried out on albino hairless mice Skh:hr-1 (8 weeks old, Charles River Laboratories) (4 animals/condition), with one control non-irradiated group, one group daily exposed to UV-A radiations (20 J/cm2 daily, up to 600 J/cm2), one group treated with polyethylene glycol (PG) (solvent for carnosine) and daily exposed to UV-A, and one group treated by carnosine (1% in PG) and exposed to UV-A. Carnosine and PG were spread over the back at the end of UV-A exposure. After animal sacrifice, samples of skins from mouse backs were recovered and stored at - 80 ◦C until use (10).

2.3 Sample preparation

Each sample was homogenized by glass bead beating (3 cycles, 60″, 350 rpm) in 100 µL of protein extraction buffer (8 M urea in 50 mM Tris- HCl, 30 mM NaCl at 8.5 pH and 1% of protease inhibitor

cocktail). The supernatant was collected in fresh tubes and centrifuged at 14000×*g*, 4 ◦C for 10 min and sonicated by probe. The amount of proteins was quantified by the Bradford Reagent following the standard procedure. 20 µg of proteins in 50 mM NH_4HCO_3 were reduced with 5 mM DL-dithiothreitol (DTT) for 30 min at 52 °C shaking, then centrifuged at 500 rpm and alkylated with 15 mM iodoacetamide for 20 min in the dark at room temperature. The protein digestion was performed in 1:100 lysC: protein ratio (w/w) for 3 h at 37 °C shaking at 650 rpm followed by 1:20, trypsin: protein ratio (w/w) overnight at 37 ◦C shaking at 650 rpm.

2.4 High-resolution mass spectrometry analysis (nLC-HRMS)

To increase the quality of instrumental analysis, the digested samples were further purified and concentrated by 0.6 µL C-18 resin ZipTip. Tryptic peptides were analyzed using a Dionex Ultimate 3000 nano-LC system (Sunnyvale CA, USA) connected to Orbitrap Fusion™ Tribrid™ Mass Spectrometer (Thermo Scientific, Bremen, Germany) equipped with a nano-electrospray ion source (nESI). Peptide mixtures were pre-concentrated onto an Acclaim PepMap 100 - 100 µm × 2 cm C25 and separated on EASY-Spray column, 25 cm × 75 µm ID packed with Thermo Scientific Acclaim PepMap RSLC C18, 3 µm, 100 Å. The temperature was set to 35 ◦C and the flow rate was 300 nL min-1. Mobile phases were the following: 0.1% formic acid (FA) in water (solvent A), 0.1% FA in water/acetonitrile with 2/8 ratio (solvent B). The elution gradient was from 96% buffer A to 40% buffer B for 110 min. MS spectra were collected over an *m/z* range of 375–1500 Da at 120,000 resolutions, operating in data dependent scan mode, cycle time 3 s between master scans. Higher-energy collision dissociation (HCD) was performed with collision energy set at 35 eV in positive polarity. Each sample was analysed in three technical replicates.

2.5 Data analysis

The instrumental raw files were processed by MaxQuant software v1.6.6.0 (29) set on the *Uniprot_Mus Musculus* (mice) database against the Andromeda search engine. The quantification

of peptides and related proteins for each control and treated sample in biological duplicate and technical triplicates was based on the LFQ intensities. Lys-C and trypsin as the digestive enzymes, variable modification of carbamidomethylation of cysteine (+57.021 Da), fixed modification of methionine oxidation (+15.995 Da), N-terminal acetylation (+42.011 Da) and LFQ minimum ratio count to 2 were set as further parameters. The interpretation and visualization of results obtained from MaxQuant software were performed by a two-sample *t*-test using Perseus (v1.6.1.3, Max Planck Institute of Biochemistry, Germany). Statistical parameters ($p < 0.05$; $q < 0.05$, q = FDR adjusted p-value) were set to identify the differentially expressed proteins between samples (log2 fold changes). The proteins were selected with a minimum of two peptides. Variability of biological replicates were measured using the scatter plot with Pearson correlation coefficient values of the LFQ intensities. The network protein analysis related to significantly altered proteins was carried out by Ingenuity Pathways Analysis software (IPA; last release; Qiagen) based on Gene Ontology database. The statistical enrichment of involved pathways is performed by the right-tailed Fisher's exact test, in correlation with QIAGEN Knowledge Base, assigning a p-value and z-scores (https://digi talinsights.qiagen.com/products/features/analysis-match/).

3. RESULTS AND DISCUSSION

The objectives of this study were to analyse whether and how carnosine prevents the modifications of skin proteome evoked by the exposure of hairless mice to UV-A. For this purpose, the skin samples recovered from Negre-Salvayre's previous study showing that UV-A generate lipid peroxidation products (like HNE, acrolein) in the skin dermis of hairless mice chronically exposed to UV-A were prevented by a topical application of carnosine (10). Skin samples were analysed by applying a high-resolution mass spectrometry (MS)-based label-free quantitative (LFQ) proteomic technique, which first led to quantify a total of 2480 proteins, whose expression has been compared for each condition. 89 proteins resulted significantly altered by UV-A exposure vs control (n=30

up-regulated, 59 down-regulated; Figure 1A), 252 proteins comparing UV-A plus carnosine (UVAC) to UV-A without carnosine (UVA) (n=173 up-regulated, 79 down-regulated; Figure 1B). Multi-scatter plots confirmed the quality and reproducibility of biological and technical replicates (Pearson correlation coefficient values ≥ 0.98).

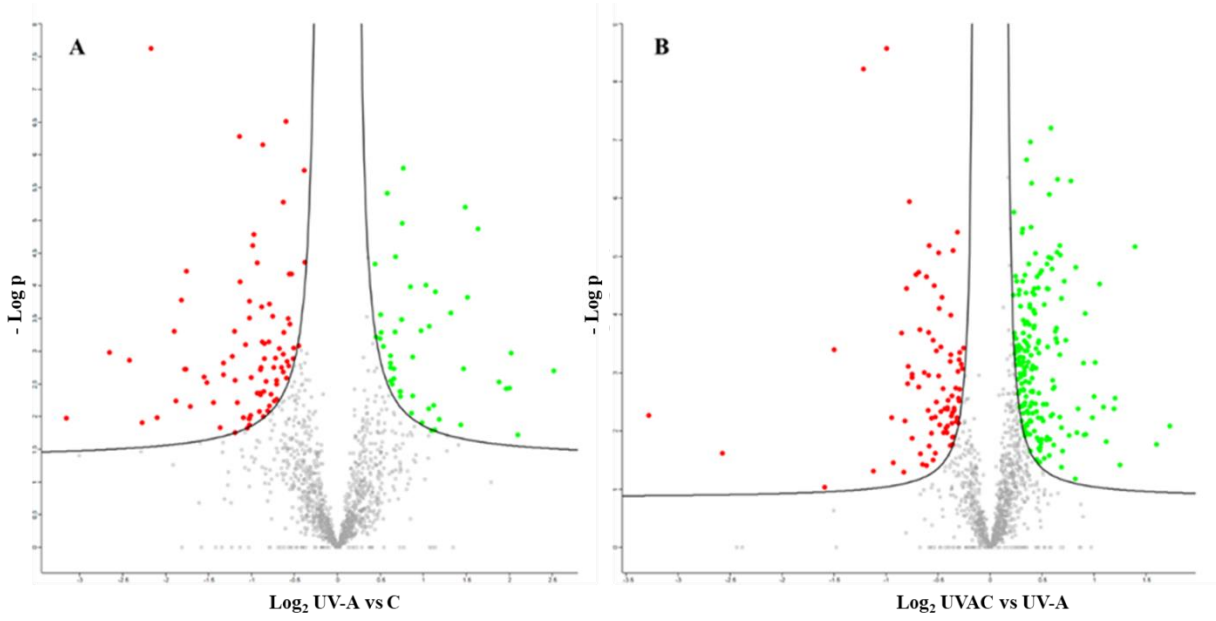

Figure 1. Distribution of differentially regulated proteins induced by a) UV-A exposure vs Control, b) UV-A exposure w/wo carnosine. Green colour indicates up-regulation (log_2 ratio ≥ 0.6), red colour represents down-regulation (log_2 ratio ≤ -0.6); Scatter plots of log_2 ratio on x-axis against -log_{10} p-value on y-axis of significantly quantified proteins (Perseus v 1.6.1.3).

The identification and quantification of proteins differentially regulated for each condition (control, UVAC, UV-A) were followed by an analysis of the protein network to describe the functional modules and pathways altered by UV-A radiations *w/wo* carnosine. In Figure 2, we show the most prominent canonical pathways obtained by IPA software comparing UVA vs control (Figure 2A) and UVAC vs UVA (Figure 2B). The functional modules are based on statistical analyses and are associated with a p-value and z-score. In addition, the protein expression in each module was correlated with literature databases to predict the de/activation of the functional or disease modules.

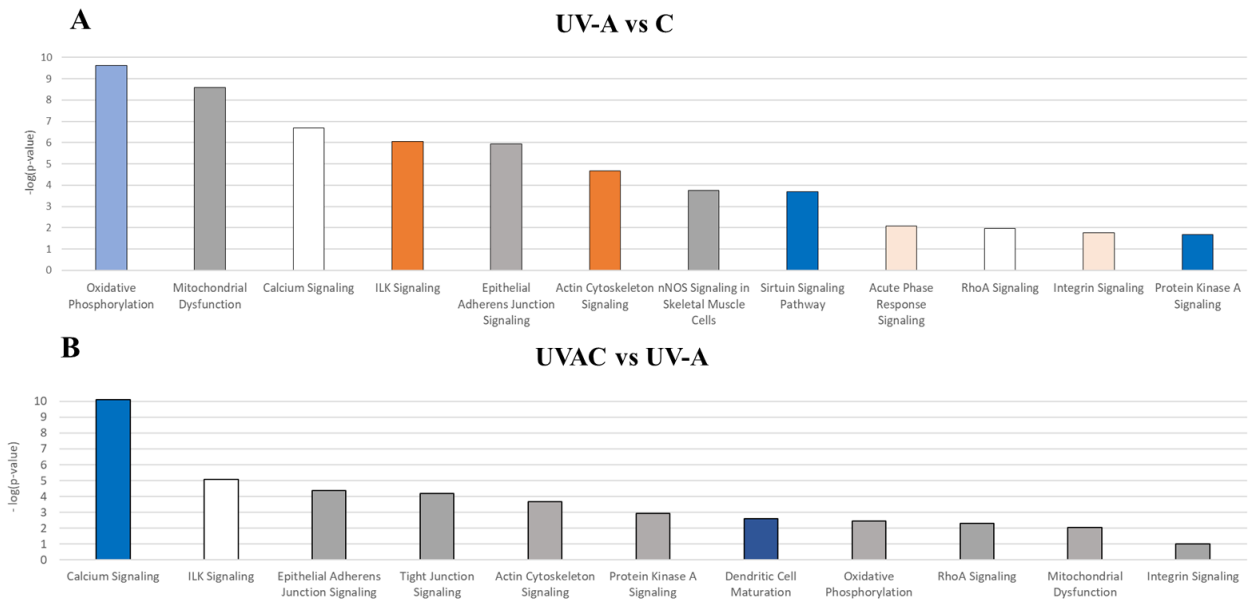

Figure 2. Main canonical pathways obtained comparing A) UV-A vs control and B) UVAC vs UV-A (IPA). Orange: increased pathways (positive z-score); blue: decreased pathways (negative z-score); white: no change (zero as z-score); grey: uncertain changes.

3.1 Changes of skin dermis proteome evoked by UV-A exposure

Several pathways were significantly altered by UV-A exposure, among them oxidative phosphorylation (p-value= 2.48 e-10), mitochondrial dysfunction (p-value= 2.54 e-09), integrin-linked kinase (ILK) signaling (p-value= 8.66 e-07) and contraction as evidenced by the increase of calcium signaling (p-value= 1.96 e-07; Figure 3A), contractile and strength of muscular tissue pathway (p-value= 6.91 e-07; Figure 4), nNOS signaling (p-value= 1.80 e-07; Figure 5A), fibrogenesis and filaments formation (p-value= 5.83 e-06; Figure 6A).

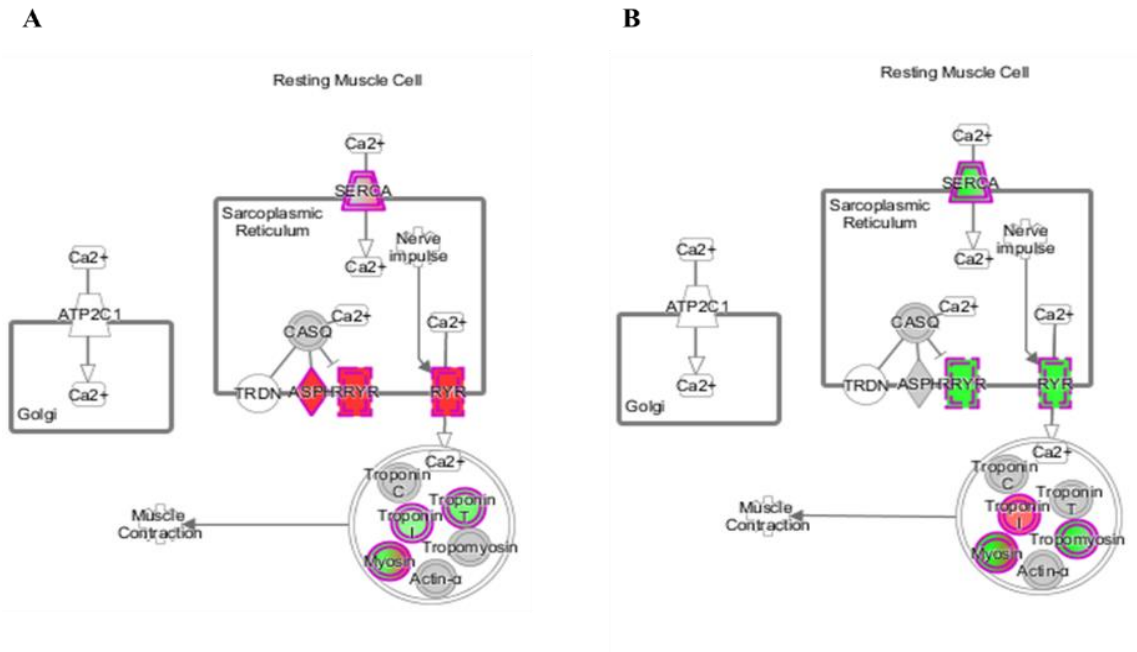

Figure 3. Calcium signaling pathway enhanced in A) UV-A vs control and decreased in B) UVAC vs UV-A (IPA). In red the increased proteins-related genes, in green those decreased. The colour intensity is positively related to the up- or down- regulation.

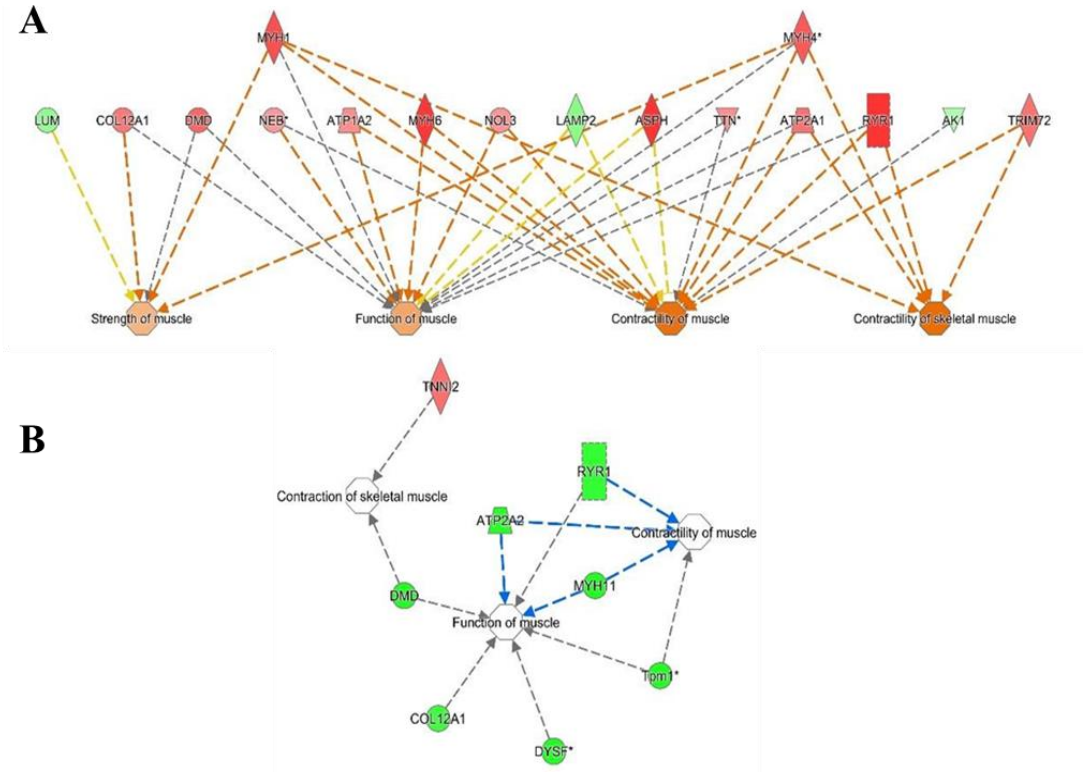

Figure 4. Contraction related pathways in A) UV-A vs Control and B) UVAC vs UV-A (IPA). In red the increased proteins-related genes, in green those decreased. The colour intensity is positively related to the up- or down- regulation; orange line leads to activation, blue lines lead to deactivation, yellow lines for findings inconsistent with state of downstream molecule, grey line for effect not predicted.

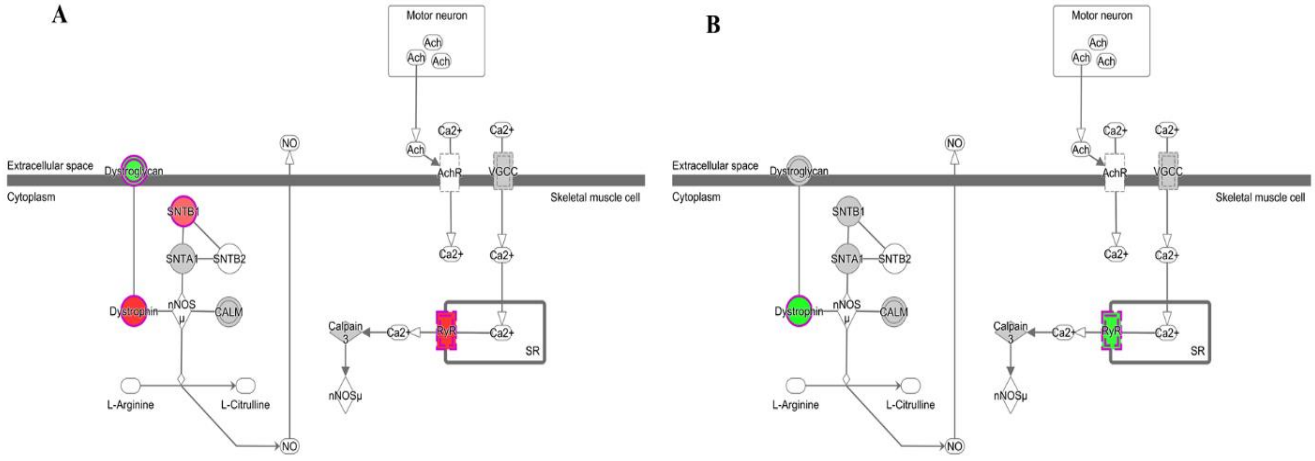

Figure 5. nNOS signaling pathway enhanced in A) UV-A vs Control, B) decreased in UVAC vs UV-A (IPA). In red the increased proteins-related genes, in green those decreased. The colour intensity is positively related to the up- or down- regulation.

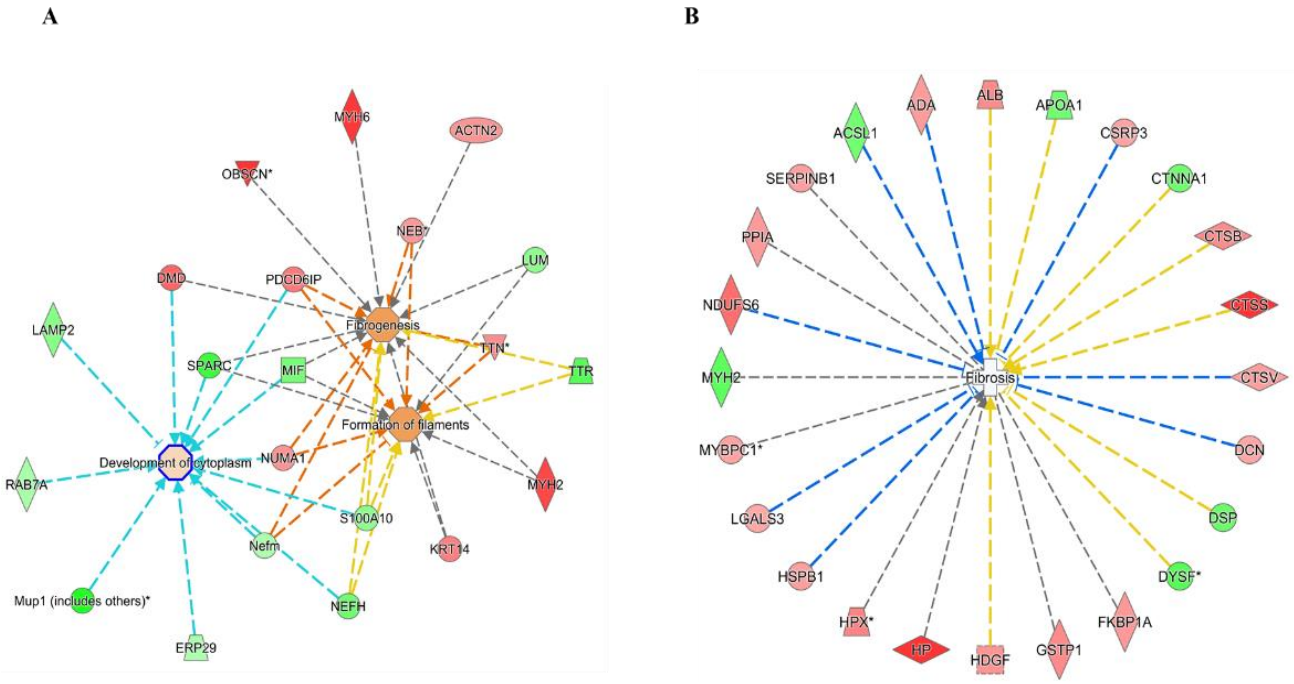

Figure 6. Fibrosis related pathways in A) UV-A vs Control and B) UVAC vs UV-A (IPA). In red the increased proteins-related genes, in green those decreased. The colour intensity is positively related to the up- or down- regulation; orange line leads to activation, blue lines lead to deactivation, yellow lines for findings inconsistent with state of downstream molecule, grey line for effect not predicted.

Indeed, a significant increase could be observed for several cytoskeletal and contractile proteins or complexes such as dystrophin (DMD, log2 ratio = 0.99), keratin 31 (KRT31, log2 ratio= 2.00), myosin heavy chain 11 (MYH11, log2 ratio= -0.82) or ryanodine receptor (RyR-1, log2 ratio= -0.75) (Table 1).

Ryanodine receptor 1 (RyR-1) is expressed at the more external layer of the epidermis in the keratinocyte and has a role in barrier homeostasis (30). RyRs are also actively involved in the regulation of intracellular calcium levels. In particular, the inhibition of RyR-1 was shown to accelerate the barrier recovery of the skin in the presence of wounds (31). RyR-1 is not the unique regulator of calcium signaling altered by UV-A. Indeed, upon UV-A exposure we also observed a significant up-regulation related to aspartate beta hydroxylase (ASPH, log2 ratio = 2.10), involved in calcium homeostasis as well further than different isoforms of heavy chain of myosin involved in calcium binding and contraction, and DMD, a myosin binding protein. Moreover, the overexpression of myosin was related to fibrosis, showed by the accumulation of collagens, such as collagen alpha-1 (XII) chain (col12a1, log2 ratio = 0.87) and by the alteration of growth factor expression, regulated by integrin-linked kinase (ILK) pathway (z-score= 1.90). The fibrotic process indeed is physiologically linked with the calcium signaling regulation as well as with the cell's damage induced, in this case, by UV-A. At this regard, calcium signaling has shown an active role on the inflammasome activation leading to fibrotic pathways (32). Homeostasis of calcium regulates also the nNOS activity and its interaction with DMD, affecting NO signaling. On the skin, UVA radiation induced an upregulation of DMD (log2 ratio = 0.99) and Beta-1- syntrophin (log2 ratio = 0.68), the adapter protein involved in the formation of dystrophin glycoprotein complex. DAD1, dystrophin-associated glycoprotein 1 was highly down-expressed (log2 ratio = - 0.701). The deregulation of nNOS signaling was also attested by the upregulation of RyR1 (Figure 5A).

Table 1. Top up-/down-regulated proteins by UV-A or UVAC exposure involved in calcium signaling and fibrogenesis processes.

Gene name	Protein name	UniProt/Swiss-Prot Accession	UVA vs C Log_2 Ratio	UVAC vs UVA Log_2 Ratio	Functional module
ATP2A2	ATPase sarcoplasmic/endoplasmic reticulum Ca2+ transporting 2	Q5DTI2	0.16	-0.80	Ca^{2+} signaling
ATP2A3	ATPase sarcoplasmic/endoplasmic reticulum Ca2+ transporting 3	Q8C213	0.84	-0.69	Ca^{2+} signaling
CAMK2G	calcium/calmodulin dependent protein kinase II gamma	Q6ZWS7	0.60	-0.78	Ca^{2+} signaling
MYH11	myosin heavy chain 11	A0A338P6K2	-0.05	-0.82	Ca^{2+} signaling
MYL3	myosin light chain 3	P09542	NaN	1.00	Ca^{2+} signaling
MYL9	myosin light chain 9	Q9CQ19	-0.78	0.73	Ca^{2+} signaling
RYR1	ryanodine receptor 1	K3W4M2	2.52	-0.75	Ca^{2+} signaling
TNNI2	troponin I2, fast skeletal type	A2A6K0	-0.85	0.64	Ca^{2+} signaling
Tpm1	tropomyosin 1, alpha	A0A2R2Y2P8	-0.45	-1.12	Ca^{2+} signaling
MYH2	myosin heavy chain 2	G3UW82	1.18	-0.79	Ca^{2+} signaling / fibrogenesis
ACTN2	actinin alpha 2	Q9JI91	0.68	0.03	fibrogenesis
DMD	Dystrophin	P11531	0.99	-0.85	fibrogenesis
KRT14	keratin 14	Q61781	0.82	-0.07	fibrogenesis
LUM	lumican	P51885	-0.90	0.11	fibrogenesis
MIF	macrophage migration inhibitory factor	Q545F0	-1.10	0.33	fibrogenesis
MYH6	myosin heavy chain 6	B2RQQ1	1.28	-0.59	fibrogenesis
NEB	nebulin	A2AQB2	0.65	-0.53	fibrogenesis
NEFH	neurofilament heavy	Q80TQ3	-1.14	0.33	fibrogenesis
Nefm	neurofilament, medium polypeptide	P08553	-0.65	0.26	fibrogenesis
NUMA1	nuclear mitotic apparatus protein 1	E9Q7G0	0.69	-0.42	fibrogenesis
OBSCN	obscurin, cytoskeletal calmodulin and titin-interacting RhoGEF	A2AAJ9	1.88	-0.49	fibrogenesis
PDCD6IP	programmed cell death 6 interacting protein	Q9WU78	0.85	-0.08	fibrogenesis
S100A10	S100 calcium binding protein A10	Q3UF30	-0.89	0.09	fibrogenesis
SPARC	secreted protein acidic and cysteine rich	Q5NCU4	-1.55	0.58	fibrogenesis
TTN	titin	A2ASS6	0.73	-0.49	fibrogenesis
TTR	transthyretin	Q9D6A4	-1.34	0.09	fibrogenesis

On the contrary, epithelial adherens junction signaling (p-value = 1.18 e-06), immune response especially mediated by monocytes (p-value = 3.73 e-03) and phagocytosis (p -value = 4.44 e-03) were decreased related to controls. The two isoforms SH3 domain binding glutamate rich protein (SH3BGR and SH3BGRL3), belonging to thioredoxin like protein superfamily and involved in the redox homeostasis were also downregulated, indicating an impairment of ROS related pathways (33). The metabolism of ROS was also down-regulated (p-value = 4.43 e-03) (34). Interestingly, sirtuin signaling was severely decreased upon UV-A treatment related to controls (p-value = 2.47 e-02), suggesting an alteration of sirtuin activity and the turnover of acetylated proteins. These data agree with a recent report showing a decreased expression of the sirtuin SIRT1 in skin samples of hairless mice and in dermis fibroblasts exposed to UV-A, directed related with photoaging (10). Sirtuins are nicotinamide dinucleotide (NAD+)-dependent deacylases, able to stabilize the chromatin structure and histone diacylation and promote the repair of DNA double-strand breaks (35,36). Sirtuins may also protect against photoaging (37) by inhibiting the expression and activity of metalloproteases (MMPs) and the degradation of collagen, while their knockdown, (particularly SIRT1) increases the levels of MMP-1 and -3 (36). Overall, these results indicate that cell environment has been compromised (p-value range= 6.89 e-07 to 3.54 e-13) as suggested by an alteration of several processes for instance related to cytoskeletal assembly and organization (p-value range= 6.89 e-03 to 4.90 e-12), cell morphology (p-value range= 6.89 e-03 to 6.51 e-07), energy production (p-value range= 6.89 e-03 to 7.23 e-07) or nucleic acid metabolism (p-value range= 6.89 e-03 to 7.23 e-07).

3.2 Effect of carnosine on skin proteome evoked by UV-A exposure

The treatment by carnosine prevented almost all conditions substantially altered by single UV-A exposure. Indeed, we found a reactivation of oxidative phosphorylation (p value = 2.59 e-03) with an up regulation of Cytochrome C oxidase 6B1 (Cox6b1, log2 ratio= 1.25) and NADH ubiquinone oxidoreductase S8 (log2 ratio= 0.92), improving the functionality of mitochondria (p-value= 9.06

e-03). In addition, we observed a decrease of calcium signaling (p-value= 8.73 e-11; Figure 3B), fibrosis (p-value= 1.99e-08; Figure 6B), cell migration (p-value= 2.27 e-03) and nNOS pathway (p-value= 4.75 e-03; Figure 5B). We also found an increase of integrin-linked kinase (ILK) and actin signaling (p-value= 8.18 e-06; 2.19 e-04 respectively), epithelial adherens junctions signaling (p-value= 4.05 e-05), immune response mediated by neutrophils and leukocyte migration (p-value= 2.60 e-04), attesting the regulation of signal transduction mediated by integrins and activation of immunity system.

Carnosine treatment was able to repristinate calcium homeostasis. Proteins related to contraction and fibrotic processes such as DMD (log2 ratio= -0.85) or MYH11 (log2 ratio= -0.82) were reduced (Table 1). RYR1 (log2 ratio= -0.75), sarcoplasmic/endoplasmic reticulum calcium ATPase (2Atp2a2, log2 ratio= -0.80) and calcium/calmodulin-dependent protein kinase II subunit gamma (Camk2g, log2 ratio= -0.78) as support of calcium channel´s block (Table 1) were also significantly down-regulated. The reduction of fibrosis (Figure 6B) and the regulation of NO signaling evoked by carnosine treatment were associated with a reversion of DMD and dystroglycan 1 expression (DAG1, log2 ratio= 0.35). The cellular organization and growth were enhanced (1.09e-08 to 4.43 e-08 and 9.98 e-03 to 1.83 e-05 as p value range, respectively) as well as function and maintenance (p-value range = 7.50 e-03 to 2.55 e-05). At this regard, proteins involved in nuclear functions, energetic metabolism, or reduction of oxidative stress as well as complement factor D (CFD, log2 ratio 1.39), glyceraldehyde-3-phosphate dehydrogenase (GAPCP2, log2 ratio= 1.73) or Cox6b1 (log2 ratio= 1.25) were significantly up-regulated (34). The thioredoxin like protein superfamily (SH3BGR and SH3BGRL3) were overexpressed after carnosine treatment, showing the regulation of redox homeostasis. Overall, these data confirm the benefit of a preventive carnosine treatment on cell and skin recovery after the UV-A injury.

Note that sirtuin signaling was partially improved by carnosine acting on genes' expression such as NDUFS8 (UVA vs C log2 ratio=-1.90 vs 0.91) or NDUFA4 (log2 ratio= -0.77 vs 0.33), in

agreement with Salvayre's recent observation (12) showing that carnosine restores sirtuin activity in skin fibroblasts exposed to UV-A radiations.

Despite the use of murine model has greatly contributed also to the dermatological research, interspecies differences with humans must be considered to properly interpret the results. Among them, skin thickness, immunologic response, mechanism of contraction (38). Moreover, a recent gene array study demonstrated as the most conserved skin genes between mice and humans are related to barrier structure or function, structure (cell-to-cell junctions), cell proliferation and communication (39). Nevertheless, the use of hairless mice allowed us to mimic human skin UV-A response more accurately compared to unmodified models. Indeed, intrinsic and extrinsic skin damages to hairless mice are similar to that of humans (40,41).

4. CONCLUSIONS

In conclusion, this study describes a high-resolution mass spectrometry (MS)-based label-free quantitative proteomic analysis of UV-A exposed murine skin and the effect of carnosine. We show here that several major protein systems are altered by UV-A treatment including calcium signaling, mitochondrial function or sirtuin expression, which were all restored by a preventive treatment of the skins by a topical application of carnosine. These results suggest that proteomics alterations could result (at least in part) from ROS generated by UV-A (and inhibited by carnosine), or/and the generation of lipid oxidation products (HNE, acrolein) resulting from the peroxidation of polyunsaturated fatty acids in the irradiated skins. These agents post-translationally modify proteins by forming adducts on free amino groups and thiol residues, which progressively alters protein expression and function, and trigger inflammatory and apoptotic responses (42–46). The implication of such agents is emphasized by the potent efficacy of carnosine in restoring a normal proteomic profile of UV-A-treated skins, in accordance with its ability to neutralize the formation of adducts on proteins and their subsequent modification, thereby restoring their function (16,47). Beyond

these observations, the high sensitivity of our proteomics approach should enable future analyses of murine or human skin, to check the protective potential of agents able to prevent or delay the mechanism of photoaging.

REFERENCES

1. M. Berneburg, H. Plettenberg, J. Krutmann, Photoaging of human skin, Photodermatol. Photoimmunol. Photomed. 6 (2000) 239–244.
2. G.J. Fisher, The pathophysiology of photoaging of the skin, Cutis 75 (2 Suppl) (2005) 5–8, discussion 8-9.
3. M. Yaar, Gilchrest B.A. Aging versus photoaging: postulated mechanisms and effectors, J. Invest. Dermatol. Symp. Proc. 3 (1998) 47–51.
4. M. Zhang, T. Zhang, Y. Tang, G. Ren, Concentrated growth factor inhibits UVA induced photoaging in human dermal fibroblasts via the MAPK/AP-1 pathway, Biosci. Rep. 40 (2020) 7.
5. E.C.C. Lan, Y.T. Hung, A.H. Fang, C.S. Wu, Effects of irradiance on UVA-induced skin aging, J. Dermatol. Sci. 94 (1) (2019) 220–228.
6. J. D'Orazio, S. Jarrett, A. Amaro-Ortiz, T. Scott, UV radiation and the skin, Int. J. Mol. Sci. 14 (6) (2013) 12222–12248.
7. B.A. Gilchrest, Photoaging. J Invest Dermatol. 133 (E1) (2013) E2–E6.
8. M. Rinnerthaler, J. Bischof, M.K. Streubel, A. Trost, K. Richter, Oxidative stress in aging human skin, Biomolecules 21 (2015) 545–589.
9. K.E. Burke, Photoaging: the role of oxidative stress, G. Ital. Dermatol. Venereol.145 (2008) 445–459.
10. P. Larroque-Cardoso, C. Camar´e, F. Nadal-Wollbold, M.H. Grazide, M. Pucelle, S. Garoby-Salom, et al., Elastin modification by 4-hydroxynonenal in hairless mice exposed to UV-A. Role in photoaging and actinic elastosis, J. Invest. Dermatol. 135 (7) (2015) 1873–1881.
11. J.H. Rabe, A.J. Mamelak, P.J. McElgunn, W.L. Morison, D.N. Sauder, Photoaging: mechanisms and repair, J. Am. Acad. Dermatol. 55 (1) (2006) 1–19.
12. A. Swiader, C. Camar´e, P. Guerby, R. Salvayre, A. Negre-Salvayre, 4-Hydroxynonenal contributes to fibroblast senescence in skin photoaging evoked by UV-A radiation, Antioxidants 10 (3) (2021) 365.
13. R. Pandel, B. Polj˘sak, A. Godic, R. Dahmane, Skin photoaging and the role of antioxidants in its prevention, ISRN Dermatol 2013 (2013) 930164.
14. M.C.B. Hughes, G.M. Williams, H. Pageon, A. Fourtanier, A.C. Green, Dietary antioxidant capacity and skin photoaging: a 15-year longitudinal study, J. Invest. Dermatol. 141 (4S) (2021) 1111–1118.e2.
15. A. Altomare, G. Baron, E. Gianazza, C. Banfi, M. Carini, G. Aldini, Lipid peroxidation derived reactive carbonyl species in free and conjugated forms as an index of lipid peroxidation: limits and perspectives, Redox Biol 17 (2021) 101899.

16. G. Aldini, R.M. Facino, G. Beretta, M. Carini, Carnosine and related dipeptides as quenchers of reactive carbonyl species: from structural studies to therapeutic perspectives, Biofactors 24 (2005) 77–87.
17. G. Aldini, M. Carini, K.J. Yeum, G. Vistoli, Novel molecular approaches for improving enzymatic and nonenzymatic detoxification of 4-hydroxynonenal: toward the discovery of a novel class of bioactive compounds, Free Radic. Biol. Med. 69C (2014) 145–156.
18. N.L. Anderson, N.G. Anderson, Proteome and proteomics: new technologies, new concepts, and new words, Electrophoresis 19 (11) (1998) 1853–1861.
19. V. Dhingra, M. Gupta, T. Andacht, Z.F. Fu, New frontiers in proteomics research: a perspective, Int. J. Pharm. 299 (1–2) (2005) 1–18.
20. B. Domon, R. Aebersold, Options and considerations when selecting a quantitative proteomics strategy, Nat. Biotechnol. 28 (7) (2010) 710–721.
21. C.M. Huang, C.A. Elmets, K.R. van Kampen, T.S. De silva, S. Barnes, H. Kim, et al., Prospective highlights of functional skin proteomics, Mass Spectrom. Rev. 24 (5) (2005) 647–660.
22. B. Dyring-Andersen, M.B. Løvendorf, F. Coscia, A. Santos, L.P. Møller, A.R. Colaço et al., Spatially and cell-type resolved quantitative proteomic atlas of healthy human skin, Nat. Commun. 11 (2020) 5587.
23. G. Fredman, L. Skov, M. Mann, B. Dyring-Andersen, Towards precision dermatology: emerging role of proteomic analysis of the skin, Dermatology (2021),
24. L. Trilla-Fuertes, A. G´amez-Pozo, G. Prado-V´azquez, A. Zapater-Moros, M. Díaz-Almir´on, C. Fortes, et al., Melanoma proteomics suggests functional differences related to mutational status, Sci. Rep. 9 (1) (2019) 7217.
25. T. Agner, P. Elsner, Hand eczema: epidemiology, prognosis and prevention, J. Eur. Acad. Dermatol. Venereol. 34 (Suppl 1) (2020 Jan) 4–12.
26. E. Sz´el, R. Boz´o, ´E. Hunyadi-Guly´as, M. Manczinger, K. Szab´o, L. Kem´eny, et al., Comprehensive proteomic analysis reveals intermediate stage of non-lesional psoriatic skin and points out the importance of proteins outside this trend, Sci. Rep.9 (1) (2019) 11382.
27. A. Srivastava, E. Barth, M.A. Ermolaeva, M. Guenther, C. Frahm, M. Marz, O. W. Witte, Tissue-specific gene expression changes are associated with aging in mice, Dev. Reprod. Biol. S1672–0229 (20) (2020) 30133–30139.
28. Q. Qi, Q. Li, H. Zhu, H. Lu, X. Yang, Y. Wu, et al., Triptolide analog LLDT-8 ameliorates psoriasis-like dermatitis in BALB/c mice via suppressing the IL-36α signaling pathway, Pharmacol. Res. 169 (2021) 105678.
29. J. Cox, M.Y. Hein, C.A. Luber, I. Paron, N. Nagaraj, M. Mann, Accurate proteome wide label-free quantification by delayed normalization and maximal peptide ratio extraction, termed MaxLFQ, Mol. Cell. Proteomics 13 (9) (2014) 2513–2526.
30. S. Denda, J. Kumamoto, K. Takei, M. Tsutsumi, H. Aoki, M. Denda, Ryanodine receptors are expressed in epidermal keratinocytes and associated with keratinocyte differentiation and epidermal permeability barrier homeostasis, J. Invest. Dermatol. 132 (1) (2012 Jan) 69–75.
31. D. Degovics, P. Hartmann, I.B. N´emeth, N. ´Arva-Nagy, E. Kaszonyi, E. Sz´el, et al., A novel target for the promotion of dermal wound healing: ryanodine receptors, Toxicol. Appl. Pharmacol. 366 (2019) 17–24.

32. Carol M. Artlett and James D. Thacker.Antioxidants & Redox Signaling.May 2015.1162-1175.http://doi.org/10.1089/ars.2014.6148
33. M. Mazzocco, M. Maffei, A. Egeo, A. Vergano, P. Arrigo, R. Di Lisi, et al., The identification of a novel human homologue of the SH3 binding glutamic acid-rich (SH3BGR) gene establishes a new family of highly conserved small proteins related to Thioredoxin Superfamily, Gene 291 (1–2) (2002) 233–239.
34. Radrezza S, Carini M, Baron G., Aldini G, Negre-Salvayre A, D'Amato A., Study of Carnosine's effect on nude mice skin to prevent UV-A damage - Free Radical Biology and Medicine 2021
35. B.J. North, Verdin E. Sirtuins, Sir2-related NAD-dependent protein deacetylases, Genome Biol. 5 (5) (2004) 224.
36. S.H. Lee, J.H. Lee, H.Y. Lee, K.J. Min, Sirtuin signaling in cellular senescence and aging, BMB Rep 52 (1) (2019) 24–34.
37. L.M. Garcia-Peterson, M.J. Wilking-Busch, et al., Sirtuins in skin and skin cancers, Skin Pharmacol. Physiol. 30 (4) (2017) 216–224.
38. H.D. Zomer, A.G. Trentin, Skin wound healing in humans and mice: challenges in translational research, J. Dermatol. Sci. 90 (1) (2018) 3–12,
39. P.A. Gerber, B.A. Buhren, H. Schrumpf, B. Homey, A. Zlotnik, P. Hevezi, The top skin-associated genes: a comparative analysis of human and mouse skin transcriptomes, Biol. Chem. 395 (2014) 577–591.
40. C.F. Hung, C.L. Fang, S.A. Al-Suwayeh, S.Y. Yang, et al., Evaluation of drug and sunscreen permeation via skin irradiated with UVA and UVB: comparisons of normal skin and chronologically aged skin, J. Dermatol. Sci. 68 (2012) 135–148.
41. P.S. Peres, V.A. Terra, F.A. Guarnier, R. Cecchini, A.L. Cecchini, Photoaging and chronological aging profile: understanding oxidation of the skin, J. Photochem.Photobiol., B 103 (2011) 93–97.
42. F. Gu´eraud, M. Atalay, N. Bresgen, A. Cipak, P.M. Eckl, L. Huc, et al., Chemistry and biochemistry of lipid peroxidation products, Free Radic. Res. 44 (10) (2010) 1098–1124.
43. P. Jørgensen, L. Milkovic, N. Zarkovic, G. Waeg, S.I.S. Rattan, Lipid peroxidation derived 4-hydroxynonenal-modified proteins accumulate in human facial skin fibroblasts during ageing in vitro, Biogerontology 15 (1) (2014) 105–110.44. G. Vistoli, D. De Maddis, A. Cipak, N. Zarkovic, M. Carini, G. Aldini, Advanced glycoxidation and lipoxidation end products (AGEs and ALEs): an over-view of their mechanisms of formation, Free Radic. Res. 47 (Suppl 1) (2013) 3–27.
44. H. Zhang, H.J. Forman, 4-hydroxynonenal-mediated signaling and aging, Free Radic. Biol. Med. 111 (2017) 219–225.
46. N. Rabbani, P.J. Thornalley, Dicarbonyl stress in cell and tissue dysfunction contributing to ageing and disease, Biochem. Biophys. Res. Commun. 458 (2) (2015) 221–226.
47. A.A. Boldyrev, G. Aldini, W. Derave, Physiology and pathophysiology of carnosine, Physiol. Rev. 93 (4) (2013) 1803–1845.

IV

Lipidomics

Characterization and relative quantification of fatty acid esters of hydroxy fatty acids (FAHFAs) in human white adipose tissue of obese patients

(Confidential data: in submission)

ABSTRACT

The importance of adipose tissue in the organism wellness is now well established as well as the different lipids characteristics and properties. Among them, a new bioactive lipid class named 'fatty acid esters of hydroxyl fatty acids (FAHFAs) was recently discovered in mammalian adipose tissue and in blood plasma showing great promises for treating metabolic diseases like diabetes and obesity as well as inflammatory ones. Due to their low abundance, incorporation into triacylglycerols and presence of many regiosteroisomers, the detection and quantification is still challenge. Considering their biological importance in metabolic conditions, the first aim of this project was to develop a reliable protocol for the characterization and relative quantification through liquid chromatography-high resolution mass spectrometry (LC-HRMS) of FAHFAs in abdominal visceral and subcutaneous human white adipose tissue (WAT) of 86 individuals including obese patients (insulin sensitive or insulin resistant) vs lean subjects. Optimized procedures from sample preparation to the instrumental analysis allowed us to identify, for the first time in clinical samples, 61 FAHFAs isoforms expressed at least in the 70% of samples of which 16 significantly altered based on metabolic status and WAT subtype. For 4 of 16 the identification of regioisomer level was possible too. Further analyses are on-going to deepen the biological meaning of the significantly altered FAHFAs.

1. INTRODUCTION

White adipose tissue (WAT) is nowadays recognized not only as a passive energy depot and thermo insulation organ, but also as an active endocrine and paracrine actor in regulation of organism homeostasis. Indeed, in the past two decades, an increasing number of studies has shown its active roles in many physiological processes gaining interested as potential therapeutic target. Since its complexity as endocrine organ, adipose tissue shows properties of systemic energy regulator as well as an involvement in inflammation, organs protection and thermoregulation. On the contrary, its dysregulation is implicated in many cellular impairments (such as activation of inflammatory response, fibrosis, hypoxia, altered mitochondrial function or adipokine secretion) as well as metabolic diseases, including obesity and diabetes type 2 (T2DM) (1–3).

Obesity, reaching pandemic proportions including over 25% of the world population, has become one the most relevant metabolic health problem of our society (4,5). As consequences, other metabolic and cardiovascular diseases, chronic inflammatory status, or malignancies are increasing too. Obesity is also the primary cause of T2DM due to the development of insulin resistance in liver, white adipose tissue (WAT) and skeletal muscle (6,7). Despite its multifactorial clinical signs, obesity is mainly characterized by a WAT expansion and dysregulation (4,8). Therefore, a precise knowledge of WAT lipidome profile in healthy and obese conditions is fundamental to better understand this pathology and identify potential therapeutic targets. At this regards, AdipoAtlas database offers a complete, reliable, and free source of information about human (subcutaneous and visceral) WAT lipidome reporting over 1600 and 700 lipids species on qualitative and quantitative levels, respectively, detected in lean and obese subjects (9).

In general, high levels of circulating fatty acids are associated with diabetes and obesity. However, certain fatty acids (dietary ω-3 fatty acids, endogenous palmitoleate etc.) have positive metabolic effects partially reverting these conditions. Similarly, a new class of endogenous lipids belonging to lipokines family and called fatty acid esters of hydroxy fatty acids (FAHFAs), which are

synthesized in adipose tissue, kidney, pancreas, and serum, have shown analogous biological activities (10).

16 families of FAHFAs are known so far based on the composition of their acyl chains including a huge number of regiosteroisomers that differ by the branched ester position on the hydroxyl fatty acid (*i.e.*, palmitic-acid-9-hydroxy-stearic acid or 9-PAHSA; Figure 1) and by the number of fatty acids chains carbons (n=16-18 carbons are the most common).

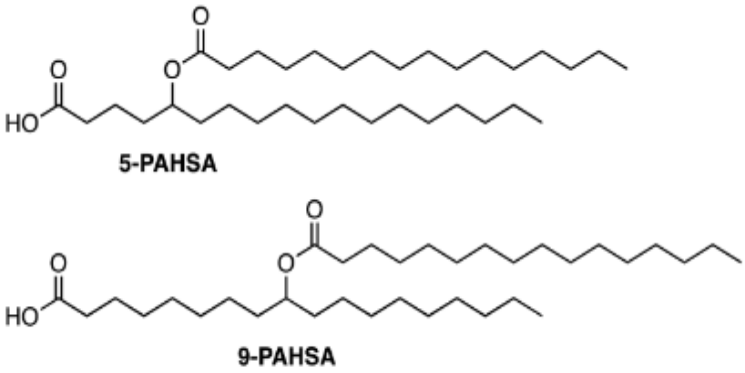

Figure 1. Example of FAHFAs´structure; palmitic-acid-5-hydroxy-stearic acid or 5-PAHSA and palmitic-acid-9-hydroxy-stearic acid or 9-PAHSA

FAHFAs' synthesis occurs in WAT and brown adipose tissue (BAT) in response to fasting conditions. On the contrary, their expression is decreased by the consumption of a high-fat diet and in insulin-resistant animals and humans. Indeed, although the precise mechanisms are still not entirely clear, the main biosynthetic pathways seem to be regulated by both GLUT4-mediated glucose uptake and carbohydrate response element-binding protein (ChREBP) by stimulation of de novo lipogenesis (DNL) and thus providing fatty acid substrates (*i.e.*, palmitate) for FAHFAs synthesis (11). From adipose tissue, FAHFAs can be exported as free-FAHFAs and, above all, incorporated into triacylglycerols (TGs) which allows their storage and then their releasing by hydrolases to cleave the FAHFAs estolide bond in a stereospecific way.

The biological importance of FAHFAs (palmitic acid esters of hydroxystearic acid or PAHSA family in particular) was demonstrated *in vivo* and in clinical studies although in FAHFAs family's dependent manner. Indeed, exogenous administration of 5-PAHSA and 9-PAHSA *in vivo*

has improved glucose tolerance increasing Glucagon-like peptide 1 (GLP-1) secretion and on insulin sensitivity binding G-protein coupled receptor 120 (GPR120) in adipocytes. Moreover, 5-PAHSA in particular seems able to impact on lipolysis and DNL resulting on the stimulation of triacylglycerol/fatty acid cycling and regulation of WAT metabolic response to cold exposure (11,12). Besides, studies on insulin-resistant models which have lower PAHSAs concentrations in serum and adipose tissue suggest that FAHFAs deficiency may contribute to metabolic diseases (10,11). Furthermore, FAHFAs, particularly 9-PAHSA and 5-PAHSA, have shown anti-inflammatory and immunomodulatory effects (13).

Increasing evidence on the physiological roles of FAHFAs motivates a more extensive characterization of these lipids as possible biomarkers and therapeutic targets for pathological conditions such as diabetes or obesity. Nevertheless, the low concentration in human tissues paired to the large structure heterogeneity of this lipids challenge their accurate identification and quantification. Moreover, the major amount of FAHFAs in cells is incorporated into triacylglycerols by esterification to the glycerol backbone, and thus TG hydrolysis step is needed to quantify FAHFAs (14).

So, considering the relevance of FAHFAs lipids class for our health status and the current analytical limitations, the main aim of this project conducted under Dr. Maria Fedorova's supervision (University of Leipzig) was to develop a reliable, reproducible, and fast methodology based on liquid chromatography-high resolution mass spectrometry (LC-HRMS) for the characterization and relative quantification of FAHFAs in human white adipose tissue of obese patients (insulin sensitive or insulin resistant) vs lean subjects.

2. MATERIAL AND METHODS

2.1 Chemicals and lipids standards

Chroloform ($CHCl_3$) and ethyl acetate (EtOAc) were purchased from Merck (KGsA, Darmstadt, Germany); methanol (MeOH), acetonitrile (MeCN), 2-propanol (*i*-PrOH) and formic acid (FA) (all ULC/MS-CC/SFC grade) were purchased from Biosolve (Valkenswaard, Netherlands); ammonium formate (NH_4HCO_2) MS grade, Triethylamine (TEA, ≥99.9%), lithium hydroxide (LiOH) and hydrochloric acid (HCl, 37%) were purchased from Sigma-Aldrich (Taufkirchen, Germany); hexane ROTISOLV® HPLC (Hex), acetone (≥99.9%) and acetic acid (CH_3COOH, 100% p.a. HPLC;) were purchased from Carl Roth (GmbH+Co. KG, Germany). Water was purified in-house (resistance >18 MΩ cm^{-1}; total organic content <10 ppb) on a PureLab Ultra Analytic System (ELGA Lab Water, Celle, Germany).

Fatty acid esters of hydroxy fatty acids (FAHFA) standards (ISTDs; 5-PAHPA, 7-PAHPA, 5-OAHPA, 7-OAHPA, 9-OAHPA, ω-OAHPA, 9-PAHPA, 5-PAHSA, 7-PAHSA, 9-PAHSA, 7-OAHSA, 10-OAHSA, (12*Z*)-10-OAHC18) were synthetized by Thierry Durand's lab (University of Montpellier, France); 5-PAHSAd9, 9-PAHSAd9, Triacylglycerols (TGs) ISTDs including TG 14:1, TG 16:1, TG 18:1, TG 20:3, TG mix (TG 6:0, TG 7:0, TG 8:0, TG 9:0, TG 10:0), and fatty acids (FAs; DHA, LA, AA, FA 18:1) were purchased from Avanti Polar Lipids Inc. (Alabaster, AL, USA).

2.2 Samples

Samples of human white adipose tissue (WAT) from 86 donors were provided by Matthias Blüher as a part of Leipzig Obesity BioBank and stored at -80 °C until the analyses. Samples corresponded to abdominal visceral (VAT) and subcutaneous (SAT) fat depots of obese insulin sensitive patients (IS, n=34; BMI > 40kg/m²), obese insulin resistant patients (IR, n=47; BMI > 40kg/m²) and lean subjects used as controls (L, n=5; BMI < 25kg/m. Tissue collection was approved by the Ethics

committee of the University of Leipzig (approval number: 159-12-21052012) and all subjects gave written informed consent before taking part in the study.

2.3 Method development

To ensure optimal FAHFAs coverage we optimized each step of the pre-analytical workflow from sample preparation to instrumental analyses using chemically defined standards, then verified using WAT lipid extract pool, and finally applied the developed protocols to the individual samples.

2.3.1 Optimization of TG-FAHFAs hydrolysis

TG esterified FAHFAs were released using LiOH hydrolysis. For method optimization a mixtures of TGs (TG 18:0, TG 21:0, TG 24:0, TG 27:0, TG 30:0, TG 42:3, TG 48:3, TG 54:3, TG 60:3; 5 µg each), FAHFAs (5-,7-PAHPA; 5-,7-,9-,ω-OAHPA; 9-, 5-,7-,9-PAHSA; 7-,10-OAHSA, (12Z)-10-OAHC18; 250 ng each), or combination of both were dried under vacuum and dissolved in $CHCl_3$:MeOH (2:1, v/v). LiOH (in water or methanol) was added to the final concentrations of 0.1 or 0.2 mol/L and samples were incubated under constant shaking (650 rpm) at room temperature, 37° C, or 42 °C. For each reaction conditions, an equivolumetric aliquots were taken after 0, 4, 6, 8, and 24h. Reaction was stopped by adding HCl (2 mol/L) and lipids were extracted using mixture of $CHCl_3$:MeOH:H_2O (2:1:1, v/v). Among others hydrolytic agents (i.e., NaOH, KOH), LiOH was selected to induce a mild alkaline hydrolysis preserving FAHFAs intact structure. After centrifugation (1000 x g, 10 min, 4°C), lower phase was collected and dried under *vacuum* (Eppendorf concentrator 5301, 5 mbar).

2.3.2 Solid phase extraction

Two solid-phase extraction (SPE) protocols were tested to enrich FAHFAs from TG containing samples. Normal phase (Strata S1-1 Silica 55 µm, 70 A, 200 mg/3mL; Phenomenex Inc.) and amino-propyl–NH_2 (Strata NH2, 55 µm, 70 A, 200 mg/3mL; Phenomenex Inc.) SPE cartridges were

conditioned with hexane (6 mL), lipids dissolved in $CHCl_3$:MeOH (2:1, v/v; 300 µL) were loaded, and the flow-through fraction was collected. Neutral lipids (NL) were washed with hexane:ethyl acetate (95:5, v/v; 6 mL), and FAHFAs were eluted with ethyl acetate (4 mL for normal phase SPE) or acetic acid in ethyl acetate (4 mL 2% v/v for the amino-propyl cartridge).

Then, to separate FAHFAs from free fatty acids (FFA) release by TG hydrolysis, C18-RP (Discovery© DSC-18, 500 mg/3 mL, Supelco) and hydrophilic lipophilic balance (HLB; 30 mg/1 mL, Oasis ©) SPE cartridges were tested. Cartridges were conditioned with 6 mL of MeCN:H_20 (1:1 v/v, containing 5 mmol/L NH_4HCO_2 and 0.1% FA, v/v). Lipids (in *i*-PrOH, 300 µL) were loaded, washed with conditioning solvent (4 mL) and gradually eluted with 10, 30, 50, 60, 70 and 100 % of solvent containing *i*-PrOH:MeCN:H_20 (85:10:5, v/v, containing 5 mmol/L NH_4HCO_2 and 0.1% FA, v/v; 4 mL each).

2.3.3 Thin layer chromatography

Dried lipids were dissolved in $CHCl_3$:MeOH (2:1 v/v; 40 µL) and separated using HPTLC on Silica gel 60 © plates (Merck KGsA, Darmstadt, Germany). Additionally, reference mixtures consisting of unprocessed lipid class specific standards were loaded on each plate to assist data interpretation. For each lipid class a TLC plates were developed using either $CHCl_3$:TEA:EtOH:H_2O (5:5:5:1 v/v; polar lipids separation) or Hex:Et_2O:HOAc (8:2:1 v/v; unpolar lipids separation) solvent mixtures. Lipids were stained using primuline (0.05% primuline in acetone/H_2O, 8:2 v/v) and images were acquired on CCD camera (Bio-Rad ChemiDoc MP, Bio-Rad; Ex: Blue Epi light illumination; Em: Filter 530/28). Densitometric analysis was performed with Image Lab (Version 5.2.1, Bio-Rad).

2.3.4 White adipose tissue (WAT) lipid extraction

For this project I received the samples corresponding to the neutral lipids fraction obtained from previous extractions conducted in the same lab starting from 50 mg of WAT (9).

The neutral lipid extracts obtained by liquid-liquid extraction (LLE) were reconstituted in 500 µL of $CHCl_3$:MeOH (2:1 v/v), moved into new vials (400 µL of 500 µL), and dried again. Once reconstituted in 240 µL of $CHCl_3$:MeOH (2:1 v/v), each sample (n=173, 169 + 4 QCs) was spiked with 5-PAHSAd9 as internal standard (200 ng in 10 µL of $CHCl_3$:MeOH 2:1 v/v), reaching 250 µL as final volume.

Lipids were re-extracted by adding H_2O (378 µL), MeOH (378 µL), and $CHCl_3$ (756 µL) and vortexed for 15 s. Afterwards, the samples were centrifuged to separate aqueous and organic phase (10 min, 4°C, 1000 x g). The bottom organic phase was collected into a new vial and dried under *vacuum*.

For the protocol validation (see *2.3.1* section) before the single samples analyses, a large pool was created mixing 20 µL of each WAT samples (n=169) after resuspension in 1800 µL $CHCl_3$:MeOH (2:1 v/v) and aliquoted. The same procedures for TG hydrolysis and FAHFAs separation and enrichment were then applied to the single samples after the re-extraction.

2.4 Targeted LC-MS/MS analysis of FAHFAs

Lipid were separated using reverse phase chromatography on a Vanquish Horizon system (Thermo Fisher Scientific, Bremen, Germany) equipped with an Accucore C18 column (150 × 2.1 mm; 2.6 µm, 150 Å; Thermo Fisher Scientific, Bremen, Germany). Gradient elution with solvent A (MeCN/H_2O, 1:1, v/v) and B (*i*-PrOH /MeCN/H_2O, 85:10:5, v/v), both containing 5 mM ammonium formate (NH_4HCO_2) and 0.1% FA (v/v) was used. Separation was performed at 50 °C with a flow rate of 0.3 mL/min using the following gradient: 0-10 min 72-77% B; 11-21 min 95% B; 21.1-26 min 72% B. Mass spectrometry detection was performed with a Q-Exactive Plus Hybrid Quadrupole-Orbitrap ™ mass spectrometer (Thermo Fisher Scientific, Bremen, Germany) equipped with a HESI probe. Mass spectra were acquired in negative mode with the following source parameters: sheath gas—40 L/min, auxiliary gas—10 L/min, sweep gas—1 L/min, spray voltage—2.5 kV, spray current—10 µA, capillary temperature—300 °C, S-lens RF level—35, and aux gas

heater temperature—370 °C. A parallel reaction monitoring (PRM) method was used at a resolution of 17.500 at m/z 200, AGC target of 2e5, and a maximum injection time of 60 ms. An isolation window for precursor selection was 1.0 m/z and a normalized collision energy (40) was used for HCD.

2.5 Data Analysis

FAHFAs lipids and related isoforms were manually identified based on the precursor, a set of specific fragments, and retention time windows using Xcalibur v 4.0.27.21. Further validation and relative quantification were performed using Skyline v. 20.2.0.343 (https://skyline.ms/project/home/software/Skyline/begin.view?). The peak boundaries were delimited and further manually corrected. Once exported, the area of each sample was normalized for the internal standard and the original amount of adipose tissue. Only transitions present in 70% of the samples in at least in two groups were considered. Finally, MetaboAnalyst v 5.0 online software (https://www.metaboanalyst.ca/) was used to perform statistical analysis.

3. RESULTS AND DISCUSSION

3.1 Hydrolysis optimization using STD mixtures

Since TGs are the major reservoir of FAHFAs, at first, we identified the optimum conditions that would release esterified FAHFAs from TGs but would not hydrolyse FAHFAs itself. To do that, we used FAHFAs and/or TGs ISTD mixtures in $CHCl_3$:MeOH (2:1 v/v) and tested the hydrolysis under the different conditions (LiOH in H_2O or MeOH; 0.1 mol/L or 0.2 mol/L; at room temperature, 37° C, or 42 °C; for 0, 4, 6, 8 and 24 hours).

Based on thin-layer chromatography (TLC) imaging and densitometry and the amount of free FA (FFA) released at each temperature (Figure 2a), LiOH 0.2 mole/L at 37 °C and 42 °C resulted in

more efficient TG hydrolysis, however leading to the significant loss of FAHFAs as well. Based on obtained results, the following parameters were selected: room temperature, 0.1 mole/L LiOH in MeOH for 24 hours.

3.2 Optimization of solid phase extraction (SPE) protocol for FAHFAs enrichment from hydrolysed TGs and potential separation from FFA

Due to low physiological abundance of FAHFAs in human tissue, SPE enrichment and potential separation of FAHFAs from FFA released by TG hydrolysis was needed. Once the hydrolysis procedure was optimized, we tested different conditions for normal phase silica-SPE (Strata S1-1 Silica) or amino-propyl (Strata NH2) solid phase extraction (SPE) for the best FAHFAs enrichment using FAHFAs and TGs ISTD pools. Then, the SPE performances were checked by TLC. With silica-cartridge the FAHFAs fraction seemed to elute together neutral lipids (NL) fraction. On the other hand, with amino-propyl cartridge FAHFAs were successfully separated from NL. Moreover, combining hydrolysis (24h, RT, LiOH 0.1 mol/L in MeOH) with SPE procedure the results were confirmed (Figure 2b). So, amino-propyl cartridge was selected for the samples' processing.

Amino-propyl-SPE protocol successfully separated FAHFAs from neutral lipids. However, elution with 2% acetic acid in ethyl acetate results in simultaneous enrichment of both FAHFAs and FFAs. Considering the low abundance of endogenous FAHFAs in adipose tissue samples and the expected large amounts of FFAs released from hydrolysed TGs, it was necessary to find the conditions allowing separation of these two lipid classes. Here, C18- reverse phase (C18-RP) and hydrophilic lipophilic balance (HLB) SPE protocols were tested for separation of FFAs STDs (DHA, LA, AA, FA 18:1; 12.5µg/each) from FAHFAs STDs (5-PAHSA and 9- PAHSA; 2.5µg/each). The obtained fractions were checked by TLCs and compared to the control pool (not processed by SPE). C18-RP SPE was efficient in separating FFAs (eluting with 60% B) and FAHFAs (eluting with 100%) lipids while a co-elution was showed with HLB cartridge (Figure 2c).

To summarize, we found the following optimum conditions to achieve a good FAHFAs enrichment and separation:

- TG esterified FAHFAs hydrolysis: 0.1 mol/L LiOH in MeOH, room temperature for 24 hours
- FAHFAs separation from hydrolysed TGs: aminopropyl-SPE cartridges, 6 mL of hexane:ethyl acetate 95:5 (v/v) to elute the NL fraction followed by 4 mL of 2% acetic acid in ethyl acetate for fraction containing FAHFAs
- FAHFAs separation from FFAs: C18-RP SPE stepping the elution from 60% to 100% (4 mL) of i-PrOH:MeCN:H_20 (85:10:5 v/v), NH_4HCO_2 5 mM in 0.1% FA

3.3 Protocol validation in WAT pool

Considering the complexity and wide dynamic range of concentrations of lipids in adipose tissue samples, protocols optimized on lipids standards were further evaluated using pooled neutral lipid extracts of human white adipose tissue (WAT) (n=169, 20 µL/each) obtained by liquid-liquid extraction (LLE) fractionation of polar and apolar AT lipids.

TG esterified FAHFAs hydrolysis and FAHFAs separation from hydrolysed TGs procedures were successfully replicated on WAT pool as previously described. Nevertheless, to a complete FAHFAs separation from FFAs the elution volume was increased (from 4 mL to 6 mL of 60% *i*-PrOH:MeCN:H_20 (85:10:5 v/v), NH_4HCO_2 5 mM in 0.1% FA) probably due to a cartridge overload for the higher lipid content in the WAT pool compared to the standards previously used. In Figure 2d some examples of endogenous FAHFAs identified in WAT pool.

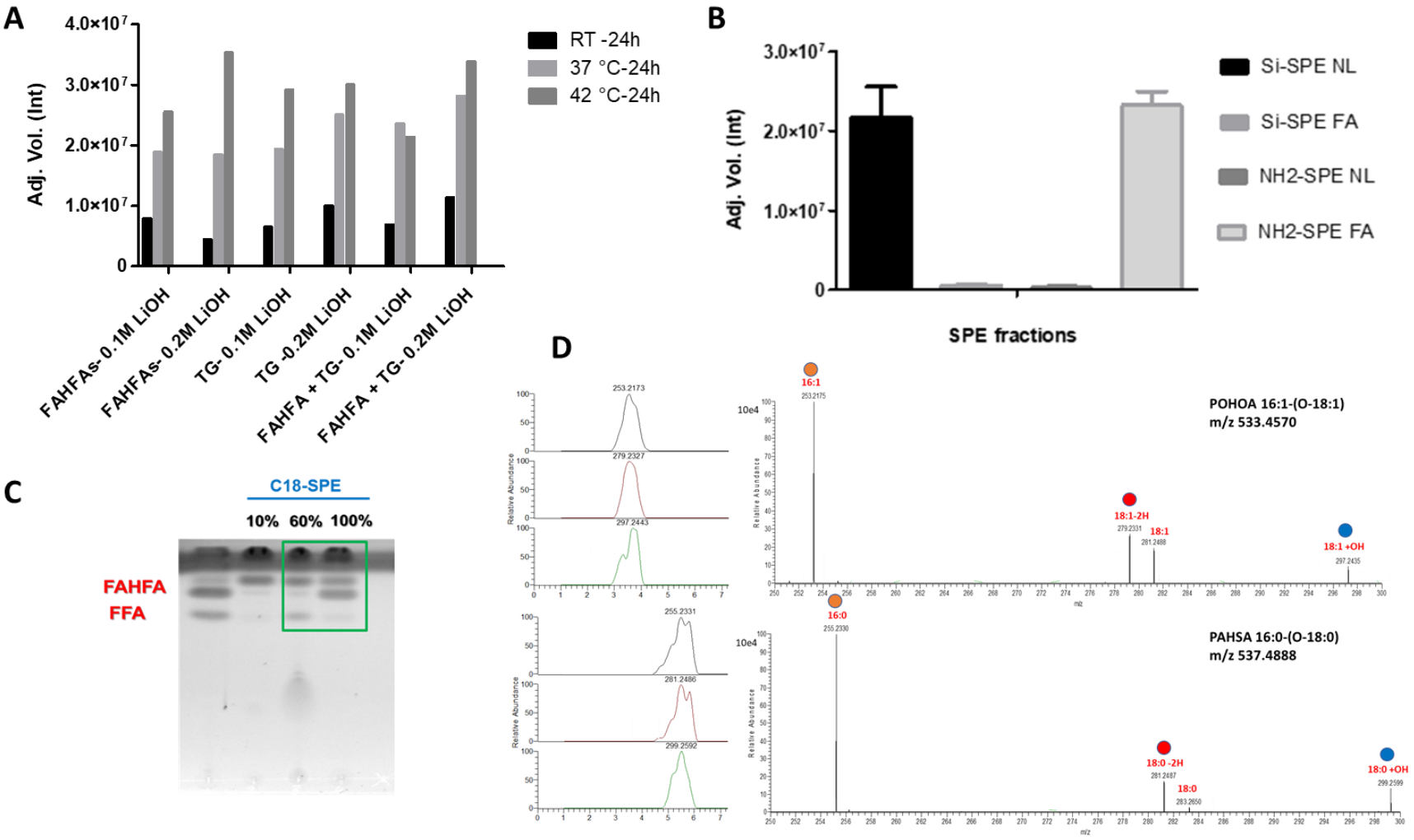
A
Adj. Vol. (Int)
4.0×10^7
3.0×10^7
2.0×10^7
1.0×10^7
0
RT -24h
37 °C-24h
42 °C-24h
FAHFAs- 0.1M LiOH
FAHFAs- 0.2M LiOH
TG- 0.1M LiOH
TG -0.2M LiOH
FAHFA + TG- 0.1M LiOH
FAHFA + TG- 0.2M LiOH
B
Adj. Vol. (Int)
3.0×10^7
2.0×10^7
1.0×10^7
0
Si-SPE NL
Si-SPE FA
NH2-SPE NL
NH2-SPE FA
SPE fractions
C
C18-SPE
10% 60% 100%
FAHFA
FFA
D
253.2173
279.2327
297.2443
255.2331
281.2486
299.2592
Relative Abundance
16:1
253.2175
18:1-2H
279.2331
18:1
281.2488
18:1 +OH
297.2435
16:0
255.2330
18:0 -2H
281.2487
18:0
283.2650
18:0 +OH
299.2599
10e4
m/z
POHOA 16:1-(O-18:1)
m/z 533.4570
PAHSA 16:0-(O-18:0)
m/z 537.4888

Figure 2. A) TLC based quantitative analysis of FFAs released upon hydrolysis of lipids standard mixtures at different temperatures using 0.1 or 0.2 mol/L of LiOH for 24 h; B) TLCs quantification analysis of FAHFAs in the separated fractions obtained from silica (Si-SPE) and amino-propyl (NH2-SPE) SPEs columns, respectively. Before SPEs procedure the lipid hydrolysis was performed at room temperature 0.1 mole/L of LiOH for 24 hours. NL= neutral lipids fraction; FA= FAHFAs containing fraction; C) TLCs analysis of fractions´ separation obtained from C18 SPEs columns that shows good FAHFAs and FFAs separations stepping the elution from 60% to 100% of i-PrOH:MeCN:H20 (85:10:5 v/v) + 5 mM NH4HCO2 in 0.1% FA; D) Examples of parallel reaction monitoring (PRM) mass confirmation spectra in WAT pool of POHOA 16:1-(O-18:1) (m/z 533.457) and PAHSA 16:0-(O-18:0) (m/z 537.488) with the corresponding fragmentation pattern showing the characteristics losses of principal FA chains (coloured dots).

3.4 Individual WAT samples analyses

The optimized and validated protocols for FAHFAs release, extraction, enrichment, and separation were then applied to the randomized single (n=169) and QCs (n=4) samples before of LC-MS/MS analyses. A parallel reaction monitoring (PRM) method was used to track lipids of interest identified as described below. Briefly, based on a public FAHFA in-silico MS/MS library (https://fiehnlab.ucdavis.edu/projects/fahfa-lipids-library; (15)) we selected and combined the most common FA chains in human AT and the related FAHFAs obtaining a starting list of 120 potential entries (unique elemental compositions). WAT pool aliquots spiked with ISTD (9-PAHSAd9) were used to verify the FAHFAs presence based on characteristics fragments identification and for the instrumental method optimization. 23 FAHFAs transitions (unique elemental compositions) were finally selected for the individual WAT sample analyses.

After the instrumental analysis, all the possible isoforms for each transition collected into FAHFA in-silico MS/MS library (15) were manually checked (Xcalibur v 4.0.27.21) in the lean samples for a total of 206 potential FAHFAs. The lean group was selected as reference since the alleged increased FAHFAs abundance compared to obese subjects. Only the isoforms identified at least in two of five samples were considered for the further analyses (n=61). Then, manual integration in Skyline for the transitions selected was applied for all samples and the area of the quantifier product (the most intense, usually those corresponded to the not-hydroxylated FA chain) exported for the normalization.

ISTD (9-PAHSAd9) quantifier product area (*m/z* 264.289) was used as normalization factor followed by the original amount of AT. 32 out of 61 FAHFAs isoforms were considered for the final analyses being present in > 70% of the samples and at least in two groups.

3.5 Data interpretation

Due to a batch effect, 39 samples have been removed for the statistical analyses (n=130 left). Comparing the abundance of the selected FAHFAs (n=32), 16 showed a significant alteration between groups (p value < 0.05; fold change >1.5). Five of them resulted up-regulated in lean subcutaneous adipose tissue (LSAT) compared to SAT of obese insulin resistant subjects (IR) and 12 showed instead an increasing in lean visceral AT (LVAT) vs VAT of obese insulin sensitive ones (IS). Opposite trend for 11 FAHFAs, downregulated in SAT of IR group respect to VAT of the same individuals supporting a different response based not only on the metabolic status (lean vs obese) but also on the type of adipose tissue (SAT vs VAT). Any statistically significant difference was demonstrated instead according to the insulin sensitivity (IR o IS group). In the Table 1 the FAHFAs significantly altered with their average concentration and standard deviation (SD) and in the Figure 3 an example of MS2 used for the identification.

Table 1. List of significantly changed endogenous FAHFAs (corrected p-value and fold change) with related concentration.

			LSAT-VS-IR-SAT		LVAT-VS-IS-VAT		IR-SAT-VS-IR-VAT	
		ng/µL (SD)	***corr p-value***	***Fold change***	***corr p-value***	***Fold change***	***corr p-value***	***Fold change***
LAHPA	18:2-(O-16:0)	2.94 (3.35)	3.56E-02	3.31			4.73E-02	-1.89
POHOA	16:1-(O-18:1)	2.65 (3.49)	3.56E-02	3.31			4.73E-02	-1.89
OAHSA	18:1-(O-18:0)	7.02 (9.76)	4.80E-02	2.89	1.67E-03	3.21	1.29E-02	-1.46
PAHPA	16:0-(O-16:0)	1.46 (1.75)	4.80E-02	2.48	4.38E-03	2.38	2.62E-02	-1.46
OAHPA	18:1-(O-16:0)	8.10 (6.95)	4.80E-02	3.06	1.18E-02	2.60	1.29E-02	-1.60
PAHSA	16:0-(O-18:0)	3.91 (4.83)			1.70E-04	2.92	4.73E-02	-1.33
SAHSA	18:0-(O-18:0)	0.48 (0.67)			4.84E-03	3.69		
PAHOA	16:0-(O-18:1)	8.43 (6.43)			1.18E-02	1.89	2.62E-02	-1.45
OAHOA	18:1-(O-18:1)	12.16 (13.26)			1.18E-02	1.93	1.29E-02	-1.47
LAHSA	18:2-(O-18:0)	20.38 (11.71)			1.18E-02	1.93	1.29E-02	-1.47
OAHLA	18:1-(O-18:2)	2.76 (3.03)			1.74E-02	1.82		
ALAHSA	18:3-(O-18:0)	4.42 (2.67)			1.74E-02	1.82		
PAHLA	16:0-(O-18:2)	3.33 (2.66)			4.86E-02	1.73		
SAHOA	18:0-(O-18:1)	0.57 (0.71)			4.86E-02	2.49		
POHSA	16:1-(O-18:0)	2.04 (2.50)					1.29E-02	-1.60
LAHOA	18:2-(O-18:1)	4.33 (2.88)					3.07E-02	-1.53

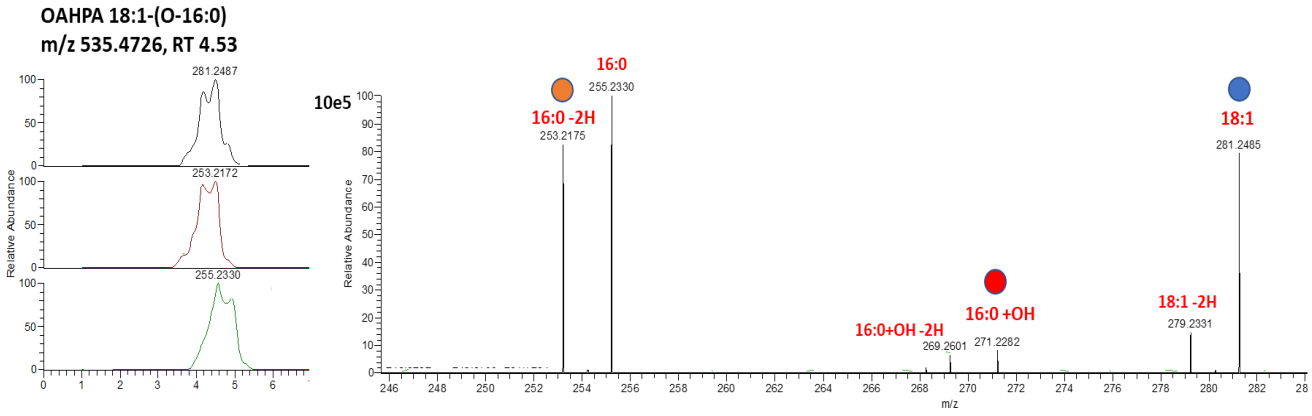

Figure 3. PRM mass spectra of OAHPA 18:1-(O-16:O) (*m/z* 535.4726) with the corresponding fragmentation pattern showing the characteristics losses of principal FA chain (18:1, blue dot). hydroxylated chain (16:0+OH, red dot) and second chain loosing $2H^+$ (16:0-2H, orange dot).

The complexity in FAHFAs research, further than their low physiological abundance and incorporation into TGs is due to their heterogeneity. Indeed, based on the composition of their acyl chains, FAHFAs are grouped into different families and each family contains multiple regiostereoisomers that differ by the branched ester position on the hydroxyl fatty acid carrying in some cases, also different biological activities (10).

Considering the importance of identify FAHFAs at regiostereoisomer level, we compared the elution and fragmentation profile of identified and significantly altered FAHFAs to our available ISTDs (see 2.1 section) previously run in single and pooled. For four of 16 significantly altered FAHFAs in our samples we found a profile match allowing us to discriminate among the regiostereoisomers. See the Table 2 for the regiostereoisomers identification and Figure 4 for an example of MS2 comparison and correlation between ISTD and endogenous FAHFA.

Table 2. Regiostereoisomers identification of 16 significantly altered endogenous FAHFAs based on co-elution with FAHFAs ISTD. In red those assigned.

Endogenous FAHFAs	Structure	m/z	Matched ISTD
PAHPA	16:0-(O-16:0)	509.4578	7-PAHPA
LAHPA	18:2-(O-16:0)	533.4575	
POHOA	16:1-(O-18:1)	533.4575	
PAHLA	16:0-(O-18:2)	533.4575	
OAHPA	18:1-(O-16:0)	535.4735	ω-OAHPA
PAHOA	16:0-(O-18:1)	535.4735	
POHSA	16:1-(O-18:0)	535.4735	
PAHSA	16:0-(O-18:0)	537.489	9- or 7- PAHSA
OAHLA	18:1-(O-18:2)	559.4752	
ALAHSA	18:3-(O-18:0)	559.4752	
LAHOA	18:2-(O-18:1)	559.4752	
OAHOA	18:1-(O-18:1)	561.4888	
LAHSA	18:2-(O-18:0)	561.4888	
OAHSA	18:1-(O-18:0)	563.5048	10-OAHSA
SAHOA	18:0-(O-18:1)	563.5048	
SAHSA	18:0-(O-18:0)	565.5201	

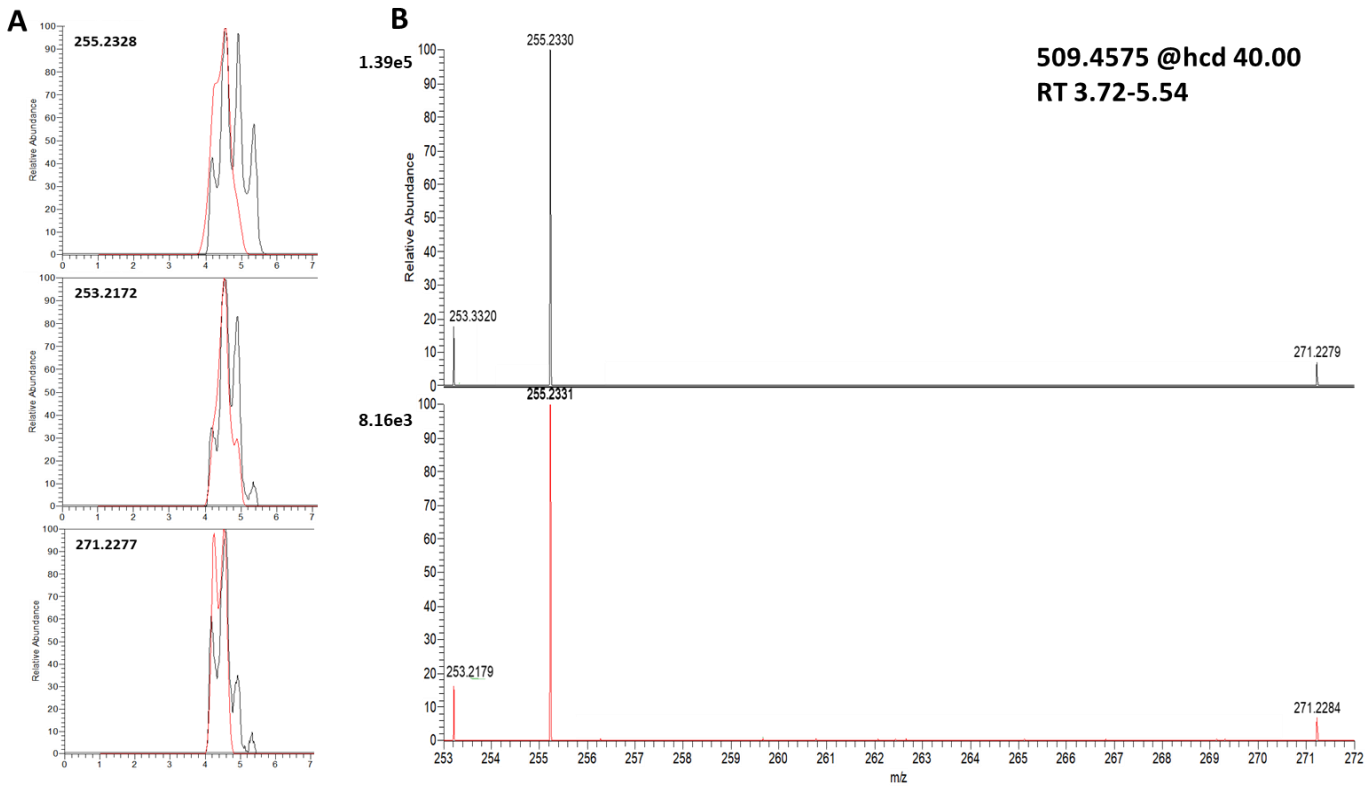

Figure 4. PRM peaks corresponding to the fragments of A) 9-, 7- and 5-PAHPA ISTDs (black) and endogenous PAHPA identified in a WAT sample (red). In B) the MS2 spectra. Based on the fragments coelution, we classified the endogenous PAHPA (*m/z* 509.457) as 7-PAHPA.

4. CONCLUSIONS

To conclude, considering the novelty and complexity of FAHFAs research (so far mainly conducted i*n vivo*), this work aimed and achieved for the first time to set up a reliable and reproducible protocol to study them in human adipose tissue giving new perspective for the treatment of metabolic diseases. Sample preparation as well as instrumental parameters were carefully considered and tested for a maximum detection coverage and reproducibility also insured by the considerable sample size (n=169). Moreover, belonging to a minor and emerging lipid class data analysis was manually curated both during method optimization and final analyses due to lack of software able to process them allowing me to gain experience to manage with a large-size dataset.

Nevertheless, despite these promising data, further biological investigations based on these results and the patients' clinical records are on-going to provide also an even better comprehension of the FAHFAs importance in human health and their potential value as biomarkers in metabolic impairments.

REFERENCES

1. Kusminski. C., Bickel. P. & Scherer P. Targeting adipose tissue in the treatment of obesity-associated diabetes. Nat Rev Drug Discov. 2016;15:639–660.
2. Sun. K., Kusminski. C. M. & Scherer PE. Adipose tissue remodeling and obesity. J Clin Invest. 2011;121:2094–2101.
3. Kusminski. C. M. & Scherer PE. Mitochondrial dysfunction in white adipose tissue. Trends Endocrinol Metab. 2012;23:435–443.
4. Blüher M. Obesity: global epidemiology and pathogenesis. Nat Rev Endocrinol. 2019;15:288–298.
5. (NCD-RisC) NRFC. Worldwide trends in diabetes since 1980: a pooled analysis of 751 population-based studies with 4.4 million participants. Lancet. 2016;9:1513–30.
6. Zhang M., Hu T., Zhang S. ZL. Associations of different adipose tissue depots with insulin resistance: A systematic review and meta-analysis of observational studies. Sci Rep. 2015;5:18495.
7. Lopes H.F., Corrêa-Giannella M.L., Consolim-Colombo F.M. EBM. Visceral adiposity syndrome. Diabetol Metab Syndr. 2016;8:40.
8. Longo M., Zatterale F., Naderi J et al. Adipose Tissue Dysfunction as Determinant of Obesity-Associated Metabolic Complications. Int J Mol Sci. 2019;20(9):2358.
9. Lange M., Angelidou G., Ni Z., Criscuolo A., Schiller J., Blüher M FM. AdipoAtlas: A Reference Lipidome for Human White Adipose Tissue. bioRxiv. 2021;
10. Yore MM., Syed I., Moraes-Vieira PM et al. Discovery of a class of endogenous mammalian lipids with anti-diabetic and anti-inflammatory effects. Cell. 2014;159:318-332.
11. Hernández-Saavedra D SK. The Regulation of Lipokines by Environmental Factors. Nutrients. 2019;11:2422.
12. Paluchova V., Oseeva M., Brezinova M. et al., Lipokine 5-PAHSA Is Regulated by Adipose Triglyceride Lipase and Primes Adipocytes for De Novo Lipogenesis in Mice. Diabetes. 2020;69:300–12.
13. Matthew J. Kolar ATNTC et al. Faster Protocol for Endogenous Fatty Acid Esters of Hydroxy

Fatty Acid (FAHFA) Measurements. Anal Chem. 2018;90:5358–5365.

14. Dan Tan., Meric Erikci, Ertunc. Srihari Konduri et al. Discovery of FAHFA-Containing Triacylglycerols and Their Metabolic Regulation. J Am Chem Soc. 2019;141.

15. Ma. Y., Kind. T., Vaniya A et al. An in silico MS/MS library for automatic annotation of novel FAHFA lipids. J Cheminform. 2015;7.

V

Integratomics

Study 1

Integratomics analysis of human dermal fibroblasts treated with low-molecular-weight hyaluronic acid (LMW-HA)

(doi.org/10.3390/molecules26165096)

ABSTRACT

Hyaluronic acid (HA) is a glycosaminoglycan very common in commercial products from pharmaceuticals to cosmetics ones due to its widespread distribution in humans and its diversified physic-chemical proprieties. Despite its extended use and preliminary evidence showing even also opposite activities to the native form, the precise cellular effects of HA at low-molecular-weight (LWM-HA) are currently unclear. The 'omics sciences currently in development offer a new and combined perspective on the cellular and organismal environment. This work aims to integrate lipidomics analyses to our previous quantitative proteomics ones for a multi-omics vision of intra- and extra-cellular impact of different concentrations (0.125, 0.25, and 0.50%) of LMW-HA (20–50 kDa) on normal human dermal fibroblasts by LC-high resolution mass spectrometry (LC-HRMS). Untargeted lipidomics allowed us to identify 903 unique lipids mostly represented by triacylglycerols, ceramides, and phosphatidylcholines. In line with proteomics analyses, LMW-HA 0.50% was the most effective concentration also in the lipidome rearrangement especially stimulating the synthesis of ceramides involved in skin hydration and reparation, cell signaling, and energy balance. Finally, integrative analyses showed 25 nodes covering several intra- and extra-cellular functions and supporting the evidence previously observed. The more complete comprehension of intra- and extra-cellular effects of LMW-HA here pointed out will be useful to further exploit its features and improve current formulations even if further studies on lipids biosynthesis and degradation are necessary.

1. INTRODUCTION

In recent decades the use and commercial value of hyaluronic acid (HA), a glycosaminoglycan constitutively present at the extracellular matrix (ECM) level, is constantly increasing in the pharmaceutical, biomedical, and cosmetics industries thanks to its several biological functions. It shows an important role in cell signaling and proliferation, ECM structural organization, tissue reparation, angiogenesis, inflammatory, and immune response (1-4). In the cosmetic field, it is widely used for anti-aging due to its enhancement of hydration, collagen stimulation, and tissue boost (5). Nevertheless, it was demonstrated as HA's biological functions and properties are strictly dependent on its molecular weight, also showing opposite effects between high-molecular-weight (HMW, if $>10^6$ Da) and low-molecular-weight (LMW, if $\leq 10^6$ Da) HA (2.6). At this regard, LMW-HA is recently becoming popular, especially in cosmetics and topical formulations due to its easier skin penetration crossing corneum stratum and epidermis than HMW-HA, resulting in skin elasticity improvement too (7-9). Despite its increasing use, the molecular action of LMW-HA is still less known. In our previous work, we showed a significant impact of 20–50 kDa LWM-HA on the proteome profile of normal human dermal fibroblasts (HDF), especially at the highest concentration (0.50% LMW-HA) (10).

Here, applying high-resolution mass spectrometry and network analyses, we focused our attention on lipidome profile changes of human dermal fibroblasts induced by the same treatment conditions (0.125, 0.25, and 0.50% LMW-HA, 24 h). The recent development of lipidomics techniques is clearly showing the importance and diversified roles of lipids in the intra- and extra-cellular functionality, including the skin layer. Indeed, lipids are far away to be only membrane raft structural components. Based on their physical and chemical properties, they are involved in many biological processes, including cell communication and differentiation, metabolism, energy balance, inflammatory and immune response (11,12). Moreover, referring to the skin, it has been shown as an alteration of lipid composition and/or organization can influence the barrier proprieties implying several skin diseases

such as atopic dermatitis or psoriasis (13). So having a lipids perspective is fundamental to provide a complete description of LMW-HA molecular effects.

Although lipid analyses boosted by advanced mass spectrometry represent a strong point also for dermatological research (14), even more is the integrative multiscale networking involving protein and lipid interactions. In this regard, our final goal was to integrate proteomics and lipidomics data offering a preliminary vision through large-scale systems biology approaches of LMW-HA effects at the cell level which can support its use and pinpoint the potential benefits in dermocosmetics.

2. MATERIALS AND METHODS

2.1 Chemicals

Primary cell line (NHDF-Ad 28887), glutamine and penicillin-streptomycin antibiotic were purchased by Lonza Bioscence (Basel, Switzerland); Dulbecco's Modified Eagle's Medium (DMEM), trypsin-EDTA (0.5% 10×), sodium piruvate were purchased by Gibco® (Thermo Fisher Scientific, Bremen, Germany); Renovyhal 20–50 kDa here referred as low-molecular hyaluronic acid (LMW-HA) was purchased by Soliance (Pomacle, France); Fetal bovine serum (FBS) and phosphate buffered saline (PBS) were purchased by Euroclone® (Milano, Italia); methanol (MeOH), acetonitrile (MeCN), 2-propanol (i-PrOH), and formic acid (FA) (all ULC/MS-CC/SFC grade) were purchased from Biosolve (Valkenswaard, Netherlands); Methyl-tert-butyl-ether (≥99%, MTBE), ammonium formate (NH4HCO2) MS grade was purchased from Sigma-Aldrich (Taufkirchen, Germany); SPLASH® LIPIDOMIX® Mass Spec Standard was purchased by Avanti Polar Lipids Inc, (Alabaster, AL, USA). Water was purified in-house (resistance > 18 MΩ cm−1; total organic content < 10 ppb) on a PureLab Ultra Analytic System (ELGA Lab Water, Celle, Germany).

2.2 Cell Culture and Treatment

The adult normal human dermal fibroblasts (NHDF-Ad 28887) were cultured as a monolayer in DMEM containing 10% FBS, 1% glutamine, and 1% penicillin-streptomycin antibiotic, at 37 °C in a humidified atmosphere of 5% CO_2 as previously described (10). Three experimental conditions were planned considering the results of cell viability assays and the usual concentrations in the cosmetic products. NHDF-Ad (7^{th} passage) seeded in T75 flasks were treated in biological duplicate with 0.125, 0.25, and 0.50% LMW-HA (w/v, in milliQ-H_2O) respectively for 24 h considering the physiological turn-over. Untreated cells were used as control. The viability of cells was evaluated using MTT reduction assay (Sigma-Aldrich) and Real-Time Glo-MT kit assay (Promega, Madison, WI, USA) as previously described (10).

2.3 Sample Preparation

Upon 24 h treatment, cells were trypsinized (3 mL of 0.05% trypsin-EDTA, v/v in PBS), transferred into tubes, counted using the automatic counter TC20™ (Bio-Rad®), pelleted in cold PBS by two cycles of centrifuging (400× g, 4 °C for 5 min) and the supernatant removed. 500 µL of antioxidant solution (0.1% w/v BHT in water) was used for the resuspension and the solution moved into a new tube followed by centrifugation (10 min, 4 °C, 1000× g) and discharge of the supernatant. The volume of solution used for the final resuspension was adjusted based on the cell count and 50 µL corresponding to around 1.50×10^5 cells taken for lipid extraction.

2.4 Lipid Extraction

Splash® Lipidomix® (5 µL) was added to 50 µL of cell suspension in 0.1% BHT in water, left on ice for 15 min and lipids were extracted using the MTBE standard protocol (15). All solvents contained BHT (0.1% w/v) and were cooled on ice before use. Briefly, 375 µL of MeOH were added to each sample and vortexed for 5 s. Then, 1250 µL of MTBE was added, followed by 5 s vortex and incubation (1 h, 4 °C, 210 rpm). The phase separation was induced by adding 315 µL of H2O, vortex

for 5 s and 10 min of incubation (4 °C, 210 rpm). Once centrifugated (4 °C, 10 min. 2000× g), the upper phase was collected into a new tube, dried under *vacuum* (Eppendorf concentrator 5301, 1 mbar). Before the LC-MS analyses, lipids extracts were dissolved in 100 µL i-PrOH and vortexed. Total quality control samples (QCs, n = 4) were obtained mixing 10 µL each and group pool samples mixing 10 µL of 2 replicates for a total of 16 samples (n = 4, *i.e.*, Ctrl A_B, LMW-HA 0.125% A_B, LMW-HA 0.25% A_B, LMW-HA 0.50% A_B).

2.5 Mass Spectrometry

Lipid were separated using reverse phase chromatography on a Vanquish Horizon system (Thermo Fisher Scientific, Bremen, Germany) equipped with an Accucore C18 column (150 × 2.1 mm; 2.6 µm. 150 Å; Thermo Fisher Scientific, Bremen, Germany). Gradient elution with solvent A (MeCN/H2O, 1:1. v/v) and B (i-PrOH /MeCN/H2O, 85:10:5. v/v), both containing 5 mM ammonium formate (NH_4HCO_2) and 0.1% FA (v/v) was used. Separation was performed at 50 °C with a flow rate of 0.3 mL/min using the following gradient: 0–20 min 10–86% B; 20.1–22 min 86–95% B; 22.1–26 min 95% B; 26.1–34 min 10% B. Mass spectrometry detection was performed with a Q-Exactive Plus Hybrid Quadrupole-Orbitrap mass spectrometer (Thermo Fisher Scientific, Bremen, Germany) equipped with a HESI probe. Mass spectra were acquired in positive and negative mode with the following source parameters: sheath gas, 40 L/min; auxiliary gas, 10 L/min; sweep gas, 1 L/min; spray voltage 3.5 kV (−2.5 kV); spray current 10 µA; capillary temperature 300 °C; S-lens RF level 35 and aux gas heater temperature 370 °C.

Full MS spectra were acquired at a resolution setting for m/z 200 at 140,000, scan range 380–1200 m/z (negative), and 250–1200 m/z (positive), automatic gain control (AGC) target 1e6 counts, maximum injection time (IT) 100 ms, MS/MS spectra were acquired applying a data-dependent acquisition (DDA, top 15) method was used at a resolution of 17,500 at m/z 200, AGC target of 2e5, and a maximum IT of 60 ms. An isolation window for precursor selection was 1.2 m/z and a stepped collision energy (CE 10-20-30) was used for HCD.

2.6 Data Analysis

Lipids identification strategy was based on merged results obtained by LipidHunter 2 RC_3 (https://github.com/SysMedOs/lipidhunter) (16), LipoStar (version 1.3.2 × 64, Molecular Discovery, Hertfordshire, UK) (17) and MSDial (http://prime.psc.riken.jp/compms/msdial/main.html) (18) followed by manual annotation in Skyline v. 20.2.0.343. Relative quantification was based on the determination of area under the curve (AUC) for each lipid correctly identified then normalized by AUC of the used ISTD to the corresponding lipid species and original the cell number. Then, MetaboAnalyst v 5.0 online software (https://www.metaboanalyst.ca/) was used to perform statistical analyses (19).

Finally, integratomics analyses between lipidomics and previously obtained proteomics data (10) were done through Ingenuity Pathways Analysis software (IPA, Qiagen, last release). Briefly, each of the significantly altered lipids was assigned to an ID corresponded to KEGG (Kyoto Encyclopaedia of Genes and Genomes), HMDB (Human Metabolome Database), PubChem, or ChEBI (Chemical Entities of Biological Interest) database. Based on the ID frequency matches, we selected HMDB as the source for the integration. Protein's gene name and related log2 ratio were then included for the final input database (See Table S3 in Radrezza et al. 2021 (20) for the complete list).

3. RESULTS AND DISCUSSION

Label-free proteomics analyses conducted in our previous study showed a significant alteration of human dermal fibroblasts proteins profile induced by LMW-HA, mainly at 0.50% of concentration (Table 1A) (10). Indeed, proteins representing pathways such as cell proliferation and growth, extracellular matrix reorganization, proteoglycans biosynthesis, mitochondrial activity, cell adhesion, or wound healing were significantly upregulated. At the highest concentration (0.50%), LMW-HA also induced moderate upregulation of proteins involved in immune responses and inflammation processes, however, without any impact on overall cells viability. Lipid metabolism-related proteins,

such as ADP-ribosylation factor 1-3 (ARF1-3; log2 FC= 5.42), Sterol Carrier protein 2 (SCP2; log2 FC= 2.11), Basement membrane-specific Heparan Sulfate Proteoglycan core protein (HSPG2; log2FC 2.97) and Hexosaminidase Subunit Beta (HEXB; log2 FC= 1.94) were also influenced by the treatment with 0.50% LMW-HA inducing an up-regulation.

Table 1. (A) Summary of detected, filtered, and significantly altered features in lipidomics and proteomics analyses (10); * unique by structure, ** Volcano plot; FC > 2, p value < 0.05; (B) Total identified lipids at bulk and structure level divided by classes; CE = cholesterol esters, Cer = ceramides, Hex1- Hex2Cer = 1-2-hexosylceramide, SM = sphingomyelin, TG = triacylglycerols, DG = diacylglycerols, PC = phosphatidylcholines, LPC = lyso-phosphatidylcholines, PE = phosphatidylethanolamines, LPE = lyso-phosphatidylethanolamines, PI = phosphatidylinositols, PG = phosphatidylglycerol, PS = phosphatidylserine.

A			
	Conditions	***Lipidomics***	***Proteomics***
Identified features*		903 (694 in Pos)	2328
Significantly altered**	**0.50 % LMW-HA vs C**	433	495
	0.25 % LMW-HA vs C	/	149
	0.125 % LMW-HA vs C	/	39
B			
Class	***Bulk (n)***	***Unique by elemental composition (n)***	***%***
CE	27	27	3.0
Cer	54	109	12.1
Hex1Cer	21	56	6.2
Hex2Cer	6	12	1.3
SM	26	26	2.9
TG	116	408	45.2
DG	31	56	6.2
PC	40	102	11.3
LPC	3	3	0.3
PE	32	75	8.3
LPE	4	4	0.4
PI	11	12	1.3
PG	3	3	0.3
PS	10	10	1.1
Tot	**384**	**903**	100

Based on these results here we extended our study to access the effect of LMW-HA on cellular lipidome with the aim to support multi-omics data integration.

3.1 Untargeted Lipidomics Profiling

Untargeted lipidomics analyses supported detection of 1380 lipids and the subsequent manual identification of 903 lipid molecular species (Table 1), of which triacylglycerols (TGs), ceramides (Cers), and phosphatidylcholines (PCs) represented 45.2, 12.1 and 11.3% of identified lipidome, respectively.

Analysing the general lipidome profile, 563 out of 903 features were significantly altered upon treatment with LMW-HA (one-way ANOVA, adjusted p-value < 0.05, post-hoc analyses using Fisher's LSD). Moreover, principal component analysis (PCA) showed a clear cluster separation between cells treated with 0.50% LMW-HA and the remaining (controls, 0.125 and 0.25% LMW-HA groups) (Figure 1A). Insignificant differences instead between 0.125% LMW-HA vs controls and 0.25% LMW-HA vs controls based on the two-sample t-test and Wilcoxon rank sum test ($p < 0.05$) was observed suggesting a significant cellular effect related only to the 0.50% LMW-HA as previously shown by the proteomics analyses (10, 20). In the box plot charts and hierarchical heatmap (Figure 2) the definite 0.50% LMW-HA effect compared to the other groups on lipidome is well represented. Among the treatment conditions investigated, 0.50% LMW-HA led to significant changes in cells lipid composition, therefore only these results are here discussed. See Table S1-S2 in Radrezza et al. 2021 (20) for the complete lists of identified and significantly altered lipids.

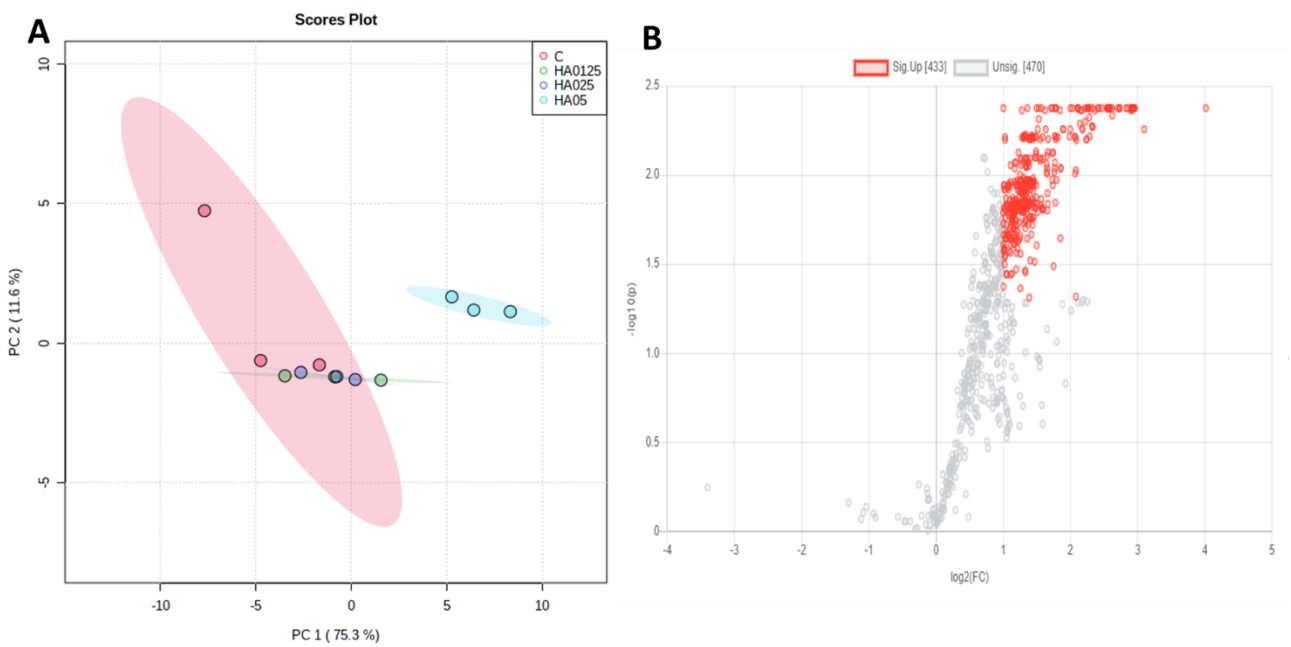

Figure 1. A) Scoring plots reconstructed using PCA (PC1 vs. PC2). The red group corresponds to the control samples; green to those treated with 0.125% LMW-HA; violet to 0.25% LMW−HA and light blue to 0.50% LMW−HA treatment group; B) Volcano Plot of LMW−HA 0.5% vs C. In red the features significantly altered (fold change (FC) > 2, Adjusted *p*-value < 0.05.

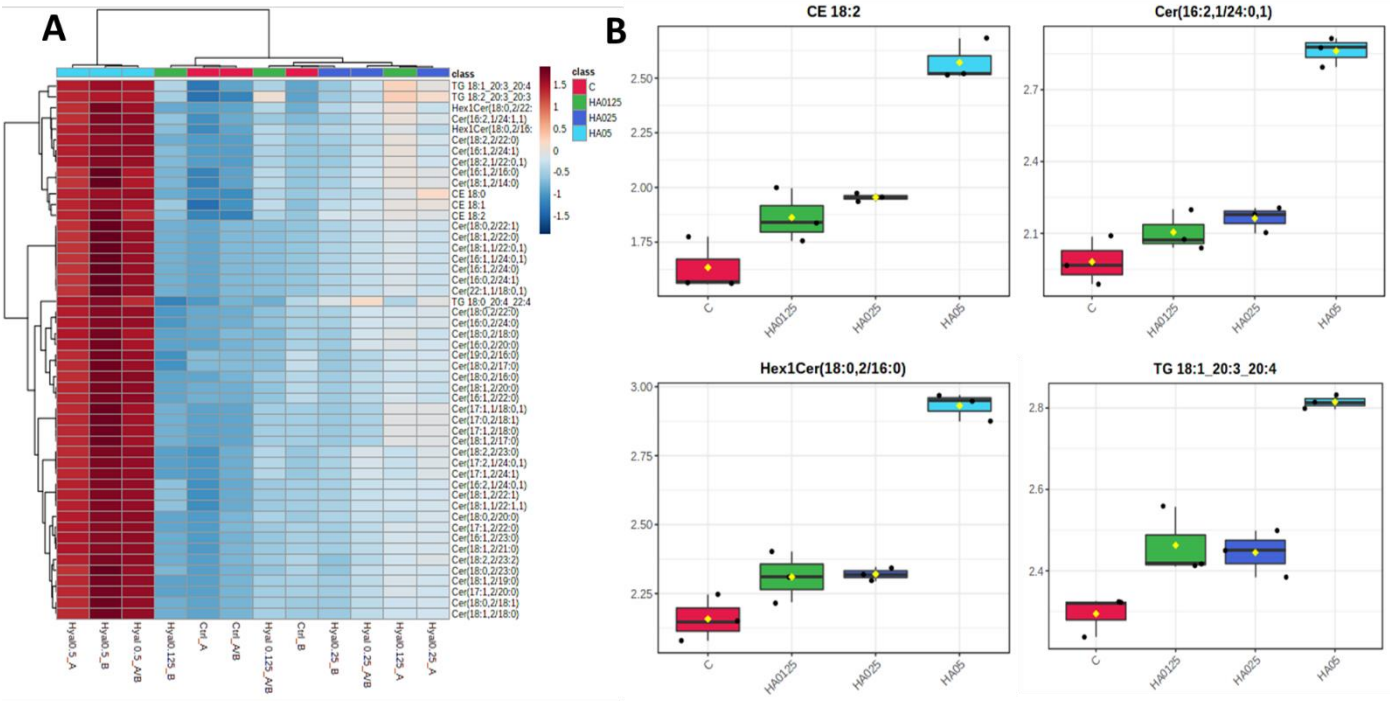

Figure 2. A) Hierarchical clustering heatmap of the 50 most significant altered lipids (one-way ANOVA and post-hoc analysis, $p < 0.05$) of all four groups. In red, the more expressed and related to the 0.50% LMW−HA group. Each coloured cell on the map corresponds to a concentration value (in red those more expressed, in dark blue those with the lowest value) with samples in the rows and

features in the columns; B) box plot charts for representative altered lipids belonging to the main classes driving by one-way ANOVA (adjusted *p*-value (FDR) cut-off 0.05).

The 0.50% LMW-HA treatment induced a significant alteration (log2 fold change >1) of 433 features (out of 903, 47.95%; Figure 1B) belonging to triacylglycerols (TG; n = 257), ceramides (Cer; n = 105), hexosylceramides (Hex1Cer; n = 39), cholesterol esters (CE; n = 4), diacylglycerols (DG; n = 13) and sphingomyelin (SM; n = 7) vs controls. Similar increasing but not significant for 0.125% and 0.25% LMW-HA treatments. On the contrary, phospholipids classes *i.e.*, phosphatidylcholines (PC), lyso-phosphatidylcholines (LPC), phosphatidylethanolamines (PE), lyso-phosphatidylethanolamines (LPE), phosphatidylinositols (PI), phosphatidylglycerols (PG) and phosphatidylserines (PS) were not statistically altered (n = 470. p > 0.05, FC < 1), except for LPC(18:0), LPE(18:0), PI(18:1_20:4) and five PS(PS 16:0_18:1, PS 18:0_18:1, PS 18:0_20:4, PS 18:0_22:6 and PS 18:1_18:1).

Among those most differentially regulated by the treatment we found lipids belonging to cholesterol esters class such as CE (18:0) (log2 FC = 4.01) or CE (18:2) (log2 FC = 3.09) (Figure 2B). Indeed, the major hyaluronan receptor (*i.e.,* CD44) has demonstrated to induce keratinocyte differentiation and synthesis of cholesterol, precursor of CEs (21).

Further than CEs, there was an increasing of several ceramides and Hex1Cer including Cer(16:1, 2/23:0) (log2 FC = 2.96) (Figure 2B), Cer(18:1,2/21:0) (log2 FC = 2.94), Hex1Cer(18:0,2/22:0) (log2 FC = 2.73) (Figure 2B) or Hex1Cer(18:0,2/16:0) (log2 FC = 2.55).

Among the lipid classes in the skin, sphingolipids and ceramides are among the most important functional molecules at the stratum corneum and deeper fibroblasts layer and playing a crucial role in the formation and maintenance of the skin barrier integrity (22-24). Moreover, ceramides are necessary to link corneocytes into a waterproof barrier and enhance skin hydration that has an impact on cell morphology at the surface and deeper layers of the epidermis.

Sphingolipid composition can influence the identity, transition path and lipid metabolic pathway in the establishment of wound repair of fibroblasts (24). Nevertheless, being their activity depended on cell type and belonged subclasses, sphingolipids were further classified according to their structure

obtaining 43 (41%) non-hydroxy-sphingosine-ceramides, 26 (25%) sphingadienine-ceramides, 19 (18%) dihydro-ceramides, 10 (10%) phyto-ceramides, 6 (6%) deoxy-ceramides, and one (1%) dihydro-deoxy-ceramides, in line with what previously demonstrated (22.25).

Further than sphingolipids, 0.50% LMW-HA also induced an increase in TGs expression. The metabolism of TGs was observed to be influential in epidermal differentiation and in the skin's barrier function, such as permeability (26). Despite their role in softness and skin's barrier functionality, the general increase of ceramides and triacylglycerols could also suggest deposition of lipid droplets that, at a certain level, can induce detrimental effects. Accumulation of TGs is often a way for the cells to get rid of an excess of toxic free fatty acids too. Therefore, more focused researches on lipid droplets' accumulation and a potential increasing of fatty acids synthesis in the condition under study are needed in the future.

3.2. Network Analyses Based on Integratomics

Although separated proteomics and lipidomics analyses allowed us to understand the cellular LWM-HA effects, integrating them in a multi-omics description provided an even further comprehension about its impact. To do that, we matched the significantly altered proteins (*n*= 495) and lipids by 0.50% LMW-HA treatment using Ingenuity Pathways Analysis software (IPA). In total, 344 of 433 significantly altered lipids in the 0.50% LMW-HA group vs control were associated to the corresponding ID, needed for the integration, consulting genomic and molecular database such as KEGG, HMDB, PubChem, or ChEBI.

Twenty-five networks including 26 lipids belonging to different classes were found covering several intra- and extra-cellular functions, including lipids, vitamins and mineral metabolisms, cell signaling, and molecular transport (20).

Among all, integratomics analyses sustained a noticeable mitochondrial activity with LWM-HA 0.50%, in line with the previous proteomics analyses (10). Indeed, as showed in Figure 3A, we observed an up-regulation of respiration and energy providing proteins, including cytochrome C

(CYCS) that plays an important role in cellular respiration, aspartate aminotransferase (GOT2) implied in the metabolite exchange and in the long-chain free fatty acids uptake, ADP/ATP translocase 3 (SLC25A6) required for the accumulation of coenzyme A in the mitochondrial matrix and mannose-specific lectin (LMAN1) involved in the sorting or recycling of proteins, lipids, or both. As involved lipids, we found cholesteryl oleate (CE (18:1(9Z))), D-erythro-C16-ceramide (Cer(d18:1/16:0)) and sphingomyelin SM(d18:1/18:0), all increased and with a role on cell signaling and differentiation, membrane stabilizer, energy storage and lipids transport. In addition, it was shown as ceramide synthesis is enhanced along with the rate of keratinocyte differentiation both in vitro and in vivo, supporting our hypothesis of induction of fibroblast maturation by the treatment (7). Among their roles, intracellular ceramides act as the second messenger with pro-apoptotic functions in several tissues and cells as demonstrable by the modulation of related genes. Among them, we found MAT2B and CSPG4, both involved in cell proliferation pathways, CYCS also involved in cell death pathways, and apoptosome, a proteic complex needed for the apoptosis trigger (Figure 3A). Moreover, we saw a down-expression of SERPINB2, a negative regulator of apoptosis, related to the tumor necrosis factor (TNF) pathway, also involved in the process as an apoptotic enhancer **(**Figure 3B). In the skin, this activity could be explained as a self-renewal process applied to the regulation of keratinocyte proliferation/differentiation balance by exerting anti-proliferative and pro-apoptotic effects (27). Apoptosis in human fibroblasts is also related to the contractility of the extracellular matrix (28). In our case, the integratomics data also showed that LMW-HA 0.50% induced a fine, regulated apoptosis with a negative overall score associated with this pathway (z score = −2.23), supporting the hypothesis of controlled apoptosis.

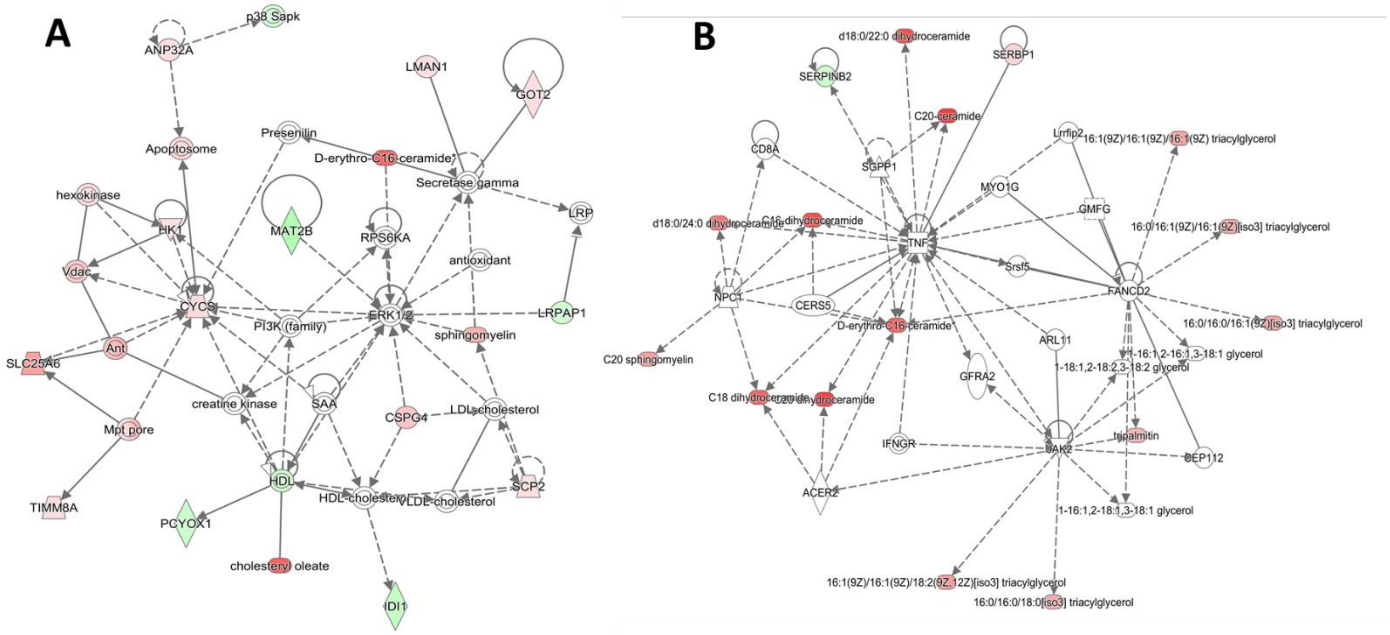

Figure 3. Networking between significantly altered proteins and lipids by LMW-HA 0.50% related to **A)** mitochondrial activity and **B)** inflammation.

The moderate activation of TNF-mediated inflammation in response to the treatment previously showed by proteomics was also confirmed in lipidomics (Figure 3B), involving several lipids belonging to Cers, TGs, and SMs classes such as Cer(d18:0/18:0), TG(16:0/16:0/18:0) or SM(d18:1/20:0) (in the figure referred respectively as C18 dihydroceramide, 16:0/16:0/18:0(iso3) triacylglycerol and C20 sphingomyelin). In this case, ceramides and their derivatives have been largely investigated in the context of inflammation and immune response. In fact, several inflammatory cytokines, including TNF-alpha, have been implicated in the regulation of ceramides production.

Hence, considering their diversified roles, the equilibrium between ceramide synthesis and degradation is essential for maintaining epidermal renewal and normal homeostasis. Indeed, an excessive accumulation may cause harmful inflammation and damages as, for example, UV-induced ones (29). At the same time, upregulation of SREBP1 was observed (Figure 3B). SREBP1 can promote the resolution of inflammatory responses by inducing enzymes that synthesize suppressive

unsaturated fatty acids supporting a good balance in the inflammation and the overall cell wellness (30,31).

Further than mitochondrial activity and moderate inflammation, integratomics showed a lipids involvement in networks related to cell signaling, mobility, and transcription regulation cells proliferation and peroxisomal beta-oxidation pathway of fatty acids (20). In the transcription one, as involved lipids, we found an up-regulation of Cer(d18:1/24:0), Cer(d18:1/22:0), and PC (16:0/22:0) all acting also in the cell signaling pathway. Moreover, as proteins related to lipids, we saw a down-regulation of Platelet Activating Factor Acetylhydrolase 1b Catalytic Subunit 2 (PAFAH1B2) with a rule in lipid degradation, Mesoderm Development LRP Chaperone (MESD) that binds low-density lipoprotein receptors.

Up-regulated proteins are also linked to cell reorganization, proliferation, and transcription, such as Dynein light chain 1 (DYNLT1), active in the actin cytoskeleton regulation, and Acidic leucine-rich nuclear phosphoprotein 32 family member P (ANP32P), while multifunctional proteins are also involved in cell proliferation, cell cycle progression, and transcription. As acting lipids in cell proliferation network, we found CE(18:0), Cer(d18:1/18:0), and LysoPC(18:0/0:0) all up-regulated and mainly involved in energy storage, membrane stabilization, and cell signaling processes. As proteins related to lipid processing, we saw a down-regulation of IAH1, operating in lipid degradation.

In the end, despite having sparse connections in the beta-oxidation network, we found an up-regulation of PC(14:0/20:4), PC(16:0/18:3), PC(18:2/20:4), SM(d18:1/22:0), and Cer(d18:1/23:0) acting in the network centered on PPARG that controls the peroxisomal beta-oxidation pathway of fatty acids and is a key regulator of adipocyte differentiation and glucose homeostasis. Up-regulation also of MGLL, a protein related to the conversion of monoacylglycerides to free fatty acids and glycerol.

4. CONCLUSIONS

To conclude, this study highlights as both proteome and lipidome of normal human dermal fibroblasts are influenced by low-molecular-weight hyaluronic acid, in particular at 0.50% of concentration. Moreover, to our knowledge, this is the first study that describes LMW-HA in *vitro* effects combining proteomics and lipidomics analyses in a multi-omics approach. The previous proteomics results (10) were not only confirmed but also corroborated by lipidomics and integratomics ones. Indeed, mitochondria functionality, cells maturation, and lipids metabolism were demonstrated as well. About lipidome changes, we saw a particular increase of ceramides, hex-ceramides, triacylglycerols and cholesterol esters involved in the skin moisturizing and epidermis renewal, supporting the beneficial role of low-molecular-weight as a cosmetic ingredient. Nevertheless, the correct balance between their synthesis and metabolism is essential for skin wellness, and further studies aim to verify the lipids droplets and the increasing of toxic free fatty acids hypotheses are necessary.

5. REFERENCES

1. Fallacara. A., Baldini. E., Manfredini. S., Vertuani. S. Hyaluronic acid in the third millennium. Polymers 2018. 10. 7

2. Snetkov. P., Zakharova. K., Morozkina. S., Olekhnovich. R., Uspenskaya. M. Hyaluronic acid: The influence of molecular weight on structural. physical. physico-chemical. and degradable properties of biopolymer. Polymers 2020. 12. 1800.

3. Ciccone. V., Zazzetta. M., Morbidelli. L. Comparison of the effect of two hyaluronic acid preparations on fibroblast and endothelial cell functions related to angiogenesis. Cells 2019. 8. 1479

4. Jiang. D., Liang. J., Noble. P.W. Hyaluronan in tissue injury and repair. Annu. Rev. Cell. Dev. Bio. 2007. 23. 435–461

5. Bukhari. S.N.A., Roswandi. N.L., Waqas. M., Habib. H., Hussain. F., Khan. S., Sohail. M., Ramli. N.A., Thu. H.E., Hussain. Z. Hyaluronic acid. a promising skin rejuvenating biomedicine:

A review of recent updates and pre-clinical and clinical investigations on cosmetic and nutricosmetic effects. Int. J. Bio. Macromo. 2018. 120. 1682–1695

6. Cyphert. J.M., Trempus. C.S., Garantziotis. S. Size Matters: molecular weight specificity of hyaluronan effects in cell biology. Int J Cell Biol. 2015. 2015. 563818

7. Cilurzo. F., Vistoli. G., Gennari. C.G.M., Selmin. F., Gardoni. F., Franze. S., Campisi. M., Minghetti. P. The role of the conformational profile of polysaccharides on skin penetration: the case of hyaluronan and its sulfates. Chem. Bio. 2014. 11. 551–561

8. Pavicic. T., Gauglitz. G.G., Lersch. P., Schwach-Abdellaoui. K., Malle. B., Korting. H.C., Farwick. M. Efficacy of cream-based novel formulations of hyaluronic acid of different molecular weights in anti-wrinkle treatment. J. Drugs Dermatol. 2011. 10. 990–1000.

9. Essendoubi. M., Gobinet. C., Reynaud. R., Angiboust. J.F., Manfait. M., Piot. O. Human skin penetration of hyaluronic acid of different molecular weights as probed by Raman spectroscopy. Skin Res. Tec. 2016. 22. 55–62

10. Radrezza. S., Baron. G., Nukala. S.B., Depta. G., Aldini. G., Carini. M., D'Amato. A. Advanced quantitative proteomics to evaluate molecular effects of low-molecular-weight hyaluronic acid in human dermal fibroblasts. J. Biopharm. Biomed. Anal. 2020. 185. 113199

11. Sezgin. E., Levental. I., Mayor. S., Eggeling. C. The mystery of membrane organization: composition. regulation and roles of lipid rafts. Nat. Rev. Mol. Cell Bio. 2017. 18. 361–374

12. Storck. E.M., Ozbalci. C., Eggert. U.S. Lipid cell biology: A focus on lipids in cell division. annual review of biochemistry. 2018. 87. 839–869

13. Sjovall. P., Skedung. L., Gregoire. S., Biganska. O., Clement. F., Luengo. G.S. Imaging the distribution of skin lipids and topically applied compounds in human skin using mass spectrometry. Sci. Rep. 2018. 8. 16683

14. Gruber. F., Kremslehner. C., Narzt. M.S. The impact of recent advances in lipidomics and redox lipidomics on dermatological research. Free Radic. Bio. Med. 2019. 144. 256–265.

15. Matyash. V., Liebisch. G., Kurzchalia. T.V., Shevchenko. A., Schwudke. D. Lipid extraction by methyl-tert-butyl ether for high-throughput lipidomics. J. Lipid Res. 2008. 49. 1137–1146.

16. Ni. Z.X., Angelidou. G., Lange. M., Hoffmann. R., Fedorova. M. LipidHunter Identifies Phospholipids by high-throughput processing of LC-MS and shotgun lipidomics datasets. Anal. Chem. 2017. 89. 8800–8807

17. Goracci. L., Tortorella. S., Tiberi. P., Pellegrino. R.M., Di Veroli. A., Valeri. A., Cruciani. G. Lipostar. a Comprehensive platform-neutral cheminformatics tool for lipidomics. Anal. Chem. 2017. 89. 6258–6265

18. Tsugawa. H., Cajka. T., Kind. T., Ma. Y., Higgins. B., Ikeda. K., Kanazawa. M., VanderGheynst. J., Fiehn. O., Arita. M. MS-DIAL: Data-independent MS/MS deconvolution for comprehensive metabolome analysis. Nat. Methods 2015. 12. 523–526

19. Chong. J., Wishart. D.S., Xia. J. Using MetaboAnalyst 4.0 for comprehensive and integrative metabolomics data analysis. Curr. Protoc. Bioinforma. 2019. 68. e86

20. Radrezza. S., Aiello. G., Baron. G., Aldini. G., Carini. M., D'Amato. A. Integratomics of Human Dermal Fibroblasts Treated with Low Molecular Weight Hyaluronic Acid. Molecules 2021.*26*. 5096

21. Kage. M., Tokudome. Y. Hyaluronan tetrasaccharides stimulate ceramide production through upregulated mRNA expression of ceramide synthesis-associated enzymes. Arch. Dermatol. Res. 2016. 308. 95–101

22. Luczaj. W., Wronski. A., Domingues. P., Domingues. M.R., Skrzydlewska. E. lipidomic analysis reveals specific differences between fibroblast and keratinocyte ceramide profile of patients with psoriasis vulgaris. Molecules 2020. 25. 630

23. Coderch. L., Lopez. O., de la Maza. A., Parra. J.L. Ceramides and skin function. american journal of clinical Dermatology 2003. 4. 107–129

24. Capolupo. L., Khven. I., Mazzeo. L., Glousker. G., Russo. F., Paz Montoya. J., Ho. S., Bhandari. D., R., Bowman. A.P., et al. Sphingolipid control of fibroblast heterogeneity revealed by single-cell lipidomics. Biorxiv. 2021

25. Morales. A., Lee. H., Goni. F.M., Kolesnick. R., Fernandez-Checa. J.C. Sphingolipids and cell death. Apoptosis 2007. 12. 923–939

26. Radner. F.P.W., Fischer. J. The important role of epidermal triacylglycerol metabolism for maintenance of the skin permeability barrier function. Biochim. Et Biophys. Acta-Mol. Cell Bio. Lip. 2014. 1841. 409–415

27. Mizutani. Y., Sun. H., Ohno. Y., Sassa. T., Wakashima. T., Obara. M., Yuyama. K., Kihara. A., Igarashi. Y. Cooperative synthesis of ultra long-chain fatty acid and ceramide during keratinocyte differentiation. Plos One 2013. 8. e67317

28. Fluck. J., Querfeld. C., Cremer. A., Niland. S., Krieg. T., Sollberg. S. Normal human primary fibroblasts undergo apoptosis in three-dimensional contractile collagen gels. J. Investig. Dermatol. 1998. 110. 153–157

29. Yang. K., Gao. B.A., Ming. X.J., Huang. Z.P., Wang. M.H., Dong. J.B., Wang. J.X. Synthesis and evaluation of xanthone derivatives as acid sphingomyelinase inhibitors: Potential treatment for UV-induced skin damage. Future Med. Chem. 2017. 9. 1887–1898

30. Oishi. Y., Spann. N.J., Link. V.M., Muse. E.D., Strid. T., Edillor. C., Kolar. M.J., Matsuzaka. T., Hayakawa. S., Tao. J.H., et al. SREBP1 contributes to resolution of pro-inflammatory tlr4 signaling by reprogramming fatty acid metabolism. Cell Metab. 2017. 25. 412–427

31. Kusnadi. A., Park. S.H., Yuan. R.X., Pannellini. T., Giannopoulou. E., Oliver. D., Lu. T., Park-Min. K.H., Ivashkiv. L.B. The cytokine tnf promotes transcription factor srebp activity and binding to inflammatory genes to activate macrophages and limit tissue repair. Immunity 2019. 51. 241–257

Study 2

Analysis of proteome and lipidome profile changes induced by γ-Oryzanol prevention treatment in obese-induced rats

- An example of research that makes you (re)think -

ABSTRACT

Grains are the most common staple food consumed worldwide and among them, rice (*Oryza sativa*) is the top one. Therefore, it is very important to consider its constituents, such as γ-Oryzanol (Orz). Orz has shown several biological activities and it's often associated with fat and cholesterol-lowering, anti-inflammatory etc., also recently becoming a great candidate in metabolic disorders like obesity. The mechanisms under all these effects are still not completely clarified also considering as the studies so far are mainly conducted through biological tests in tissues and fluids. So, the main goal of this work was to describe and relatively quantify plasma proteome and lipidome changes in 32 rats (obese-induced rats treated or not with Orz vs lean controls) by liquid chromatography coupled to high-resolution mass spectrometry. Despite the widespread use of plasma to study drugs and active substances effects *in vivo*, this model didn't provide for this project the best example in terms of reproducibility and estimation of treatment efficacy both in proteome and lipidome. Further thoughts and experiments are needed to confirm the biological relevance of Orz only showed in biological tests so far.

1. INTRODUCTION

Grains are the most common staple food consumed worldwide and among them, rice (*Oryza sativa*) is the top one. Therefore, it is very important to consider its constituents. such as γ-Oryzanol (Orz) that is present in the bran layer and comprises a mixture of ferulic acid esters and phytosterols (sterols and triterpenic alcohols) (1). Among them, cycloartenyl, 24-methylenecycloartanyl, campesteryl and sitosteryl ferulate are the most expressed (Figure 1).

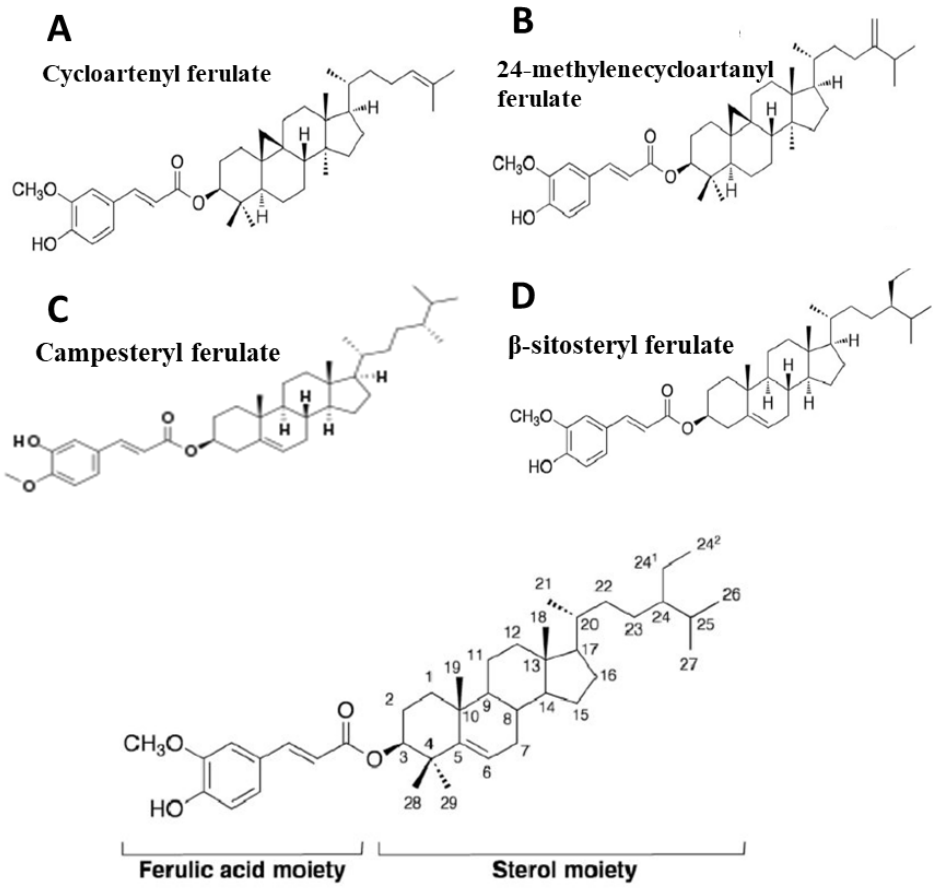

Figure 1. Molecular structures of the four main Orz components (A–D). Chemical structures are composed by ferulic acid and steryl ferulates. In mammals, Orz can be metabolized to ferulic acid and sterol moiety.

Orz has shown several biological activities and it's often associated with cholesterol-lowering, anti-inflammatory, anti-cancer, anti-diabetic effects, and antioxidant ones by blocking lipid peroxidation (2–4). Preliminary positive results were also obtained in amelioration of cardiorenal metabolic

syndrome as showed by Francisqueti FV et al., (5) and Leite J. et al., (data not published). Moreover, Orz is also recently become a great candidate in metabolic disorders like obesity thanks to its alleged capacity to reducing fat accumulation. It seems also to act at the central nervous system affecting the preference for high-fat diet as demonstrated in *vivo* by Masukaki et al., (3).

Obesity is one of largest health problems on the world that has shifted from being a problem in rich countries, to one that spans all income levels. Indeed, it is common to 13% of adults worldwide being responsible of 8% of global deaths (WHO 2017) (6). So, additional alternatives for its treatment and/or prevention are required.

Although all the benefits linked to Orz, the mechanisms under its effects, decreasing of fat accumulation included, are still not completely clarified also considering as the studies so far are mainly conducted through biological tests in tissues and fluids (2). To reduce this gap, the main goal of this work was to describe and (relatively) quantify plasma proteome and lipidome changes in obese-induced rats treated or not with Orz vs lean controls by high-resolution mass spectrometry.

2. MATERIALS AND METHODS

2.1 Chemicals

γ-Orizanol was purchased by Tokyo Chemical Industry Co., Ltd (Toshima, Kitaku, Tokyo; lot. 5ZZYLPJ); BCA kit, protease inhibitor cocktail, DL-dithiothreitol (DTT), iodocetamide (IAA), ammonium bicarbonate (NH_4HCO_3), ammonium formate (NH_4HCO_2), methyl-tert-butyl-ether (≥99%, MTBE), acetonitrile (MeCN), methanol (MeOH), 2-propanol (i-PrOH), chloroform (CH_3Cl) and formic acid (FA) (all UHPLC/MS-CC/SFC grade) were purchased from Sigma-Aldrich (Taufkirchen, Germany); Trypsin Sequencing Grade were purchased by Roche (Monza, Italy); TMT6-plex Isobaric Label Reagent Set (2x6x0.8 mg) and Pierce™ High pH Reversed-Phase Peptide Fractionation Kit were purchased by Thermo Fisher Scientific (San Jose, CA, United States); SPLASH® LIPIDOMIX® Mass Spec Standard was purchased by Avanti Polar Lipids Inc,

(Alabaster, AL, USA), Water was purified in-house (resistance > 18 MΩ cm−1; total organic content < 10 ppb) with a Milli-Q H2O purification system (Millipore, Bedford, MA, USA).

2.2 Animals and Experimental Protocol

Plasma samples used in this work were kindly provided by Camila Renata Corrêa's lab (São Paulo State University – Unesp- Medical School, Botucatu, Brazil) and stored at -80°C. All the experiments and procedures were approved by the Animal Ethics Committee of Botucatu Medical School (1150/2015) and were performed in accordance with the National Institute of Health's Guide for the Care and Use of Laboratory Animals. Briefly, 32 male Wistar rats (±187 g) were kept in an environmental controlled room (22 °C ± 3 °C; 12 h light-dark cycle and relative humidity of 60 ± 5 %) and randomly divided into 4 experimental groups. Over 30 weeks the animals received: control diet (C, n= 8), control diet + gamma-oryzanol (C + γ-Orz, n= 8), high sugar-fat diet (HSF, n= 8), and high sugar-fat diet + gamma-oryzanol (HSF + γ-Orz, n= 8) (Table 1). HSF groups also received water + sucrose (25%). γ-Orizanol was administered in prevention so since the beginning of the study. The diets and water were *ad libitum*.

2.3 Diet based on γ-Orizanol and metabolic parameters

To simulate γ-Orizanol regular way of consumption and due to its nonpolar characteristics, it was added to diets to reach 0.5% of final concentration (*w/w*). Diets and the period of treatment were based on the work of Son et al., (2011) (7) and on the daily consumption of rice of an adult individual in Brazil according to data from the Family Budget Survey (POF) 2008–2009 (8). For the complete diet composition and nutritional values refer to Francisqueti FV et al. (2017) (5). Food consumption was measured daily and body weight weekly. Total triglycerides were measured with an automatic enzymatic analyser system (Chemistry Analyzer BS-200, Mindray Medical International Limited, Shenzhen, China). After euthanasia, the fat deposits visceral (VAT), epididymal (EAT) and

retroperitoneal (RAT) were used to calculate the adiposity index (AI) by the following formula: [(VAT + EAT + RAT)/FBW] ×100.

Table 1. Diet composition in control and high-fat high-sugar group (HSF) (5).

Components	Control	HSF
Soybean meal (g/kg)	335	340
Sorghum (g/kg)	278	80
Soy hulls (g/kg)	188	116
Dextrin (g/kg)	146	20
Sucrose (g/kg)	-	80
Fructose (g/kg)	-	180
Soybean oil (g/kg)	14	-
Lard (g/kg)	-	154
Minerals (g/kg)	25	25
Salt (g/kg)	4	8

2.4 Proteomics analyses

2.4.1 Samples preparation and TMT-^{6}plex labelling

The amount of proteins in non-depleted plasma (n=32) was quantified by the BCA following the standard procedure. Three subgroups of each condition expressing 100 µg/µL of proteins were obtained grouping 2 or 3 samples obtaining 12 final samples for the next analyses (C1, C2, C3, CY1, CY2, CY3, OB1, OB2, OB3, OBY1, OBY2, OBY3). Quantitative proteomics analyses were done through tandem mass tag (TMT) assay following the standard protocol. Briefly, a suitable plasma volume was dissolved by triethylamonium bicarbonate (TEAB) to reach the final proteins concentration of 2.0 µg/µL, 25 µL of 100 mM TEAB and 2.5 µL of the reducing agent Tris(2-carboxyethyl) phosphine hydrochloride (TCEP) 200 mM (55°C for 1 hour) were added to the 25 µL of pre-dissolved sample. Protein alkylation was done adding 2.5 µL of 375 mM iodoacetamide (IAA) for 30 mins in the dark. Then, the protein digestion was performed with 2.5 µL of trypsin 0.5 µg/µL in solubilization reagent (enzyme: protein ratio 1:40) at 37°C overnight.

The samples were labelled using TMT6-plex Isobaric Label Reagent Set according to the manufacturer's protocols. Each peptide solution was incubated for 1 h at room temperature with 20.5 µL TMT Label Reagent then quenched for 15 min with 8 µL of 5% hydroxylamine solution in water. Two sets of analyses were obtained mixing 30 µL of each tagged sample (n=6 each) and dried under *vacuum* (Eppendorf concentrator 5301, 1 mbar).

TMT-labelled samples were divided into 8 fractions using Pierce™ High pH Reversed-Phase Peptide Fractionation Kit applying the standard protocol. Then, fractions were dried in under *vacuum* and dissolved in 40 µL of 1% formic acid (FA) taking off aliquots (3 µL) for mass spectrometry analysis.

2.4.2 Mass spectrometry (nLC-HRMS)

All samples have been analysed at Unitech OMICs (University of Milano, Italy) using: Dionex Ultimate 3000 nano-LC system (Sunnyvale CA, USA) connected to Orbitrap Fusion™ Tribrid™ Mass Spectrometer (Thermo Scientific, Bremen, Germany) equipped with nano electrospray ion source. Peptide mixtures were pre-concentrated onto an Acclaim PepMap 100 – 100µm x 2cm C18 (Thermo Scientific) and separated on EASY-Spray column ES803, 50 cm x 75 µm ID packed with Thermo Scientific Acclaim PepMap RSLC C18, 3 µm, 100 Å using mobile phase A (0.1 % formic acid in water) and mobile phase B (0,1% formic acid in acetonitrile 20/80, v/v) at a flow rate of 0.300 µL/min. Separation was performed at 35 °C with a flow rate of 0.3 µL/min using the following gradient: 0-100 min from 4 to 28% B; 101- 160 min from 28 to 60% B followed by washing and column re-equilibration up to 240 min. The sample injection volume was 3 µL and analysed in technical duplicate.

MS spectra were collected in positive ion mode, in the data-dependent (DDA) - Synchronous Precursor Selection (SPS) - MS/MS/MS (MS3) mode. Peptides were ionized with a spray voltage of 1600 kV. The instrument method included Orbitrap MS1 scans (resolution of 120,000; mass range 375−1500 m/z, automatic gain control (AGC) target $4x10^5$, max injection time of 50 ms).

During the MS2 analyses, precursor ions were filtered according to charge state (required >1z), dynamic exclusion (60 s with a ± 10 ppm window), and monoisotopic precursor selection. Precursors were isolated with quadrupole mode using a width of 0.7 m/z and were fragmented by collision induced dissociation (CID) followed by ion trap MS2 scans (CID collision energy of 35%; AGC target $1x10^4$; turbo ion trap scan rate; max injection time of 50 ms).

Quantitative SPS-MS3 scans operating in DDA mode with precursor selection range 400-1200 m/z and 10 SPS precursors were selected. For the MS3 scan, the MS1 precursor was isolated using a 2 m/z wide window (resolution of 30,000; HCD collision energy of 65%; scan range 100−500 m/z; AGC target $5x10^4$; max injection time of 54 ms).

2.4.3 Data Analysis

The instrumental raw files were processed by MaxQuant software v1.6.6.0 set on the *Rattus_Norvegicus* database against the Andromeda search engine (9,10). The quantification of peptides and related proteins for each control and treated sample in technical duplicates was based on reporter ion MS3 normalized intensities selecting "6plex TMT" option leaving the default parameters. Trypsin as the digestive enzyme, variable modification of carbamidomethylation of cysteine (+57.021 Da), fixed modification of methionine oxidation (+15.995 Da), N-terminal acetylation (+42.011 Da) were selected too. The interpretation and visualization of results obtained from MaxQuant software were performed by a two-sample *t*-test of specific ion reporter intensity' s ratio using Perseus (v1.6.1.3, Max Planck Institute of Biochemistry, Germany). Statistical parameters ($p < 0.05$; $q < 0.05$. q = FDR adjusted p-value) were set to identify the differentially expressed proteins between samples (log2 fold changes). The proteins were selected with a minimum of two peptides. Variability of biological replicates were measured using the scatter plot with Pearson correlation coefficient values of the ion reporter' intensities.

2.5 Lipidomics analysis

2.5.1 Lipid extraction

All solvents used for the extraction contained 0.1 % BHT (w/v). An aliquot of 10 µL of plasma was diluted with 40 µL of ddH_2O, then 5 µL of SPLASH® LIPIDOMIX® Mass Spec Standard in $CHCl_3$/MeOH (2:1, v/v) were added to each sample and incubated for 15 min on ice. Samples were numeric randomized *prior* lipid extraction as well as LC-MS analysis. For lipid extraction, 375 µL of MeOH and 1250 µL MTBE were added to each sample. The samples were shaken at 40 rpm at 4 °C for one hour. The phase separation was induced by the addition of 315 µL of H_2O, followed by 10 minutes of shaking. The extraction mixtures were centrifuged for 10 minutes (1000 g). The upper phase (organic phase) was collected. 500 µL MTBE/MeOH/H_2O (4:1.2:1. v/v) were added to the lower phase, vortexed (5 s), centrifuged for 10 minutes (1000 g), and the upper organic phase was collected. Both organic phases were mixed and dried in a *vacuum* concentrator (Eppendorf concentrator 5301, 1 mbar). 10 µL of the extracts were dissolved in 200 µL of $CHCl_3$/MeOH (2:1, v/v) and aliquoted in portions of 30 µL.

Total quality control samples (QCs, n=2) were obtained mixing each sample in an equivolumetric way and subdivided in aliquots corresponding to 10 µL of original plasma. Then, group quality control samples (n=4 *i.e.*, Ctrl, Ctrl+Y-Orz, Obese, Obese+Y-Orz) were done mixing 2.5 µL of samples by group (20 µL total). The extraction procedure followed that described above in duplicate volumes to maintain the single samples extraction conditions. Dried aliquots were stored at -80 °C and dissolved in 50 µL in *i*-PrOH prior to LC-MS/MS analysis.

2.5.2 Mass spectrometry (UHPLC-HRMS)

Lipid were separated using reverse phase chromatography on a Vanquish Horizon system (Thermo Fisher Scientific, Bremen, Germany) equipped with an Accucore C18 column (150 × 2.1 mm; 2.6 µm, 150 Å; Thermo Fisher Scientific, Bremen, Germany). Gradient elution with solvent A

(MeCN/H_2O, 1:1, v/v) and B (i-PrOH /MeCN/H_2O, 85:10:5, v/v), both containing 5 mM ammonium formate and 0,1 % FA (v/v) was used. Separation was performed at 50 °C with a flow rate of 0.3 mL/min using the following gradient: 0-20 min 10-86 % B; 20.1-22 min 86-95 % B; 22.1-26 min 95 % B; 26.1-34 min 10 % B. Preliminary data were obtained through the same instrumental equipment at Health, Animal Science and Food Safety "Carlo Cantoni" (VESPA) (University of Milan). Final mass spectrometry detection instead was performed with a Q-Exactive Plus Hybrid Quadrupole-Orbitrap mass spectrometer (Thermo Fisher Scientific, Bremen, Germany) equipped with a HESI probe at Dr. Fedorova's Lab (University of Leipzig). Mass spectra were acquired in positive and negative mode with the following source parameters: sheath gas—40 L/min, auxiliary gas—10 L/min, sweep gas—1 L/min, spray voltage—3.5 kV (- 2.5 kV), spray current—10 μA, capillary temperature—300 °C, S-lens RF level—35, and aux gas heater temperature—370 °C.

Full MS spectra were acquired at a resolution setting for m/z 200 at 140,000. scan range 380-1200 m/z (negative), and 250-1200 m/z (positive), automatic gain control (AGC) target 1e6 counts, maximum injection time (IT) 100 ms. MS/MS spectra were acquired applying a DDA (top 15) method was used at a resolution of 17,500 at m/z 200, AGC target of 2e5, and a maximum IT of 60 ms. An isolation window for precursor selection was 1.2 m/z and a stepped collision energy (CE 10-20-30 eV) was used for HCD.

2.5.3 Data Analysis

Lipid identification strategy was based on merged results obtained by LipidHunter 2 RC_3 (https://github.com/SysMedOs/lipidhunter) (11) and LipoStar (version 1.3.2 x64. Molecular Discovery, Hertfordshire. UK) (12) followed by manual annotation in Skyline v. 20.2.0.343. Relative quantification was based on determination of area under curve (AUC) for each lipid correctly identified then normalized by AUC of the used ISTD to the correspondent lipid specie and the protein concentrations. Range of concentration for each class was determined by the following formula: pg/ μL = (raw peak area analyte*pg ISTD)/ ISTD area.

Then, MetaboAnalyst v 5.0 online software (https://www.metaboanalyst.ca/) was used to perform statistical analyses.

3. RESULTS AND DISCUSSION

3.1 Animal model validation

Induction of obesity in HFS diet groups was verified by C.R. Correa's lab based on initial weight, weight gain and adiposity index data and total triglycerides (TGs) blood content (Table 2). Additional metabolic and hormonal factors (insulin, glucose, food intake etc.) were evaluated but not provided although previous studies were conducted by Francisquet FV et al., (5,13,14) with the same animal model and treatment aimed to verify the Orz effects on obesity and related morbidities.

Table 2. Nutritional and metabolic values supporting induction of obesity provided by Correa's Lab (data unpublished). Single values are expressed as means ± standard deviation. Comparison by two-way ANOVA with Tukey post-hoc. $p < 0.05$; * means significance.

	Ctrl	**Ctrl+Y-Orz**	**Obese**	**Obese+Y-Orz**
Initial weight (gr)	476.87 ± 43	494.65 ±60	592.88 ±57	467.24 ± 64
Weight gain (gr)	302.91± 48	300.8± 28	405.5± 65	296.87± 56
Adiposity Index	4.53 ±1	3.94± 0.8	7.13 ± 1.86	5.73 ± 1
Triglycerides (mg/dl)	60.86 ±13	58.48 ± 12	118.78 ±4	82.68 ± 14

	Significance (Turkey's Test)			
	Ctrl vs Ctrl +Y-Orz	**Ctrl vs Obese**	**Obese vs Obese+Y-Orz**	**Ctrl vs Obese+Y-Orz**
Initial weight (gr)	0.565	*<0.001	*<0.001	0.377
Weight gain (gr)	0.94	*0.001	*<0.001	0.88
Adiposity Index	0.38	*<0.001	*0.049	*0.014
Triglycerides (mg/dl)	0.711	*<0.001	*<0.001	*<0.001

3.2 Proteome analysis

329 proteins were identified at least with two peptides and quantified. Comparing the groups, no significant differences was observed by Volcano plot analysis performed with Perseus software (Figure 2).

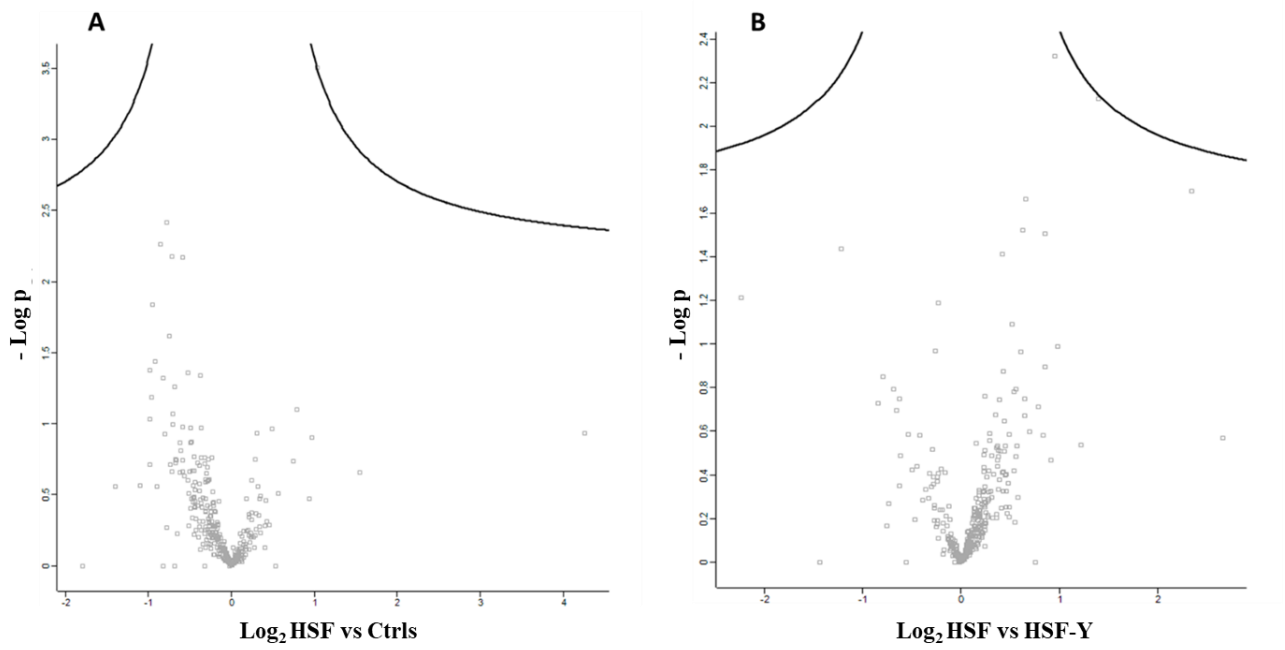

Figure 2. Proteins distribution of A) Obese vs Control groups and B) Obese vs Obese-Y groups; log2 fold change on x-axis against -log p-value on y-axis. No significant alterations were determined (log2 fold change ≥ 0.6 for up-regulation, ≤ -0.6 for down-regulation).

Nevertheless, few significant alterations (Table 3) were highlighted by manual curation considering the following threshold standard parameters: 0.57 as difference (corresponded to 1.5-fold change variation) and 1.3 as $-\log_{10}$ p-value ($\log_{10}$ 0.05= 1.3).

HFS group vs Ctrl showed a general downregulation of immune response proteins mainly belonging to the Ig-like domain family that acts in cell-cell recognition, cell-surface receptors, muscle structure and the immune system. These observations are in line with literature ones. In fact, detrimental effects on immunity linked to obesity and/or metabolic syndromes are well known (15). Moreover, proteins involved on vasodilatation and permeability, HDL metabolism and oxidative stress response showed

a downregulation in HFS. Imbalance of vasoconstriction, vascular lipids deposition and inflammatory activation are confirmed factors characterizing obesity development (16).

Partial differentiation also between HFS+γ-Orz and HFS (Table 3). Orz treatment induced a rearrangement of proteins mainly correlated with structural such as actin and transcription processes. Up-regulation instead was demonstrated by insulin-like growth factor-binding protein complex and 14-3-3 protein theta involved in the insulin internalization in tissues and membrane transport.

The multiplex proteomics approach by labelled peptides didn't seem to positively affect the coverage performance resulting in a relative low number of identified proteins. The concentration of proteins in plasma usually spans a dynamic range of 10-12 orders of magnitude causing a poor identification of those less abundant. Indeed, albumin, immunoglobulins, haptoglobin, antitrypsin and transferrin are the most expressed counting for 85-90% of total protein mass. Despite depletion of these highly abundant proteins has demonstrated (17) a greatly increasing in the number of identifiable proteins, we worked with non-depleted plasma considering the procedure's high costs and the risks to introduce further samples variability (17,18). Trying to overcome this limitation and to reduce the complexity of mixed sample to improve the detection and quantification of reporter ions we performed a fractionation of peptides coupling high pH reversed-phase chromatography to separate peptides by hydrophobicity (Thermo Scientific™ Pierce™ High pH Reversed-Phase Peptide Fractionation Kit) and high-performance liquid chromatography (Dionex Ultimate 3000 nano-LC system).

Further sample preparation and instrumental adjustments, such as extensive fractionation, increasing the number of samples and replicates, are needed for a better coverage of rat plasma proteome.

Table 3. Altered proteins (>1.5-fold change, p value < 0.05) comparing HSF vs Ctrl groups and HSF-Orz vs HSF.

HFS vs C					
	log p-value	**Difference**	**Protein IDs**	**Protein names**	**Function**
DOWN	1.38	-0.98	D3ZMS7	Ig-like domain-containing protein	immune response
	1.19	-0.96	A0A0G2K7P6	IGv domain-containing protein	extracellular space
	1.83	-0.95	P08932	T-kininogen 2	glycoprotein: Protease inhibitor, Thiol protease inhibitor, Vasoactive, Vasodilator
	1.44	-0.92	M0R9U2	Ig-like domain-containing protein	innate immune response; antigen binding, complement cascade factor
	2.26	-0.85	Q6IRS6	Fetuin-B	cysteine-type endopeptidase inhibitor activity
	1.32	-0.82	Q5PQU1	T-kininogen 1	glycoprotein: smooth muscle contraction, Thiol protease inhibitor, vasoactive, vasodilator
	2.42	-0.78	A0A0G2JZ73	Alpha-1-antiproteinase	protease binding
	1.61	-0.74	A0A0G2JX36	Ig-like domain-containing protein	immune response
	2.18	-0.72	P04638	Apolipoprotein A-II	May stabilize HDL (high density lipoprotein) structure by its association with lipids, and affect the HDL metabolism
	1.26	-0.68	A0A0G2JUY4	Ig-like domain-containing protein	immune response
	2.17	-0.59	A0A0G2K531	Glutathione peroxidase 3	response to oxidative stress
UP	1.10	0.79	D3ZQM9	Ig-like domain-containing protein	immune response
	3.50	1.03	P06238	Alpha-2-macroglobulin	acute inflammatory response to antigen stimulus
HFS-Orz vs HFS					
	log p-value	**Difference**	**Protein IDs**	**Protein names**	**Function**
DOWN	1.70	-2.35	D3ZGK7	Carboxylic ester hydrolase	hydrolase
	2.13	-1.40	F1LPR6	Immunoglobulin heavy constant mu	immune response
	2.32	-0.96	P60711	Actin, cytoplasmic 1	cytoplasmic cytoskeleton, G- and F-actin also localize in the nucleus, and regulate gene transcription and motility and repair of damaged DNA
	1.51	-0.86	A2VD04	Hyaluronan-binding protein 2	enzyme
	1.67	-0.66	M0R965	RNA helicase	Transcription
	1.52	-0.63	Q8CHN9	AT-rich interaction domain 1B	DNA binding
	1.09	-0.52	Q8K583	Fibrinogen-like protein 1	immune response
UP	1.44	1.22	F1LRE2	Insulin-like growth factor-binding protein complex acid labile subunit	access regulation of circulating IGFs to the tissues.
	1.22	2.24	P68255	14-3-3 protein theta	transmembran transport, binding

3.2 Lipidome analysis

3.2.1 Lipids Identification

Untargeted lipidomics analyses supported detection of 546 lipids unique by structure of which 299 confirmed by manual identification in Skyline. Two samples belonging to Ctrl and HSF+Orz respectively were removed from the analyses due to bad chromatographic performance. Lipids were considered "true" based on the following stringent parameters: detection on at least 70% of samples; presence of class characteristic fragments (such as 168 and 224 for phosphatidylcholines); presence of at least two fragments derived from the specific structure (except for the lyso- and cholesterol esters where one fragment is conventional accepted).

Triacylglycerols (TGs) demonstrated the higher abundance covering 76% of identified lipidome, followed by sphingomyelin (SMs, 7.3%), ceramides (Cers, 5%), phosphatidylcholines (PCs, 4.3%) and cholesterol esters (CEs, 2%). Negligible presence of diacylglycerols (DGs), phosphatidylethanolamine (PEs), lyso-phosphatidylethanolamine (LPEs), lyso- phosphatidylcholines (LPC) and phosphatidylinositol (PIs).

3.2.2 Lipids alteration

Once normalized the identified compounds, the general lipidome profiles were compared. Considering all groups, 64 lipids resulted significantly altered at least between two conditions on the basis of one-way ANOVA test (adjusted p value < 0.05, post-hoc analyses using Fisher's LSD). Partial least squares-discriminant analysis (PLS-DA) also showed a cluster separation between controls (lean) and HSF groups. On the other hand, no significant effect seemed to be correlated to Orz treatment since the overlapping with the respective untreated samples (Figure 3A-B). The invariance was demonstrated also through two sample t-test and Wilcoxon rank sum test ($p< 0.05$).

Unexpectedly, Volcano plot analysis (FC>1.5, p value< 0.05) showed only 9 statistical significant lipids comparing Ctrl vs HSF (Figure 3C) *i.e.,* 2 PCs (PC(15:0:20:4), PC(17:0_20:4)), 2 SMs (SM(41:2,2); SM(41:1,2) and one PI (PI(16:0_20:4)) that resulted more expressed in the control

samples while DG(16:0_18:1) and three TGs (TG(15:0_15:0_18:1); TG(16:0_16:0_16:1); TG(14:0_16:0_16:1)) were more abundant in HSF group.

Nevertheless, subdividing TGs based on fatty acid chains saturation level we saw a different trend based on normalized intensities between the groups despite not significant. Indeed, unsaturated and mono-unsaturated TGs are generally more expressed on samples from HSF group while polyunsaturated ones (PUFAs) in lean samples (Figure 4).

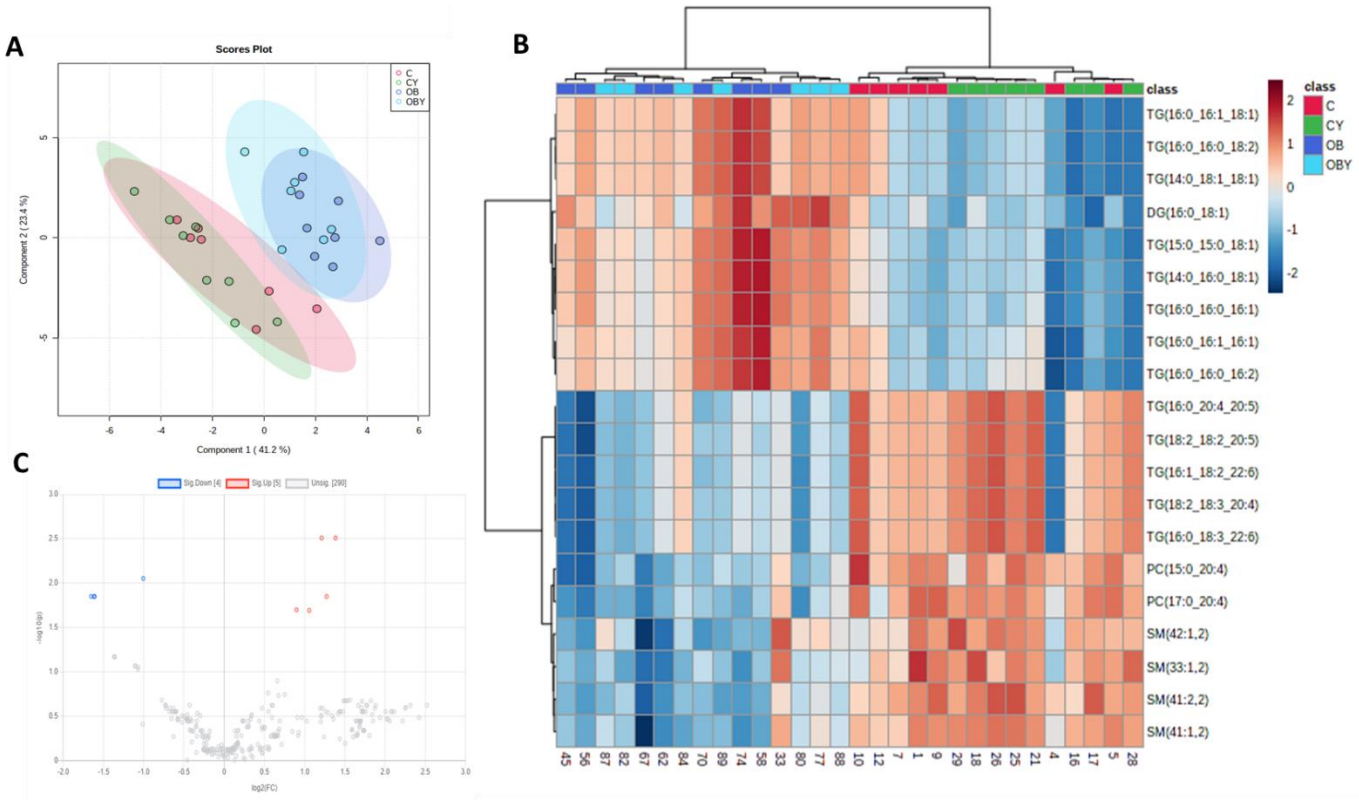

Figure 3. A) Scoring plots reconstructed using PLS-DA (PC1 vs PC2). Red group correspond to the control samples; green to Ctrl+Y-Orz; blu to HSF (obese) and light blue to HSF+ Y-Orz ones; B) Hierarchical Clustering Heatmap of the 20 most significant altered lipids (T-test/ANOVA $p < 0.05$). Each coloured cell on the map corresponds to a concentration value (in red those more expressed, in dark blue those with the lowest value) with samples in row and features in column; C) Volcano Plot of Ctrls vs HSFs. In red the features significantly altered (Fold change (FC) > 1.5, adjusted p value <0.05).

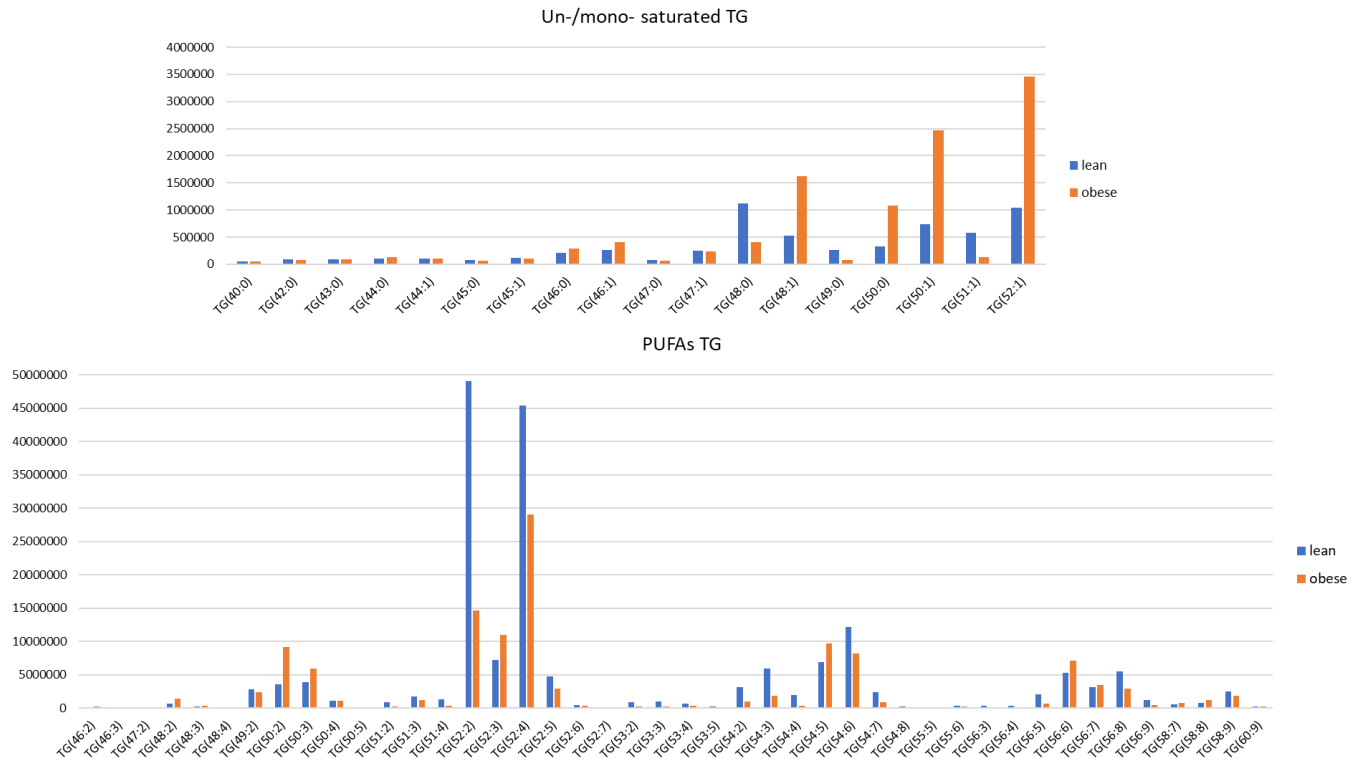

Figure 4. Normalized intensity (peak area) comparison of TGs in lean (controls) and obese groups based on saturation level. At the top those unsaturated and monosaturated, at the bottom the polyunsaturated ones (PUFAs).

Higher levels of saturated fatty acids (SFAs) and lower levels of PUFAs here observed are in line with previous studies both clinical and *in vivo*. For example, a similar lipidome profile was showed by Gowda et al., (19) in high fat diet (HFD)-induced obesity rats. Exogenous PUFAs administration also demonstrated positive effects mammalian membranes counteracting dietary lipids perturbation (typical in obesity) to maintain cellular phenotypes and functionality (20). On the contrary, no significant changes induced by Orz were recorded.

3.3 Critical analysis of the results: What was wrong? What can be fixed?

Preliminary analyses aimed to optimize method and having an initial biological vision were conducted on 4 groups QCs. Based on these data, we decided to analyse the single samples. Despite the general identification profile was similar, the significance was not reached by Orz treatment as

expected both in proteomics and lipidomics. In addition, low number of significant lipids changes were observed between control and HFS groups.

Once avoided mistakes related to the in-house sample preparation, instrumental and data analysis, I wondered what the possible reasons were and what to improve in the next future.

3.3.1 A priori considerations

- Plasma matrix was chosen based on the in-house sample type availability and its less complexity (still complex) compared to solid tissues like adipose one. Moreover, plasma samples are often used to have a reflection of the general health status as well as for the research of diseases biomarkers avoiding more invasive procedures (21–23). Nevertheless, the inter-individual and intra-day samples variability (less in rodents than humans but still present) is a considerable problem especially for lipidome analyses requiring an elevated number of samples to minimize these confounding factors. Moreover, temperature, time of storage, light and oxygen exposure are the main influencing factors that can alter both lipids and proteins profile (24)
- Rodents including mice and rats have long been used in research areas such as pharmacology, cancer, nutrition, and toxicology representing, unlike humans, higher controllable experimental model systems. However, these samples have a similar wide dynamic range in protein concentrations and lipidome diversification as seen in human samples and therefore face some of the same technological challenges (18)
- About lipidomics, there is no “one for all” extraction. By tailoring better this step, it’d be possible to increase the lipidome coverage for (here) less abundant species
- Studies of the profile of individual plasma TGs (the most abundant lipid class that we detected) are not common (25). This parameter is usually tested in adipose tissue, where TG accumulates or as total content in plasma

3.3.2 Work related considerations – what are the facts

- To induce obesity, HFS animals received a different diet both for quantity and quality (Table 1) increasing the response variability. Despite the same diet, the individual response could be different. Moreover, no data are available at the starting point to normalize the subjective response to the diet
- For the main goal of Correa's Lab's initial project, the diet was supplied for 30 weeks. Based on literature. studies to induce obesity by diet in rats (not genetically modified) are general conducted for shorter timing (8-16 weeks) (19, 26-28). For example, Panchal et al., (29) for first validated the HSF diet efficacy on induction of obesity feeding rats for 16 weeks. In addition, Wang et al., (30) with the analogue aim to evaluate Orz effects on HFS-diet induced metabolic syndrome in rats, treated rats only for 13 weeks. Aging is a well know influenced factor on lipid metabolism following diet composition and gender (31)
- Comparing the concentration of each identified lipid among groups' sample, I registered a high inter-variability as showed by relative standard deviation (RSD) in Table 4. The small sample size paired to a high variability could affect the significance of the data
- The samples I worked with were stored since 2017 causing a potential alteration of lipidome profile
- Despite double fractionation, non-depleted samples could cause an underestimation of lower abundant proteins

Table 4. Relative quantification (pg/µL) of each identified lipid classes in Ctrl and HFS groups expressed by average and relative standard deviation (RSD).

	Ctrls (pg/µl)	**Ctrls RSD**	**Obese (pg/µl)**	**Obese RDS**
SM	35.29	28.35	183.91	144.28
Cer	63.74	190.71	6.02	36.46
CE	3564.31	33.44	4285.42	22.58
DG	24.23	28.17	26.23	23.75
TG	74.59	61.70	52.66	47.47

3.3.3 Open considerations – what could it be done?

- Repeat the measurements to validate these results
- Considering the elevated number of detected TGs, lipids droplets could be an alternative lipidomics focus to investigate the HSF and Orz effects
- Consumption of diets rich in fats and fructose can lead to hepatic fat accumulation and liver dysfunctions (29). Similarly, Orz supplemented by oral intake (8 weeks) has showed to be accumulated more in liver than in plasma or other organs (2000 ng/ml in liver vs 20 ng/ml plasma for example) (32). So, liver tissue could be a better sample type to indicate Orz effects both for proteome and lipidome global profiles

4. CONCLUSIONS

Despite the preliminary data and literature evidence, in this case HRMS applied to proteomics and lipidomics analyses didn't highlighted any significant differences induced by γ-Orizanol treatment as well as (with few exceptions) between controls and HFS groups. The explanations could be related to the weakness of animal model used (reduced sample size, unstandardized and prolonged diet, inter-variability etc.) and the criticisms of samples manipulation (long storage, temperature sensibility etc.). Further studies are necessary to deepen and better understand the negative results here obtained maybe with other tissues.

REFERENCES

1. Lerma-García MJ. Herrero-Martínez JM. Simó-Alfonso EF. Mendonça CRB. Ramis-Ramos G. Composition. industrial processing and applications of rice bran γ-oryzanol. Food Chemistry. Elsevier; 2009. 115. p. 389–404.
2. Minatel IO. Francisqueti FV. Corrêa CR. Pereira Lima GP. Antioxidant activity of Y-oryzanol: A complex network of interactions . International Journal of Molecular Sciences. Multidisciplinary Digital Publishing Institute; 2016 . 17. p. 1107.
3. Masuzaki H. Kozuka C. Okamoto S. Yonamine M. Tanaka H. Shimabukuro M. Brown rice-specific γ-oryzanol as a promising prophylactic avenue to protect against diabetes mellitus and obesity in humans . J Diabetes Investig; 2019 . 10. p. 18–25.
4. Szcześniak KA. Ostaszewski P. Ciecierska A. Sadkowski T. Investigation of nutriactive phytochemical - gamma-oryzanol in experimental animal models. J Anim Physiol Anim Nutr; 2016 . 100. p. 601–17.
5. Francisqueti FV. Minatel IO. Ferron AJT. Bazan SGZ. Silva VDS. Garcia JL. et al. Effect of Gamma-Oryzanol as Therapeutic Agent to Prevent Cardiorenal Metabolic Syndrome in Animals Submitted to High Sugar-Fat Diet. Nutr 2017 Nov 29 ;9(12):1299.
6. Obesity and Overweight. In: SpringerReference 2012 . https://www.who.int/news-room/fact-sheets/detail/obesity-and-overweight
7. Son MJ. Rico CW. Nam SH. Kang MY. Effect of Oryzanol and Ferulic Acid on the Glucose Metabolism of Mice Fed with a High-Fat Diet. J Food Sci . 2011 Jan 1 ;76(1):H7–10.
8. IBGE—Instituto Brasileiro de Geografia e Estatística Pesquisa de Orçamentos Familiares (POF) 2008–2009: Análise do Consumo Alimentar Pessoal No Brasil: https://biblioteca.ibge.gov.br/visualizacao/livros/liv50063.pdf/

9. Cox J. Hein MY. Luber CA. Paron I. Nagaraj N. Mann M. Accurate proteome-wide label-free quantification by delayed normalization and maximal peptide ratio extraction. termed MaxLFQ. Mol Cell Proteomics . 2014 Sep 1;13(9):2513–26.

10. Cox J. Yu SH. Kyriakidou P. Isobaric matching between runs and novel PSM-level normalization in maxquant strongly improve reporter ion-based quantification. J Proteome Res . 2020 Oct 2;19(10):3945–54.

11. Ni Z. Angelidou G. Lange M. Hoffmann R. Fedorova M. LipidHunter Identifies Phospholipids by High-Throughput Processing of LC-MS and Shotgun Lipidomics Datasets. Anal Chem . 2017 Sep 5 ;89(17):8800–7.

12. Goracci L. Tortorella S. Tiberi P. Pellegrino RM. Di Veroli A. Valeri A. et al. Lipostar. a Comprehensive Platform-Neutral Cheminformatics Tool for Lipidomics. Anal Chem . 2017 Jun 6 ;89(11):6257–64.

13. Francisqueti FV. Ferron AJT. Hasimoto FK. Alves PHR. Garcia JL. dos Santos KC. et al. Gamma oryzanol treats obesity-induced kidney injuries by modulating the adiponectin receptor 2/PPAR-α axis. Oxid Med Cell Longev. 2018;2018.

14. Francisqueti-Ferron FV. Garcia JL. Ferron AJT. Nakandakare-Maia ET. Gregolin CS. Silva JP das C. et al. Gamma-oryzanol as a potential modulator of oxidative stress and inflammation via PPAR-y in adipose tissue: a hypothetical therapeutic for cytokine storm in COVID-19? Mol Cell Endocrinol. 2021 Jan 15;520:111095.

15. Andersen CJ. Murphy KE. Fernandez ML. Impact of obesity and metabolic syndrome on immunity . Advances in Nutrition. Oxford Academic; 2016 . 7. p. 66–75.

16. Barton M. Baretella O. Meyer MR. Obesity and risk of vascular disease: Importance of endothelium-dependent vasoconstriction . Br J Pharmacol; 2012 . 165. p. 591–602.

17. Gaun A. Lewis Hardell KN. Olsson N. O'brien JJ. Gollapudi S. Smith M. et al. Automated 16-Plex Plasma Proteomics with Real-Time Search and Ion Mobility Mass Spectrometry Enables Large-Scale Profiling in Naked Mole-Rats and Mice. J Proteome Res . 2021 Feb 5 ;20(2):1280–95.

18. Linke T. Doraiswamy S. Harrison EH. Rat plasma proteomics: Effects of abundant protein depletion on proteomic analysis. J Chromatogr B Anal Technol Biomed Life Sci. 2007 Apr 15;849(1–2):273–81.

19. Gowda SGB. Gao ZJ. Chen Z. Abe T. Hori S. Fukiya S. et al. Untargeted lipidomic analysis of plasma from high-fat diet-induced obese rats using UHPLC-Linear trap quadrupole-orbitrap MS. Anal Sci . 2020 ;36(7):821–8.

20. Levental KR. Malmberg E. Symons JL. Fan YY. Chapkin RS. Ernst R. et al. Lipidomic and biophysical homeostasis of mammalian membranes counteracts dietary lipid perturbations to maintain cellular fitness. Nat Commun . 2020;11(1):1–13.

21. Shi L. Buckley NJ. Bos I. et al. Plasma Proteomic Biomarkers Relating to Alzheimer's Disease: A Meta-Analysis Based on Our Own Studies. Front Aging Neurosci . 2021 Jul 21 ;13.

22. Surinova S. Schiess R. Hüttenhain R. Cerciello F. Wollscheid B. Aebersold R. On the development of plasma protein biomarkers . Journal of Proteome Research. American Chemical Society; 2011 . 10. p. 5–16.

23. Geyer PE. Holdt LM. Teupser D. Mann M. Revisiting biomarker discovery by plasma proteomics. Mol Syst Biol . 2017 Sep 1 ;13(9):942.

24. França CN. Mendes CC. Ferreira CES. Time collection and storage conditions of lipid profile. Brazilian J Med Biol Res . 2018 ;51(3).

25. Liakh I. Sledzinski T. Kaska L. Mozolewska P. Mika A. Sample Preparation Methods for Lipidomics Approaches Used in Studies of Obesity . Molecules; 2020 25.

26. Battault S. Meziat C. Nascimento A. Braud L. Gayrard S. Legros C. et al. Vascular endothelial function masks increased sympathetic vasopressor activity in rats with metabolic syndrome. Ajpheart. 2018 Mar 1 ;314(3):H497–507.

27. Jouenne A. Fourny N. Lan C. Varlet I. Sérée E. Pechere L. et al. In vivo and ex vivo longitudinal follow-up of resveratrol supplementation or restauration of a normal diet in female rat hearts submitted to high-fat-high-sucrose diet. Arch Cardiovasc Dis Suppl. 2021 May 1;13(2):198.

28. Yoshitsugu R. Kikuchi K. Hori S. Iwaya H. Hagio M. Shimizu H. et al. Correlation between 12α-hydroxylated bile acids and insulin secretion during glucose tolerance tests in rats fed a high-fat and high-sucrose diet. Lipids Health Dis . 2020 Jan 15 ;19(1):1–9.

29. Panchal SK. Poudyal H. Iyer A. Nazer R. Alam A. Diwan V. et al. High-carbohydrate high-fat diet-induced metabolic syndrome and cardiovascular remodeling in rats. J Cardiovasc Pharmacol . 2011 Jan ;57(1):51–64.

30. Wang O. Liu J. Cheng Q. Guo X. Wang Y. Zhao L. et al. Effects of ferulic acid and γ-Oryzanol on high-fat and high-fructose diet-induced metabolic syndrome in rats. PLoS One . 2015 Feb 3 ;10(2):e0118135.

31. Saito K. Ishikawa M. Murayama M. Urata M. Senoo Y. Toyoshima K. et al. Effects of sex. age. and fasting conditions on plasma lipidomic profiles of fasted sprague-dawley rats. PLoS One . 2014 Nov 6 ;9(11):e112266.

32. Kobayashi E. Ito J. Shimizu N. Kokumai T. Kato S. Sawada K. et al. Evaluation of γ-oryzanol Accumulation and Lipid Metabolism in the Body of Mice Following Long-Term Administration of γ-oryzanol. Nutrients . 2019 Jan 1 ;11(1).

VI

General conclusions

The 'omics sciences (*i.e.*, genomics, transcriptomics, proteomics, metabolomics etc.) are currently in development offering a new perspective of cellular and organismal environment. Despite the huge amount of information provided by a single omics, the comprehension of a biological and phenotypical phenomenon in physiological conditions as well as in diseases, exploring a drug mechanism, external factor impact etc., is related to just one point of view. Indeed, only an integrative approach can depict a complete scenario considering the complex molecular interplay.

At this regard, the main goal of my PhD was to integrate quantitative proteomics and lipidomics methodologies as potential contribution in the field of precision medicine.

Through different projects I have had the opportunity to learn, apply and merge proteomics and lipidomics techniques from the sample preparations to data analysis passing through high-resolution mass spectrometry. Paired to the analytical approaches, treating different biological matrices (both for source and type) was then a strength and challenge of this path. Indeed, sample processing, instrumental parameters, data analysis and biological interpretations were tailored based on the sample type that I worked with *i.e.*, cells, mice skin, human adipose tissue, and rats' plasma.

As main results, investigation on skin hairless mice proteome allowed me to show how carnosine is acting in defense of UV-A damages and as low-molecular-weight hyaluronic acid (LMW-HA) is involved not only in skin hydration and softness but only on remodeling of intra- and extra-cellular functionality. Lipidomics has also highlighted LMW-HA's alterations in lipid metabolism mainly through sphingolipids and cholesterol esters. Then, connections between proteome and lipidome changes were demonstrated by integratomics and networking analyses reinforcing the results previously obtained. Moreover, a new and minor class of functional lipids (FAHFAs) were successfully isolated detected and quantify from human adipose tissue revealing significant alterations based on metabolic status and adipose tissue portions. These results, for the first time obtained on human complex matrix, will be useful to better understand the biological

potentiality of this bioactive lipids in metabolic pathologies. Finally, during these last months working on γ-Orizanol capacities to contrast induced-obesity in rats, I faced issues related both instrumental and data analysis that made me think about the importance of the study design, the experimental model, and the accuracy of every project's step.

To conclude, despite the work that I've done is just a starting point of my scientific path and other omics should be included in an integrative vision (metabolomics for example), this PhD was been a multidisciplinary journey with an ambitious goal by which I appreciated the complexity and value of omics sciences in deepening our knowledges about several research fields from biological and pharmaceutical to nutrition, and environmental ones approaching more and more the precision medicine goal.

VII

Scientific Contributions

PUBLICATIONS

In preparation: Analytical solution to untangle the diversity of modified lipids in biological samples (Review)

In Submission: Characterization and relative quantification of fatty acid esters of hydroxy fatty acids (FAHFAs) in human white adipose tissue (WAT) of obese patients

Radrezza S., Aiello G., Baron G., Aldini G., Carini M., D'Amato A., Integratomics of Human Dermal Fibroblasts Treated with Low Molecular Weight Hyaluronic Acid. Molecules 2021. 26. 5096. https://doi.org/10.3390/molecules26165096

Radrezza S., Carini M., Baron G., Aldini G., Negre-Salvayre A., D'Amato A., Study of Carnosine's effect on nude mice skin to prevent UV-A damage - Free Radical Biology and Medicine 2021; doi.org/10.1016/j.freeradbiomed.2021.07.010.

Radrezza S., Baron G., Nukala SB., Depta G., Aldini G., Carini M., D'Amato A., Advanced quantitative proteomics to evaluate molecular effects of low-molecular-weight hyaluronic acid in human dermal fibroblasts. J Pharm Biomed Anal. 2020 Jun 5;185:113199. doi: 10.1016/j.jpba.2020.113199

ORAL COMMUNICATIONS

Radrezza S. - Quantitative lipidomics and proteomics in medicinal chemistry (SSPA September 2021)

Radrezza S. - Integratomics of human dermal fibroblasts treated with low-molecular weight hyaluronic acid (ECI Summer Conference, July 2021)

Radrezza S. - Hyaluronic acid at low-molecular-weight in human dermal fibroblasts: study by LC-MS/MS quantitative proteomics (Merck Young Chemists' Symposium 2019, November 2019)

POSTERS

Radrezza S., Aiello G., Altomare A., Aldini G., Carini M., D'Amato A. - Integratomics of human dermal fibroblasts treated with low-molecular weight hyaluronic acid (RDPA September 2021)

Radrezza S., Garcia J.L., Aiello G, Correa C. R., Ferron F.V.F., Chiesa L. M., Panseri S., Aldini G., D'Amato A., Carini M. - Y-oryzanol prevention treatment in obese rats: analysis of lipidome and proteome profile changing (LipidMaps Spring School, April 2021)

Radrezza S., Baron G., D'Amato A., Nukala S.B., Depta G., Aldini G., Carini M. - Advanced Quantitative Proteomics to Evaluate the Signaling Pathways Induced by Biomolecules in Human Dermal Fibroblasts (NMMC 2019)

Radrezza S., Baron G., D'Amato A., Nukala S.B., Depta. G., Aldini G., Carini M. - Advanced analytical approach for evaluating differentially regulated pathways induced by endogenous compounds and cosmetic ingredients on human dermal fibroblasts (IFSSC 2019)